

Seismic Retrofitting Project

Testing of Materials and Building Components of Historic Adobe Buildings in Peru

Research Report

Daniel Torrealva, Erika Vicente,
and Tim Michiels

In collaboration with Federica Greco,
Claudia Cancino, and Kelly Wong



Seismic Retrofitting Project

Testing of Materials and Building Components of Historic Adobe Buildings in Peru

Daniel Torrealva, Erika Vicente, and Tim Michiels

In collaboration with
Federica Greco, Claudia Cancino, and Kelly Wong

THE GETTY CONSERVATION INSTITUTE
LOS ANGELES
PONTIFICIA UNIVERSIDAD CATÓLICA DEL PERÚ
LIMA

© 2018 J. Paul Getty Trust

The Getty Conservation Institute
1200 Getty Center Drive, Suite 700
Los Angeles, CA 90049-1684
United States
Telephone 310 440-7325
Fax 310 440-7702
E-mail gciweb@getty.edu
www.getty.edu/conservation

The Getty Conservation Institute (GCI) works internationally to advance conservation practice in the visual arts—broadly interpreted to include objects, collections, architecture, and sites. The Institute serves the conservation community through scientific research, education and training, field projects, and the dissemination of information. In all its endeavors, the GCI creates and delivers knowledge that contributes to the conservation of the world's cultural heritage.

ISBN 978-1-937433-48-2 (online resource)
ISBN 978-1-937433-49-9 (print)

All images are © J. Paul Getty Trust and Escuela de Ciencias de Ingeniería at the Pontificia Universidad Católica del Perú (PUCP) unless otherwise noted.

Cover: © J. Paul Getty Trust, 2011. Photo: Scott Warren.



The Getty Conservation Institute



Contents

Project Participants	v
SRP Peer Review Group	vii
CHAPTER 1	
Project Background	
Introduction	1
Institutional Background and Project Partners	1
About This Publication	2
References	3
CHAPTER 2	
Material Properties of Adobe and Brick Masonry	
Introduction	5
Soil Analysis	6
Adobe Units	9
Adobe Wallets	10
Brick Masonry	16
Conclusions	19
References	19
CHAPTER 3	
Wood Characterization of Timber Elements	
Introduction and Methodology	21
Timber Distribution	21
Mechanical Characteristics	26
Discussion and Conclusion	28
References	29

CHAPTER 4**Quincha Testing**

Introduction to Quincha Systems	31
Testing Methodology	32
Results	38
Discussion and Conclusion	47
References	50

CHAPTER 5**Testing of Timber Connections at Ica Cathedral**

Selected Connections and Testing Methodology	51
Connection between Post and Horizontal Bracing (pin)	52
Connection between Post and Diagonal Bracing (nailed)	53
Connection between Arches and Beams (mortise and tenon)	56
Conclusions	59
References	59

CHAPTER 6**Traditional Techniques for Seismic Stabilization**

Pull-out Testing of Tie Beams	61
Testing of Corner Keys	71
Conclusions	78
References	78

CHAPTER 7

Conclusions	79
Bibliography	81

Project Participants

Seismic Retrofitting Project—Testing Phase

PROJECT DIRECTORS

Claudia Cancino

Senior Project Specialist, Getty Conservation Institute, Los Angeles

Daniel Torrealva

Professor, Pontificia Universidad Católica del Peru, Lima

PARTICIPANTS

Nicole Declat

Intern (2017-18), Getty Conservation Institute, Los Angeles

Charlotte Deschamps

Architect, Architecture School of Paris Belleville

Federica Greco

Engineering Consultant, Getty Conservation Institute, Los Angeles

Susan Macdonald

Head, Building and Sites, Getty Conservation Institute, Los Angeles

Tim Michiels

Engineering Consultant, Getty Conservation Institute, Los Angeles

Juan Carlos Parra

Engineer, Pontificia Universidad Católica del Peru, Lima

Erika Vicente

Engineer, Pontificia Universidad Católica del Peru, Lima

Kelly Wong

Former Project Specialist (2015-2017), Getty Conservation Institute, Los Angeles

SRP Peer Review Group

Organized by the Getty Conservation Institute (GCI) as part of the Seismic Retrofitting Project (SRP), the following professionals participated in peer review meetings in Lima on July 18-21, 2011 and in Cusco on January 23-27, 2017. The SRP peer review group consists of experienced professionals in seismic retrofitting, analytical modeling of historic masonry structures, and conservation of earthen architecture. The meetings, which included formal talks and site visits, were designed to provide maximum opportunity for informal discussion among a select group of experts.

The objective of the first meeting was to review the SRP Construction Assessment of selected building prototypes. The meeting also included a review of the SRP Proposal for the Testing and Modeling Phase, which was developed in collaboration with the GCI by the Escuela de Ciencias e Ingeniería of the Pontificia Universidad Católica del Perú (PUCP, SRP partner) and the Department of Architecture and Civil Engineering at the University of Bath (SRP partner from 2011 to 2014), respectively. The objective of the second meeting was to review the results of the completed testing developed by PUCP and the modeling results of the un-retrofitted and retrofitted SRP building prototypes, designed and developed by TecMinho, University of Minho (GCI consultant from 2015 to 2018).

In advance of both meetings, peer reviewers received extensive documentation of the work carried out by the SRP team. Peer reviewers' comments were highly valuable for the SRP team and enriched the methodology and results of the project. This publication serves as a testament to their voice and influence.

Eng. Rafael Aguilar **

Associate Professor, Pontificia Universidad Católica del Perú

Arch. André Aninat Jolly **

Head, Sustainable Conservation Project Workshop, Fundación Altiplano Msv, Chile

Eng. Carlos Casabonne **

Senior Principal, Gallegos, Casabonne, Arango, Ingenieros Civiles SAC

Arch. Mariana Correia **

President, ESG/Escola Superior Gallaecia, Portugal and former President, PROTERRA Iberian-American Network

Eng. Matthew DeJong ***

Senior Lecturer, University of Cambridge

Eng. Carmen Kuroiwa *

Gerente de Investigación y Normalización, Servicio Nacional de Capacitación para la Industria de la Construcción (SENCICO)

Arch. Philippe Garnier ***

Director, Human Settlements, CRAterre-ENSAG

Arch. Eng. Stephen J. Kelly ***

Secretary-General, International Scientific Committee on the Analysis and Restoration of Structures of Architectural Heritage (ISCARSAH)

Eng. Terrence Paret **

Senior Principal, Wiss, Janney, Elstner Associates, Inc.

Eng. Pere Roca **

Professor, Technical University of Catalonia

Eng. Nicola Tarque **

Associate Professor, Pontificia Universidad Católica del Perú

Eng. Julio Vargas Neumann ***

Member, International Scientific Committee on the Conservation of Earthen Architectural Heritage (ISCEAH) and World Heritage Earthen Architecture Programme (WHEAP)

Eng. Humberto Varum *

Professor, University of Porto, Member of ISCEAH

Eng. Fred Webster *

Former Member, Getty Seismic Adobe Project (GSAP)

* = Attended first meeting (July 2011)

** = Attended second meeting (January 2017)

*** = Attended both meetings

Project Background

Introduction

For nearly two decades, the Getty Conservation Institute (GCI) has been a recognized leader in developing methodologies and setting standards for the conservation of earthen architectural heritage worldwide.

Earthen buildings, typically classified as unreinforced masonry structures, are extremely vulnerable to earthquakes and subject to sudden collapse during a seismic event, particularly if a building lacks proper and regular maintenance. Historical earthen sites located in seismic areas are at high risk of being heavily damaged, even destroyed. During the 1990s, the GCI implemented the Getty Seismic Adobe Project (GSAP), a major research and laboratory testing program that investigated the performance of historical adobe structures during earthquakes and developed cost-effective retrofit methods that substantially preserve the authenticity of these buildings. Results of this research have been disseminated in a series of publications in both English and Spanish (Tolles et al. 1996, 2000, 2002).

In 2006, the GCI's Earthen Architecture Initiative convened two meetings: the Getty Seismic Adobe Project Colloquium and New Concepts in Seismic Strengthening of Historic Adobe Structures. Held at the Getty Center in Los Angeles, the meetings focused on implementation of the GSAP. Papers presented at the colloquium, as well as the main conclusions of the colloquium's roundtable discussions, were published as part of the colloquium proceedings. Participants in the colloquium concluded that the GSAP methodology was excellent and effective. However, the methodology's reliance on high-tech materials and professional expertise was a factor in preventing it from being more widely implemented (Hardy, Cancino, and Ostergren 2009).

Institutional Background and Project Partners

Building on the conclusions made during the GSAP colloquium, in 2009 the GCI created the Seismic Retrofitting Project (SRP) with the objective of adapting the GSAP guidelines for countries where equipment, materials, and technical skills are not readily available by providing low-tech, cost-effective seismic retrofitting techniques and easy-to-implement maintenance programs for historical earthen buildings that could improve their seismic performance while preserving their historical fabric.

The SRP was designed to be carried out in four phases: (1) selection and construction assessment of prototype buildings; (2) experimental and analytical investigations of the selected prototype buildings, including laboratory testing and numerical modeling; (3) testing and modeling of the designed retrofitting strategies for each prototype building; and (4) implementation and dissemination of the results and methods. During this last phase, the SRP is intended to provide guidance to those responsible for implementation (e.g.,

architects, engineers, and conservators) and to assist authorities in gaining acceptance of the designed techniques. Finally, the SRP will develop a model project in which these techniques could be implemented as case studies.

Peru was selected as the location for the project due to its acquired knowledge and experience in earthen construction and seismic retrofitting techniques for historical buildings; the existence in that country of potential partners for implementation of these techniques on model conservation projects; and background work already completed there by the GCI (Cancino 2014).

Consequently, in 2011, the GCI partnered with the Ministerio de Cultura del Perú and the Escuela de Ciencias de Ingeniería at the Pontificia Universidad Católica del Perú (PUCP) to develop the SRP in Peru. The Department of Architecture and Civil Engineering at the University of Bath and the Department of Civil, Environmental and Geomatic Engineering at University College London (UCL) served as SRP partners from 2010 to 2012 and from 2013 to 2014, respectively. In 2014, the University of Minho in Guimares, Portugal, joined the SRP as a consultant to refine and further develop the numerical analysis of the four building prototypes.

Staff of the Escuela de Ciencias de Ingeniería at PUCP started studying, testing, and publishing seismically resistant earthen constructions in the 1970s and have been key players on promoting safety on this type of building worldwide. The GCI and PUCP collaboration was established during the 1990s (Tolles, Kimbro, and Ginell 2002). However, it was the partnering in 2006 between the GCI and PUCP on a preliminary testing and research investigation into the use of geo-mesh to reinforce earthen constructions that led to a number of publications worldwide (Vargas-Neumann, Torrealva, and Blondet 2007).

About This Publication

During the first phase of the SRP, four archetypal religious and residential building types in Peru were identified, surveyed, and assessed. These prototypes represent principal building types in need of sensitive retrofitting techniques that have the potential for the most widespread application in Peru and other seismic regions in Latin America. The data acquired through historical research and on-site surveys produced an assessment of each typology construction system and are available for conservation professionals to consult at the GCI website as part of the SRP publications (Cancino and Lardinois 2012).

The second phase started in 2011 and focused on experimental and analytical investigations, including laboratory testing and numerical modeling. This phase demanded close interaction between the construction assessments developed in the first phase, the experimental testing, and the numerical analysis. Numerical models for all four building prototypes were developed first at the University of Bath to represent the actual state of each of the prototypes. The evolution of the models was transferred from Bath to UCL, which has published a series of papers describing UCL's partial results of this phase (Ferreira et al. 2013; Ferreira and D'Ayala 2014; Fonseca and D'Ayala 2012a, 2012b). Currently, the GCI is working with the University of Minho as consultants to develop numerical models to help guide the next phase of the project.

The current publication is the summary and conclusions of the more than three hundred experimental tests to characterize the materials and structural components of the four

building prototypes, carried out from 2011 to 2014 at PUCP. The performed tests were designed and conducted under the direction of the primary authors of this research report as SRP partners. Some of these tests were performed for the first time on earthen materials and/or structural components, providing valuable information to the field.

The tests also provide valuable information to the partial and global models of each of the prototypes that are currently under further development. Partial results of the testing program have been published in several international conferences (Torrealva and Vicente 2012, 2014), but this publication is intended to give a general overview and deeper understanding of the mechanical behavior of materials and structural components of historical earthen buildings in Peru.

References

- Cancino, Claudia. 2014. Estudio de daños a edificaciones históricas de tierra después del terremoto del 15 de agosto del 2007 en Pisco, Perú. Los Angeles: Getty Conservation Institute. http://hdl.handle.net/10020/gci_pubs/damage_assess_esp
- Cancino, Claudia, and Sara Lardinois. 2012. Seismic Retrofitting Project: Assessment of Prototype Buildings. 2 vols. Los Angeles: Getty Conservation Institute. http://hdl.handle.net/10020/gci_pubs/assess_prototype
- Ferreira, C. F., and D. D'Ayala. 2014. "Structural Analysis of Timber Vaulted Structures with Masonry Walls." In *Proceedings of the SAHC 2014 9th International Conference on Structural Analysis of Historical Constructions, Mexico City, Mexico, 14–17 October 2014*. Wroclaw, Poland.
- Ferreira, C. F., D. D'Ayala, J. L. Fernandez Cabo, and R. Díez. 2013. "Numerical Modeling of Historic Vaulted Timber Structures." *Advanced Materials Research*, 778, 517–25.
- Fonseca, C., and Dina D'Ayala. 2012a. "Numerical Modelling and Structural Analysis of Historical Ecclesiastical Buildings in Peru for Seismic Retrofitting." In *Proceedings of the 8th International Conference on Structural Analysis of Historical Constructions, 15–17 October 2012*. Wroclaw, Poland.
- _____. 2012b. "Seismic Assessment and Retrofitting of Peruvian Earthen Churches by Means of Numerical Modeling." In *Proceedings of the Fifteenth World Conference on Earthquake Engineering*. Lisbon.
- Hardy, Mary, Claudia Cancino, and Gail Ostergren, eds. 2009. Proceedings of the Getty Seismic Adobe Project 2006 Colloquium: Getty Center, Los Angeles, April 11–13, 2006. Los Angeles: Getty Conservation Institute. http://hdl.handle.net/10020/gci_pubs/gsap
- Tolles, E. Leroy, Edna E. Kimbro, and William S. Ginell. 2002. Planning and Engineering Guidelines for the Seismic Retrofitting of Historic Adobe Structures. GCI Scientific Program Reports. Los Angeles: Getty Conservation Institute. http://hdl.handle.net/10020/gci_pubs/seismic_retrofitting_english
- Tolles, E. Leroy, Edna E. Kimbro, Frederick A. Webster, and William S. Ginell. 2000. Seismic Stabilization of Historic Adobe Structures: Final Report of the Getty Seismic Adobe Project. GCI Scientific Program Reports. Los Angeles: Getty Conservation Institute. http://hdl.handle.net/10020/gci_pubs/seismic_stabilization
- Tolles, E. Leroy, Frederick A. Webster, Anthony Crosby, and Edna E. Kimbro. 1996. Survey of Damage to Historic Adobe Buildings after the January 1994 Northridge Earthquake. GCI Scientific Program Reports. Los Angeles: Getty Conservation Institute. http://hdl.handle.net/10020/gci_pubs/damage_adobe_structures
- Torrealva Dávila, Daniel and Erika Vicente Meléndez. 2012. Proyecto de Reforzamiento Sísmico: Evaluación Experimental del Comportamiento Sísmico de Muros de Quincha del Centro Histórico de Lima—Perú. En *11th International Conference on the Study and Conservation of Earthen Architectural Heritage*. Lima, Perú.

- _____. 2014. "Experimental Behavior of Traditional Seismic Retrofitting Techniques in Earthen Buildings in Peru." In *Proceedings of the SAHC 2014 9th International Conference on Structural Analysis of Historical Constructions, Mexico City, Mexico, 14–17 October 2014*. Wroclaw, Poland.
- Vargas-Neumann, Julio, Daniel Torrealva, and Marcial Blondet. 2007. *Construcción de casas saludables y sismorresistentes de adobe reforzado con geomallas—Zona de la costa* (1st ed.). Lima: Fondo Editorial de la Pontificia Universidad Católica del Perú.

Material Properties of Adobe and Brick Masonry

Introduction

This chapter presents the testing methodology and results of investigation of the mechanical properties of adobe and brick masonry used in some of the prototype buildings assessed in the Peru Seismic Retrofitting Project (SRP). Adobe blocks and soil mortar are used as the main construction materials in the walls of all four prototype buildings. Brick masonry with lime mortar is found in the plinths of the wall in Hotel El Comercio, as well as around the doors and windows in Ica Cathedral and Hotel El Comercio. The aim of this set of tests was to characterize the mechanical properties of the original materials used in the prototype buildings. However, given the difficulty of obtaining original historical material from all sites, historical material data tests are complemented by tests on new contemporary, yet similar, material.

Material was obtained from three of the four prototype buildings (Ica Cathedral, Hotel El Comercio, and the church of Kuñotambo); no materials were obtained from Casa Arones in Cuzco. In addition to Hotel El Comercio, materials were obtained from two other buildings in the historic center of Lima: the house next to Hotel El Comercio in the Jr. Ancash (hereafter referred to as Casa Ancash), and Casa Welsch (fig. 2.1).

Testing procedures were executed following international standards whenever those standards were available. Due to the brittle nature of adobe test specimens, it was repeatedly necessary to modify the testing protocol in order to successfully carry out the tests.

FIGURE 2.1.

Aerial view of the historic center of Lima, indicating the locations of Hotel El Comercio (1), Casa Ancash (2), and Casa Welsch (3). © 2013 Google. Image: © 2013 Digital Globe.



Therefore, each test is described briefly below, followed by a presentation of its results and a brief conclusion.

Soil Analysis

Soil samples were collected from adobe blocks in Kuñotambo, Ica Cathedral, and Hotel El Comercio. Soil samples from mortar were also obtained from Ica Cathedral and Hotel El Comercio, but not from Kuñotambo. No soil analysis on adobe or mortar was performed for Casa Arones as no material could be obtained. Additionally, soil samples were collected from two other buildings in Lima (Casa Welsch and Casa Ancash), the results of which are provided for comparative reasons. For an overview of the type and amount of soil samples tested per building, see table 2.1.

TABLE 2.1.
Number of tests performed and origin of material tested for soil samples collected from buildings in Lima.

Origin of Material	Number of Tests	
	Adobe	Mud mortar
Kuñotambo	1	–
Ica Cathedral	2	2
Hotel El Comercio	1	1
Other buildings in Lima	3	3

Particle-size Distribution

TEST DESCRIPTION AND METHODOLOGY

Particle-size distribution of the soil of the adobe units and mud mortar was identified using sieve and hydrometer analysis. The sieve analysis was performed to determine the distribution of particles with a diameter larger than 74 μm , and the hydrometer method was used to determine distribution of the finer particles. The tests were performed following ASTM Standard Test Method for Particle-Size Analysis of Soils (ASTM D422) (withdrawn 2016).

RESULTS

Granulometric curves are provided for Ica Cathedral (fig. 2.2), Hotel El Comercio (fig. 2.3), and other buildings in Lima (fig. 2.4). Figure 2.5 combines all granulometric curves of adobe blocks; figure 2.6 combines all granulometric curves for soil from the original mortar.

DISCUSSION AND CONCLUSION

In general, the soil composition of adobe units and mortars present low-plasticity clays. The soils from Ica Cathedral contain more silt. The amounts of coarse and fine particles were similar in all cases (see figs. 2.5, 2.6): 30–40% for coarse material and 60–70% for fine material. The similarity of grain-size distribution of the soil used for mortar and adobes per location confirms that traditionally the same soil was used for making both mud mortar and adobe.

The test samples from Kuñotambo and Hotel El Comercio have a low clay content (10%), which is the lower boundary recommended for adobe blocks in literature (the Peruvian Adobe Code suggests clay contents ranging from 10% to 20%) (Ministerio de Transportes 2000). The soil from the other buildings in Lima contains about 15–20% clay. Measurements of clay content for the soil in the building materials in Ica varied from 12% to 16%.

FIGURE 2.2.
Granulometric curve for Ica Cathedral, showing mud mortar (orange) and adobe (blue).

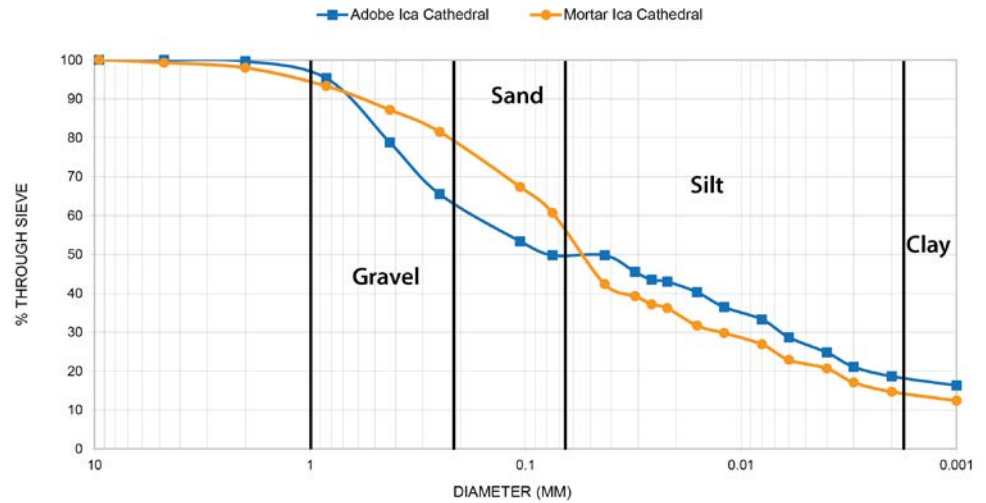


FIGURE 2.3.
Granulometric curve for Hotel El Comercio, showing mud mortar (green) and adobe (red).

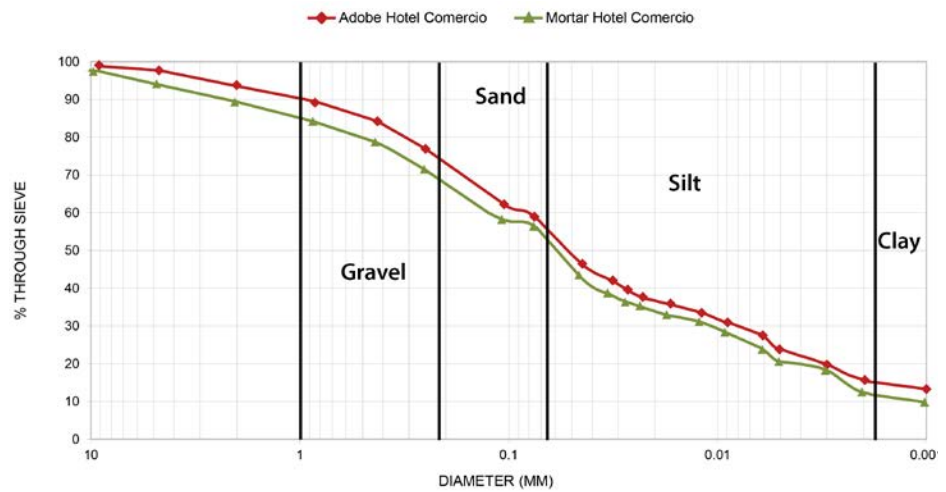


FIGURE 2.4.
Combined granulometric curves for Casa Ancash, Casa Welsch, and Hotel El Comercio.

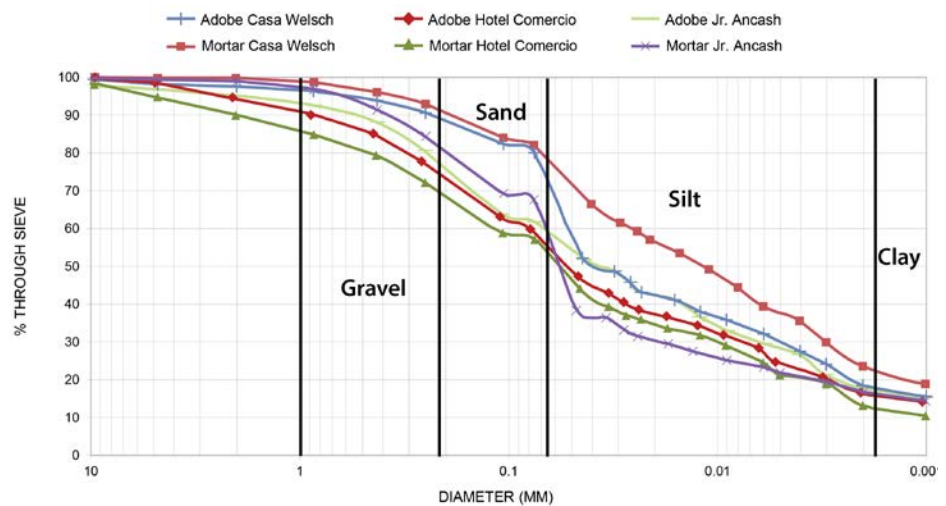


FIGURE 2.5.
Combined granulometric curves for
all adobe blocks.

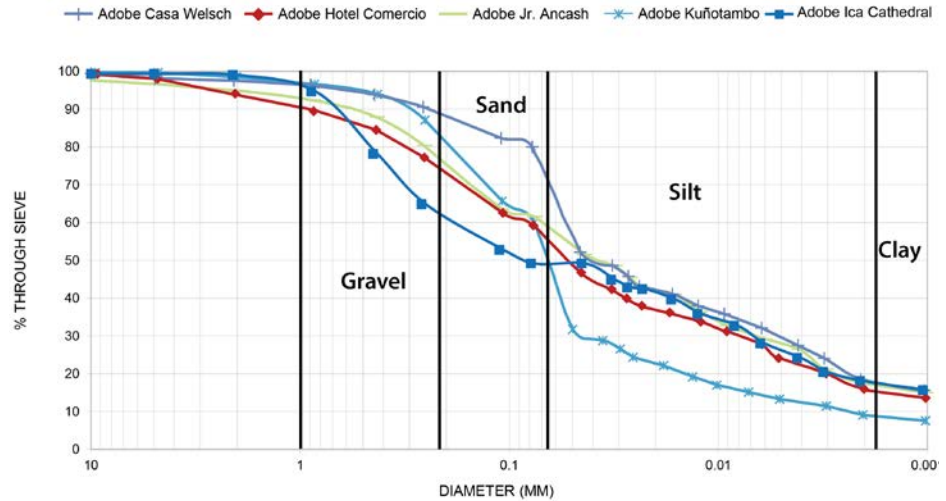
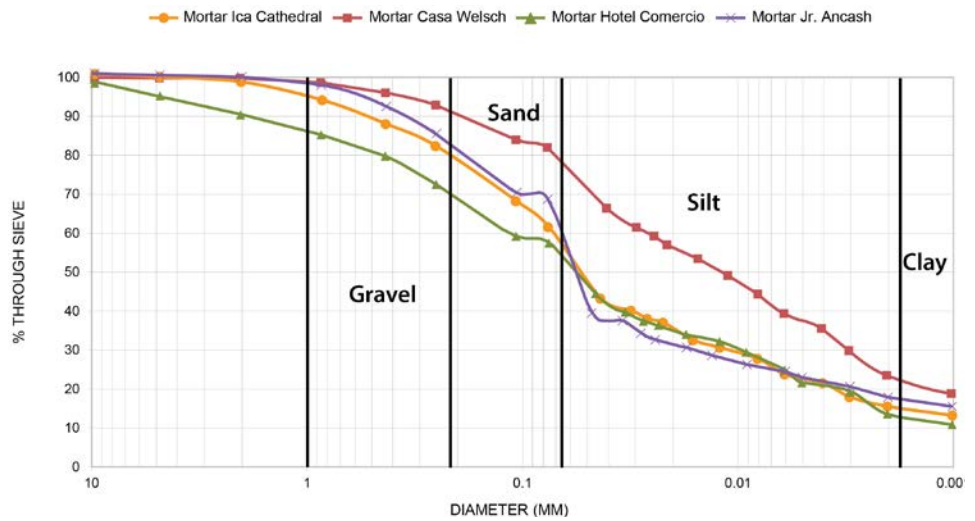


FIGURE 2.6.
Combined granulometric curves for
soil from the original mortar.



Atterberg Limits

TEST DESCRIPTION

Plastic, liquid, and shrinkage limits of a fine-grained soil, also known as Atterberg limits, were determined. Plastic limit (PL) is the water content, in percent, of a soil at the boundary between plastic and semi-solid states. Liquid limit (LL) is the water content, in percent, of a soil at the arbitrarily defined boundary between semi-liquid and plastic states. Shrinkage limit (SL) is the water content where further loss of moisture will not lead to further volume reduction. Additionally, initial moisture content of the samples and specific gravity of the soil are determined. Specific gravity is the ratio of the mass of a unit volume of soil solids to the mass of the same volume of gas-free distilled water at 20°C.

Tests were carried out following ASTM Standard Test Method for Liquid Limit, Plastic Limit, and Plasticity Index of Soils (ASTM D4318) and ASTM Standard Test Method for Shrinkage Factors of Soils by Mercury Method (ASTM D427) (withdrawn 2008).

RESULTS

Results related to Atterberg limits, moisture content, and specific gravity of fine-grained soil are shown in table 2.2.

TABLE 2.2.

Results related to Atterberg limits, moisture content, and specific gravity of fine-grained soil.

Origin	Building	Material source	UCSC	w % moisture content	LL (liquid limit)	PL (plastic limit)	PI (plasticity index)	SL (shrinkage limit)	SG (specific gravity)
Lima	Hotel el Comercio	Adobe	CL	0.06	0.32	0.2	0.12	0.15	2.65
	Casa Ancash			0.095	0.3	0.17	0.13	–	2.66
	Casa Welsh			0.041	0.27	0.16	0.11	0.13	2.64
Ica	Ica Cathedral		CL-ML	0.038	0.26	0.19	0.07	0.15	2.66
Cuzco	Kuñotambo		CL	0.039	0.3	0.19	0.11	0.14	2.58
Lima	Hotel El Comercio	Mortar	CL	0.059	0.3	0.19	0.11	0.14	2.66
	Casa Ancash			0.115	0.32	0.18	0.14	0.12	2.64
	Casa Welsh			0.05	0.3	0.18	0.12	0.15	2.65
Ica	Ica Cathedral			0.037	0.27	0.18	0.09	0.15	2.67

CONCLUSION

All soils were cataloged as inorganic clays with low to medium plasticity (see table 2.2), except for the soil from Ica Cathedral, which falls between the same group of inorganic clays and inorganic silts based on USCS soil classification (ASTM International 2006, 8).

Adobe Units

Test Description and Methodology

The uniaxial compression strength of the adobe units was tested on cubes approximately 10 × 10 × 10 cm (fig. 2.7). The cubes were tested using a displacement-controlled material testing system (MTS) machine. The tops and bottoms of the cubes were covered with a thin layer of gypsum to ensure a level testing surface. The units were collected inside the historic buildings, but their exact origin, age, and state of deterioration is unknown. Units from Ica Cathedral were obtained from a rubble pile within the cathedral; units from Hotel El Comercio were taken from the collapsed area at the rear of the building. One adobe unit

FIGURE 2.7.

Adobe test sample cubes (a) were tested for uniaxial compression strength on a displacement-controlled MTS machine (b).



was found in the sacristy of Kuñotambo. None of the historic adobe units contained straw. Table 2.3 provides the number of tests performed for each building. Furthermore, it should be noted that the adobes needed to be cut down in order to obtain relevant test samples, which could have affected the results. Deformation was not recorded.

TABLE 2.3.
Number of tests performed on the cubes and origin of the material.

Origin of Material	Number of Tests
Kuñotambo	4
Ica Cathedral	5
Hotel El Comercio	5
Other buildings in Lima	5

Results and Discussion

The compression strength of the adobe blocks differs based on geographic location. The adobes from Ica Cathedral present the lowest values, with an average compression strength of 0.59 MPa. This value is significantly lower than the average value obtained for the units from three buildings in the center of Lima, at about 1.51 MPa. It should be noted, however, that the samples from buildings other than Hotel El Comercio were only 7 cm high, which may have slightly increased their compression strength.

The average compression strength for the adobe units from Kuñotambo is 0.71 MPa. This value should be treated with great care, though, as it may not be representative. The reason for this is twofold: first, all the test samples were obtained from a single adobe unit, and second, the results within this one block vary greatly, from 0.48 to 0.87 MPa. This variation is probably caused by imperfections in the block or by damage from certain elements due to the cutting of the samples.

Overall, differences between values obtained from the different sites can be attributed to a variety of factors, such as soil composition, production process, deterioration over time, or sample size. For example, the city of Ica experienced several floods throughout history that affected large portions of the adobe walls. It is unknown, though, whether the samples were effectively subjected to this repeated flooding. Therefore, it is not possible to link with certainty the differences in strength to either soil composition or environmental conditions.

The Peruvian Adobe Code for new adobe buildings, Reglamento Nacional de Construcciones (E.080), sets the minimum adobe unit compression strength for new construction at 1.20 MPa (Ministerio de Transportes 2000). The adobe units tested from locations in Lima meet this minimum strength criterion, whereas the samples from Ica Cathedral and Kuñotambo average only about half this compression strength value. However, similar material tests on cut-down adobe units extracted from historic buildings in Ecuador showed compression stresses in the same low range, with strengths of 0.4–0.6 MPa (Haesebrouck and Michiels 2011). The strength of adobe units from both Ica Cathedral and Kuñotambo is on the lower side if compared to values found for new adobe in literature (Ottazzi et al. 1989).

Adobe Wallets

Adobe masonry is a composite of adobe blocks and mud mortar; therefore, the properties of the masonry as a whole are quantified as well. Axial compression tests on masonry piles

were performed in order to determine compression strength and Young's modulus (or elasticity modulus) of the masonry (tables 2.4, 2.5). Additionally, diagonal compression tests on adobe wallets were performed to analyze shear capacity and shear modulus of the masonry. Shear-compression tests on triplets were performed to determine friction angle and cohesion values within the adobe masonry, on the interface of the adobe and brick, and on the interface of adobe and stone shear.

TABLE 2.4.

Results of the axial compression test to determine average compression strength of the masonry.

N°	Origin	Dimensions					Area (cm ²)	Maximum Load (kN)	Compression Strength (MPa)	Average Compression Strength (MPa)
		a cm	x	b cm	x	h cm				
01	Ica Cathedral	9.5	x	10.0	x	9.0	95.0	6.20	0.65	0.59
02		9.8	x	9.9	x	9.0	97.0	5.70	0.59	
03		9.8	x	10.0	x	8.9	98.0	6.39	0.65	
04		9.9	x	9.9	x	8.9	98.0	6.06	0.62	
05		9.8	x	9.9	x	8.9	97.0	4.21	0.43	
01	Hotel El Comercio	9.9	x	10.0	x	8.7	99.0	16.34	1.65	1.67
02		9.9	x	9.9	x	8.8	98.0	14.97	1.53	
03		10.0	x	10.0	x	8.9	100.0	15.90	1.59	
04		9.8	x	9.9	x	8.8	97.0	17.81	1.84	
05		9.9	x	9.9	x	8.8	98.0	17.09	1.74	
01	Other buildings in Lima	10.1	x	10.0	x	7.1	101.0	14.65	1.45	1.35
02		10.0	x	9.9	x	7.1	99.0	12.57	1.27	
03		9.9	x	10.0	x	7.0	99.0	14.20	1.43	
04		10.0	x	9.9	x	7.1	99.0	12.70	1.28	
05		10.0	x	10.0	x	7.1	100.0	13.28	1.33	
01	Kuñotambo	13.3	x	13.0	x	14.3	172.9	14.61	0.84	0.71
02		13.6	x	13.8	x	14.7	187.7	12.23	0.65	
03		13.4	x	13.2	x	14.5	176.9	8.51	0.48	
04		13.5	x	13.5	x	14.6	182.3	15.90	0.87	

TABLE 2.5.

Results of the axial compression test to determine Young's modulus (E-modulus).

Specimen	Origin	Dimensions					Area mm ²	Compression Strength			E-Modulus	
		a mm	x	b mm	x	h mm		Load kN	Stress MPa	Stress MPa	MPa	MPa
01	Ica Cathedral	200	x	150	x	435	30000	14.0	0.47		57.1	64.0
02	Ica Cathedral	200	x	150	x	430	30000	14.4	0.48	0.46	65.1	
03	Ica Cathedral	200	x	150	x	435	30000	13.3	0.44		69.7	
04	Casa Welsch	200	x	180	x	500	36000	14.1	0.39	0.49	38.3	38.8
05	Casa Welsch	155	x	135	x	410	20925	12.2	0.58		39.4	
06	Hotel El Comercio	200	x	145	x	520	29000	12.2	0.42	0.39	57.5	50.2
07	Hotel El Comercio	200	x	145	x	20	29000	10.6	0.36		42.8	
08	Casa Ancash	205	x	150	x	515	30750	23.3	0.76	0.76	94.3	94.3

Axial Compression Testing of Adobe Wallets

TEST DESCRIPTION AND METHODOLOGY

Axial compression tests on adobe masonry piles were performed to determine compression strength and Young's modulus of the adobe wallets. A gypsum layer was placed on the surface of the piles to avoid stress concentrations due to unevenness of the masonry. The compression tests were executed on a force-controlled MTS machine at a loading rate of 1.5 kN/min. Vertical deformation was measured using a linear variable differential transformer (LVDT). The elasticity modulus, or E-modulus, of the masonry was calculated by dividing the stress level at one-third of the maximum stress by the corresponding strain.

RESULTS AND DISCUSSION

The failure mode for all specimens was a vertical crack pattern running through the units and the mortar, as can be observed in figure 2.8. The piles from Ica Cathedral provided consistent results (variation of less than 10%), with an average compression strength of 0.46 MPa. The average compression strength of the masonry from Hotel El Comercio was 0.39 MPa. The masonry of the other buildings in Lima had a compression strength ranging from 0.39 to 0.76 MPa. Overall, the obtained values for the masonry piles were in the same range. The admissible value of compression strength in Peruvian Adobe Code E-080 is 0.2 MPa, while values of experimental analysis for Peruvian new adobe masonry are between 0.77 and 3.72 MPa (Vargas and Ottazzi 1981; Vargas, Bariola, and Blondet 1983; Vargas et al. 1986).

The compression strength values of the masonry piles were significantly lower than the compression strength of the individual units. For Ica Cathedral, compression strength of the masonry piles was 22% lower than the average compression strength of the adobe units. The compression strength values for the masonry from Lima was about 75% lower than average values of the unit blocks. These large reductions in capacity could be attributed partly to the different heights of the samples, as the taller, more slender piles have less lateral confinement. These results imply that great care should be taken when extrapolating the values of unit compression tests to the properties of adobe masonry, as the unit compression tests may provide significant overestimations of the actual capacity in compression of the masonry.

Young's modulus, or E-modulus, shows dispersed values, with both lowest (38 MPa) and highest (94 MPa) values corresponding to buildings in Lima. The obtained values for E should be handled with great care because the historical material is extremely fragile and the elastic deformation of the adobe piles is very small, which severely complicates an accurate estimation of their value. However, for Ica Cathedral, quite consistent results were obtained with an average E of 64 MPa. For Hotel El Comercio, an average E value of 50 MPa was obtained. These values fall in the lower range of the values reported in literature, which vary greatly from 33 to 448 MPa.

Shear-compression Testing of Masonry Triplets

TEST DESCRIPTION AND METHODOLOGY

Cohesion and angle of friction of the masonry were tested through a combined compression-and-shear test. In this procedure, a vertical force was applied on the triplet first, followed by a horizontal force exerted on the central unit until failure occurred (fig. 2.9). Three types of triplets were considered, all using the same mud mortar made from soil obtained from Ica Cathedral, mixed with sand and straw (1 part sand, 3 parts soil, 1 part straw):

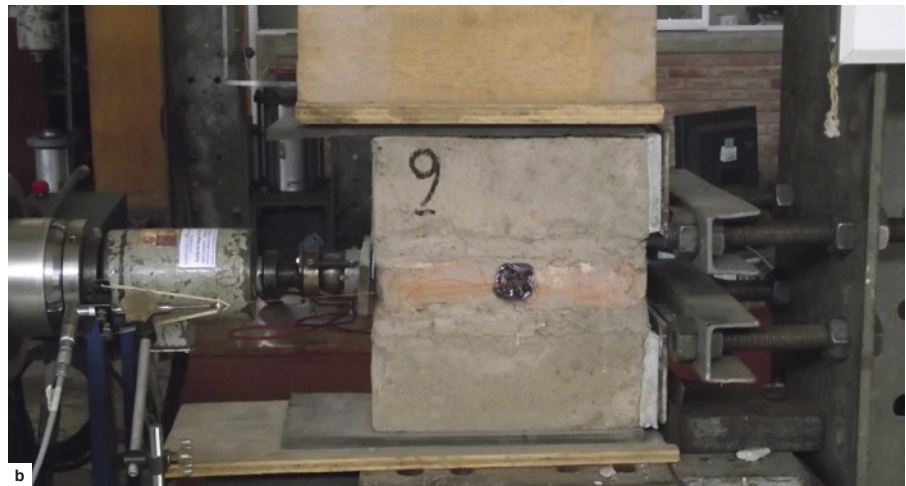


FIGURE 2.8. Compression test on adobe pile. Vertical cracks are visible in the units and the mortar.

- Adobe/adobe: three triplets were made of original adobe units from Ica; twelve triplets were made with new adobes.
- Adobe/brick: these triplets were made of original adobe units and bricks obtained from Hotel El Comercio.
- Adobe/stone: these triplets were made of original stones from Hotel El Comercio.

FIGURE 2.9.

Shear-compression tests performed on three types of triplets:
 (a) adobe/adobe;
 (b) adobe/brick;
 (c) stone/adobe.



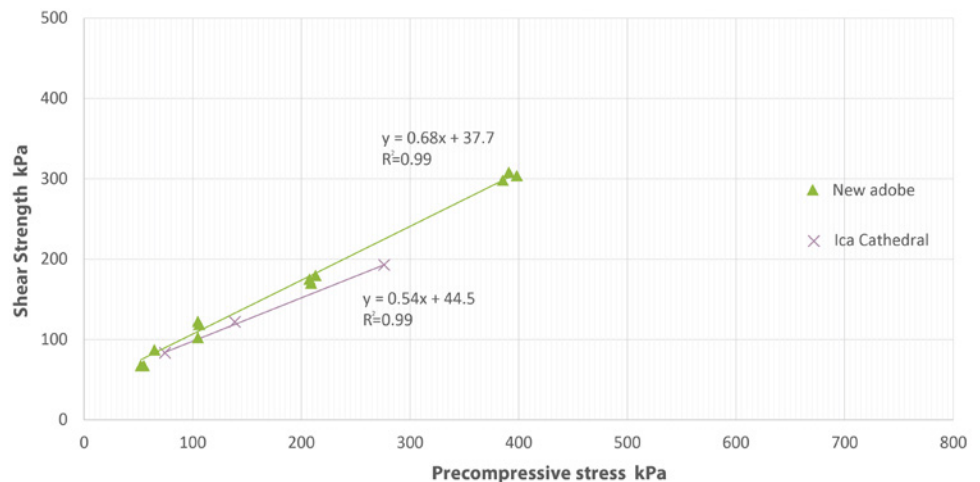
Dimensions of the adobe units were $13 \times 30 \times 10$ cm. Thickness of the mud mortar joints was 2 cm. Horizontal load rate was 150 N/s, following British Standard BS EN 1052-3 (British Standards Institution 2002).

Cohesion and friction angle values were obtained by measuring normal stress (σ) and shear stress (τ) at failure for several sets of triplets. Each tested triplet provided one data point, which was then plotted on a graph of normal stress versus shear stress. The slope of the regression line through these data points corresponds to the friction angle of the interface, while the intercept corresponds with the cohesion.

RESULTS AND DISCUSSION

The shear-compression tests on the triplets provided consistent results that allow clear estimations to be made of the cohesion and friction angle of the masonry. The adobe/adobe and adobe/brick exhibited a similar failure pattern: sliding between the interface of the mud mortar and the adobe. This is reflected in the values obtained for cohesion and friction angle, which are similar. Cohesion and friction angle values for the new adobe masonry are 38 kPa and 0.60 rad, respectively. Specimens with historical material from Ica Cathedral have a cohesion value of 45 kPa and a friction angle of 0.50 rad. The obtained cohesion and friction angle for the adobe/brick triplets were 38 kPa and 0.64 rad, respectively, almost identical to the values obtained for the new adobe/adobe masonry. It can furthermore be noted that the regression lines fit the samples extremely well, with R^2 values of 98% and higher (figs. 2.10, 2.11).

FIGURE 2.10.
Graph showing shear-compression curve for adobe/adobe triplets.



The adobe/stone triplets failed on the interface between adobe and stone, leading to cohesion and friction angle values equal to 65 kPa and 0.45 rad, respectively. This friction angle of the adobe/stone masonry is thus lower than that observed in the adobe/adobe and adobe/brick interfaces because the failure interface is no longer between the adobe and the mud mortar but along the mud mortar and stone. This lower adherence of the mud mortar to the stone, compared to the adobe or brick, can be explained by the lower porosity of the stone. It can also be observed in figure 2.12 that the regression curve does not match the data points for the mud mortar–adobe interface, mostly due to the values under higher pre-compression distorting the plot. Ignoring these data points would lead to a more realistic lower cohesion value like the one observed for the other triplets (fig. 2.13).

FIGURE 2.11.
Graph showing shear-compression curve for adobe/brick triplets.

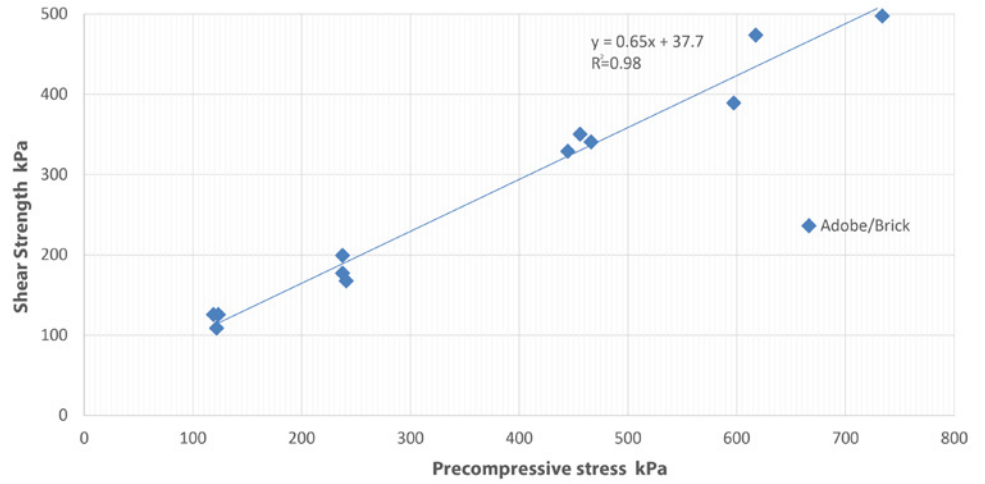


FIGURE 2.12.
Graph showing shear-compression curve for stone/adobe triplets.

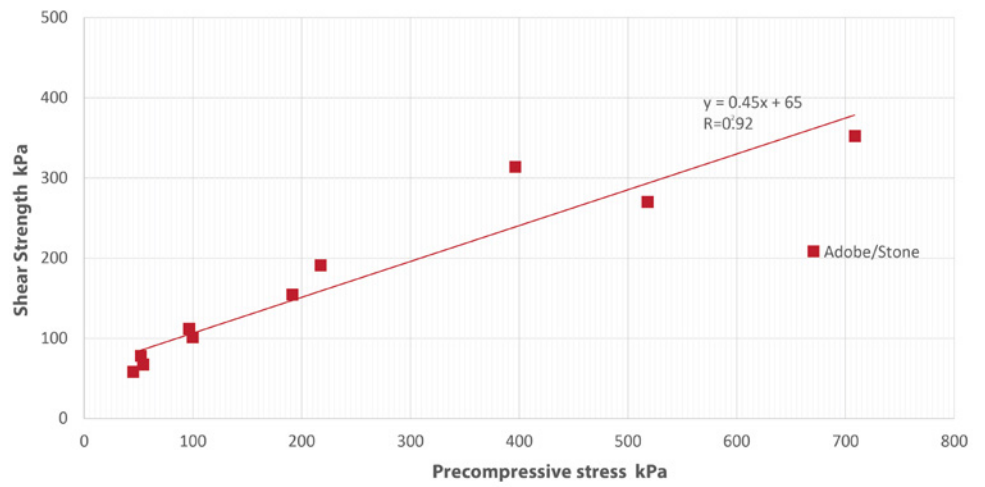
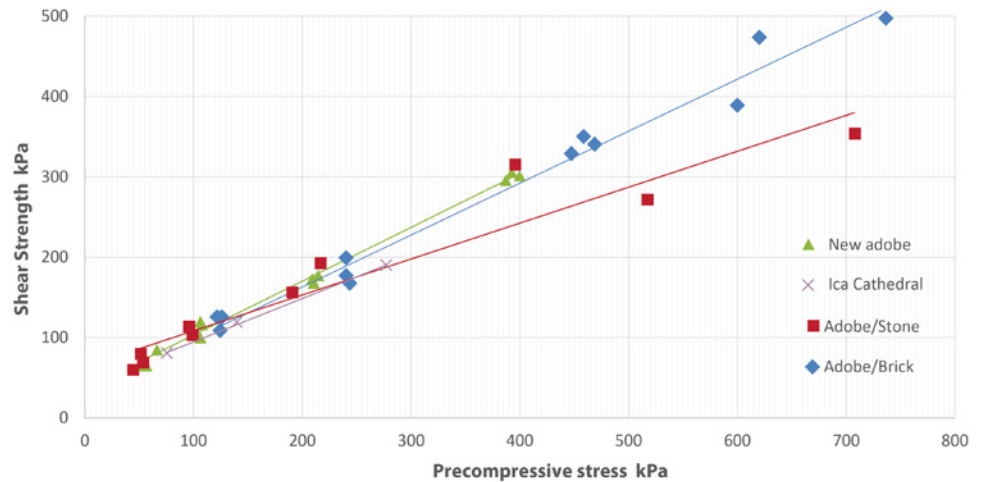


FIGURE 2.13.
Graph showing comparison of results for all triplets.



Diagonal Compression Testing of Adobe Wallets

Diagonal compression tests were executed on adobe wallets that had been rotated so that the mortar layers were inclined at 45 degrees with the horizontal axis; results are shown in table 2.6. These tests proved to be inconclusive due to the extreme fragility of the specimens, which caused several specimens to fail when placed into the testing position. Furthermore, there was no consistency in the failure mechanism, even though the test is designed to generate a crack pattern running vertical from the upper corner to the bottom corner. The results of these tests therefore varied excessively, with recorded values for shear compression strength ranging from 0.01 to 0.05 MPa (a variation of 500%). These values do fall within the wide range of shear strength for original adobe material ranging between 0.026 and 0.109 MPa (Vargas and Ottazzi 1981; Vargas et. al. 1986; Torres and Alva 1983; Varum et al. 2006; Yamin et al. 2004; Ottazzi et al. 1989; Vargas, Bariola, and Blondet 1983). The shear strength prescribed in the Peruvian Adobe Code for new buildings is 0.025 MPa.

TABLE 2.6.

Results of diagonal compression test on adobe wallets.

N°	Origin	Dimensions					Area mm ²	Shear Strength	
		a mm	x	b mm	x	e mm		Load kN	Stress MPa
01	Other buildings in Lima 1	425	x	415	x	190	112862.24	3.757	0.033
02	Other buildings in Lima 1	410	x	420	x	200	117388.24	5.868	0.050
03	Hotel El Comercio	425	x	400	x	155	90462.79	1.240	0.014
04	Ica Cathedral	415	x	375	x	150	83899.49	0.858	0.010
05	Ica Cathedral	416	x	375	x	145	81210.49	3.464	0.043
06	Ica Cathedral	410	x	430	x	150	89120.70	2.639	0.030

Brick Masonry

Brick Unit Testing

The compression strength of brick units obtained from Hotel El Comercio was determined based on Peruvian Standard E-070, Norma Técnica de edificación E.070 Albañilería de Peru (Ministerio de Transportes 2006a). Five tests were carried out on bricks approximately 25 × 13 × 5 cm (fig. 2.14). The average compression strength was 12.51 kN (table 2.7). This compression strength of the original brick units is similar to the values prescribed in the Peruvian code for the industrial bricks.

Axial Compression Testing of Brick Piles

Eight brick piles underwent axial compression testing as well. Five of these piles were directly extracted from an exposed plinth at Hotel El Comercio; the three remaining piles were constructed with bricks from Hotel El Comercio using new lime mortar. The mortar had a sand-to-lime ratio of 1:2 and an average compression strength of 3.66 MPa (measured on 9 samples).

The average compression stress for the historical brick piles was 1.7 MPa, which is very low compared to the average compression strength of the rebuild piles (6 MPa) (table 2.8). The original piles from Hotel El Comercio consisted of bricks in a good state of conservation, but the sand-lime mortar was heterogeneous and fragile and had little adherence

FIGURE 2.14.

Brick units from Hotel El Comercio used in compression strength testing.



TABLE 2.7.

Results of axial compressive test on brick units from Hotel El Comercio.

N°	Origin	Dimensions				Load kN	Compression Strength		
		a cm	x	b cm	x		h cm	MPa	Average MPa
01	Hotel El Comercio	26.6	x	13.4	x	5.3	403.8	11.3	12.5
02		26.9	x	13.4	x	5.2	409.3	11.4	
03		26.3	x	13.5	x	5.4	490.6	13.9	
04		25.9	x	13.2	x	4.8	434.1	12.7	
05		26.4	x	13.5	x	5.5	471.4	13.8	

TABLE 2.8.

Results of the axial compressive test on eight additional brick piles, comparing the historical brick with the new mortar piles.

N°	Origin	Dimensions				Area mm ²	Compression Strength			Young's Modulus (MPa)	
		a mm	x	b mm	x		h mm	Load kN	Stress (MPa)		Average Stress (MPa)
01	Hotel El Comercio	130	x	300	x	378	39000	47.1	1.21	1.70	99
02		150	x	300	x	370	45000	65.4	1.45		38
03		140	x	300	x	385	42000	63.6	1.52		199
03		160	x	300	x	265	48000	87.8	1.83		199
05		140	x	300	x	254	42000	103.7	2.47		99
07	New mortar	255	x	128	x	420	32640	211.1	6.47	6.04	579
07		260	x	130	x	420	33800	166.2	4.92		455
08		260	x	130	x	420	33800	227.5	6.73		642



FIGURE 2.15.

Brick pile (a) cut from a portion of masonry wall; brick pile (b) extracted from Hotel El Comercio for axial compression testing.

to the brick, resulting in low strength (fig. 2.15). Peruvian code E-070 for masonry states that the compression strength of piles made of cement mortar varies between 3.5 and 11.0 MPa depending on the type of brick, which is consistent with the obtained results. The E-modulus of the historical masonry piles could not be accurately measured, as measurements varied from 38 to 199 MPa (more than 500%). The average E-modulus of the newly constructed brick piles was 558 MPa.

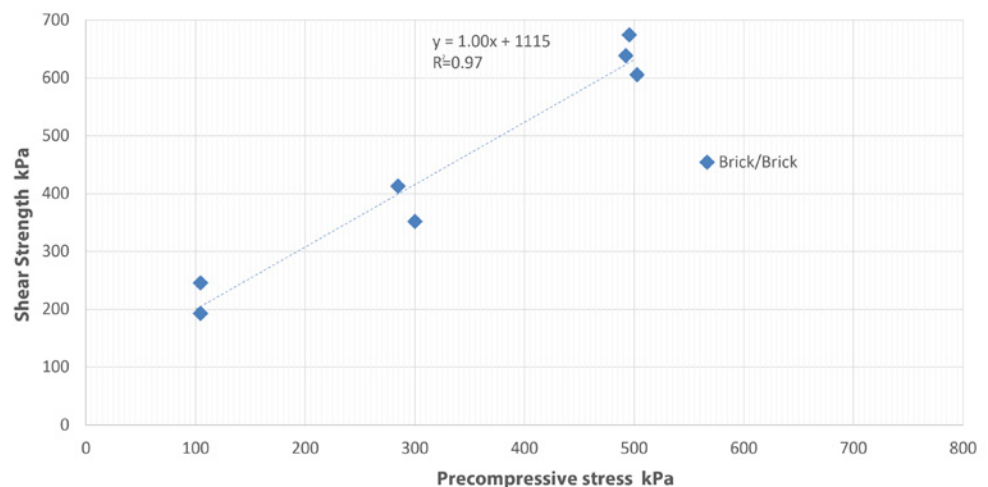
Compression strength values of the original masonry were low compared to the values stated in the Peruvian code for new masonry. The reconstructed specimens with original and new bricks do meet the minimum criteria specified by the Peruvian code. It can be concluded that the quality of the masonry is governed by the quality of the mortar. As the mortar of the original masonry was severely deteriorated, it affected the results greatly.

Shear-compression Testing of Brick Masonry

Shear-compression tests were performed to obtain cohesion and friction angle values, as the diagonal compression tests were inconclusive for the adobe masonry. Nine specimens were constructed, each consisting of three bricks from Hotel El Comercio and the same lime mortar used for the axial compression test. Specimens were tested sixty-five days after

FIGURE 2.16.

Graph showing shear-compression curve for brick triplets.



construction. The obtained cohesion value was 111 kPa and the friction angle was 1 rad, as seen figure 2.16.

Conclusions

A variety of tests were performed to characterize the adobe masonry and its components for historic sites in Peru. Data on the capacity of the masonry in compression and on cohesion and friction angle were successfully obtained. Accurate measurement of the E-modulus of adobe masonry proved to be difficult, and several attempts were unsuccessful due to the inherently brittle behavior of the adobe. Nonetheless, the testing program provided a range of estimates for the E-modulus.

Because adobe piles as well as individual adobe units were tested in uniaxial compression, it was possible to compare the results of both sets of tests. While the strength of the adobe units corresponded to the expected values reported in literature, the much lower compression strength values of the adobe masonry piles indicates that adobe unit testing can lead to an underestimation of the effective compression strength of the masonry. It should be noted, however, that the masonry piles were very slender and unconfined, which could have significantly impacted the results.

Shear-compression tests on adobe and brick triplets were successfully conducted for the first time in Peru. The tests provided consistent data that allowed the extraction of cohesion and friction angle values of the masonry. The tests also indicated that the weakest link in the adobe triplets was the interface between the adobe blocks and the mud mortar. The consistency of these results stands in stark contrast to the data obtained from the diagonal compression test for both the adobe and the brick masonry. In the diagonal compression test, the measured values as well as the observed failure mechanisms varied excessively, making it impossible to extract reliable data. It is therefore suggested that researchers consider using the shear-compression test instead of the diagonal compression test in further research.

Historical brick masonry obtained from Hotel El Comercio was also tested for compression strength. The results indicated that the strength of the masonry is determined by the quality of the mortar, which was badly deteriorated for the test samples obtained from Hotel El Comercio.

Finally, it should be noted that the variation in the results for the adobe masonry was relatively large over several tests. This was due to the inherent heterogeneity of the material and soil, as well as to the brittle nature of adobe. This particularly affected the values obtained for the E-modulus. As this value tends to be an important parameter in numerical modeling, researchers are advised *not* to rely solely on the data obtained in this report but to instead perform a parametric analysis to assess the effect of the variation of this parameter. The reported values, from testing and from literature, can be used as starting points.

References

- ASTM International. 2006. *Standard Practice for Classification of Soils for Engineering Purposes (Unified Soil Classification System)*. ASTM D2487. West Conshohocken, PA: ASTM International.
- ASTM International. 2007. *Standard Test Method for Particle-Size Analysis of Soils (Withdrawn 2016)*, ASTM D422-63(2007)e2. West Conshohocken, PA: ASTM International.

- ASTM International. 2017. *Standard Test Methods for Liquid Limit, Plastic Limit, and Plasticity Index of Soils*, ASTM D4318-17e1. West Conshohocken, PA: ASTM International.
- ASTM International. 2018. *Standard Classification of Peat Samples by Laboratory Testing*, ASTM D4427-18. West Conshohocken, PA: ASTM International.
- British Standards Institution. 2002. *Methods of Test for Masonry, Part 3: Determination of Initial Shear Strength*. BS EN 1052-3. London: BSI Group.
- Haesebrouck, L., and T. Michiels. 2011. "Improving Durability of Adobe: A Case Study for Cuenca, Ecuador." Master's thesis, University of Leuven, Belgium.
- Ministerio de Transportes, Comunicaciones, Vivienda y Construcción. 2000. *ININVI: Adobe Construction. Technical Standard for Adobe Building. Special Disposition for Seismic-resistant Adobe Building*. NTE E-080. Lima: Ministerio de Transportes, Comunicaciones, Vivienda y Construcción.
- _____. 2006a. *Albañilería*. NTE E-070. Lima: Ministerio de Transportes, Comunicaciones, Vivienda y Construcción.
- Ottazzi, G. P., J. F. L. Yep, M. S. Blondet, M. G. Villa-García, and J. F. Ginocchio. 1989. *Ensayos de simulacion sismica de viviendas de adobe*. Lima: Pontificia Universidad Católica del Perú, Departamento de Ingeniería.
- Torres, R., and J. Alva. 1983. *Propiedades físico-mecánicas de adobes no estabilizados utilizados en el Perú*. Lima: Universidad Nacional de Ingeniería, Departamento de Estructuras y Construcción.
- Vargas, J., and G. Ottazzi. 1981. *Investigaciones en adobe*. Lima: Pontificia Universidad Católica del Perú, Departamento de Ingeniería, Sección Ingeniería Civil.
- Vargas, J., J. Bariola, and M. Blondet. 1983. *Informe final del proyecto resistencia sísmica de la mampostería de adobe*. Convenio AID-PUCP. Lima: Pontificia Universidad Católica del Perú, Departamento de Ingeniería, Sección Ingeniería Civil.
- Vargas, J., J. Bariola, M. Blondet, and P. K. Mehta. 1986. "Seismic Strength of Adobe Masonry." *Materials and Structures* 19 (4): 253–58. <https://doi.org/10.1007/BF02472107>
- Varum, H., A. Costa, H. Pereira, and J. Almeida. 2006. "Comportamento estrutural de elementos resistentes em alvenaria de adobe." Paper presented at TerraBrasil 2006: I Seminário Arquitetura e Construção com Terra no Brasil / IV Seminário Arquitetura de Terra em Portugal, Ouro Preto, Minas Gerais, Brazil, November 2006.
- Yamin, L., C. Phillips, D. Reyes, and D. Ruiz. 2004. "Seismic Behavior and Rehabilitation Alternatives for Adobe and Rammed Earth Buildings." In *Proceedings of the 13th World Conference on Earthquake Engineering, Vancouver, BC*. Bogotá: CITEC, Universidad de Los Andes.

Wood Characterization of Timber Elements

Introduction and Methodology

The main structural components of Hotel El Comercio and Ica Cathedral are masonry and timber. In Hotel El Comercio, the second and third floors are made of quincha, which is a timber, cane, and mud paneling system. In Ica Cathedral, the entire roof structure is made from timber with an earthen covering and an adobe and fired-brick masonry envelope. Timber is a vital part of these structures; therefore, it is important to identify the species used and to quantify their mechanical properties. The tests described in this chapter were conducted by a team of wood experts at the Laboratorio de Anatomía e Identificación de la Madera (Wood Anatomy and Identification Laboratory) and the Laboratorio de Tecnología de la Madera (Timber Technology Laboratory) at the Universidad Nacional Agraria la Molina (UNALM, National Agrarian University of La Molina), with the participation of Pontificia Universidad Católica del Perú (PUCP).

Test samples were collected inside Hotel El Comercio and Ica Cathedral. Only samples without visible deterioration or damage were selected. Anatomic identification of the wood was performed according to the following standards: Normas de Procedimientos em Estudos de Anatomia de Madeira—Angiospermae (Coradin and Bolzon de Muniz 1991), Lista de las Características Microscópicas para la Identificación de Madera Duras (Bass, Gasson, and Wheeler 1989), and Norma de la Comisión Panamericana de Normas Técnicas (COPANT 1974): “Método para la Descripción de las Características Generales, Macroscópicas y Microscópicas de la Madera Angiospermas Dicotiledóneas.” Additionally, laboratory tests were executed to identify the mechanical properties following ASTM D143-09, Standard Test Methods for Small Clear Specimens of Timber (ASTM 2009).

Timber Distribution

Ica Cathedral

As mentioned above, Ica Cathedral has a masonry perimeter, but its entire roof structure of pillars, vaults, and domes supported by beams is built entirely with timber elements. A layer of cane covered with mud and lime plaster is nailed to these timber elements. The two towers of the church are also made of timber supported by a brick base. Figure 3.1 shows the overall structural scheme of Ica Cathedral, including the timber elements. Research showed that three wood species were employed predominantly in the cathedral: huarango (*Prosopis* sp.), sapele (*Entandrophragma* sp.), and cedar (*Cedrela odorata* L.). Distribution is determined by the structural element each species is used for:

- The beams and columns of the **towers** are made of huarango.
- The central posts and the diagonal and transversal connectors of the **pillars** are made of huarango. The posts around the center are made of sapele.

FIGURE 3.1.
Overall structural scheme of Ica Cathedral, with timber elements highlighted.

- The longitudinal **beams** of the **central nave** and **lateral nave** are made of sapele. The arches of both naves are made of cedar.
- The **main cupola**, as well as the **cupolas of the lateral nave**, are made of cedar.

A typical bay in the cathedral is shown in figure 3.2 as an example.

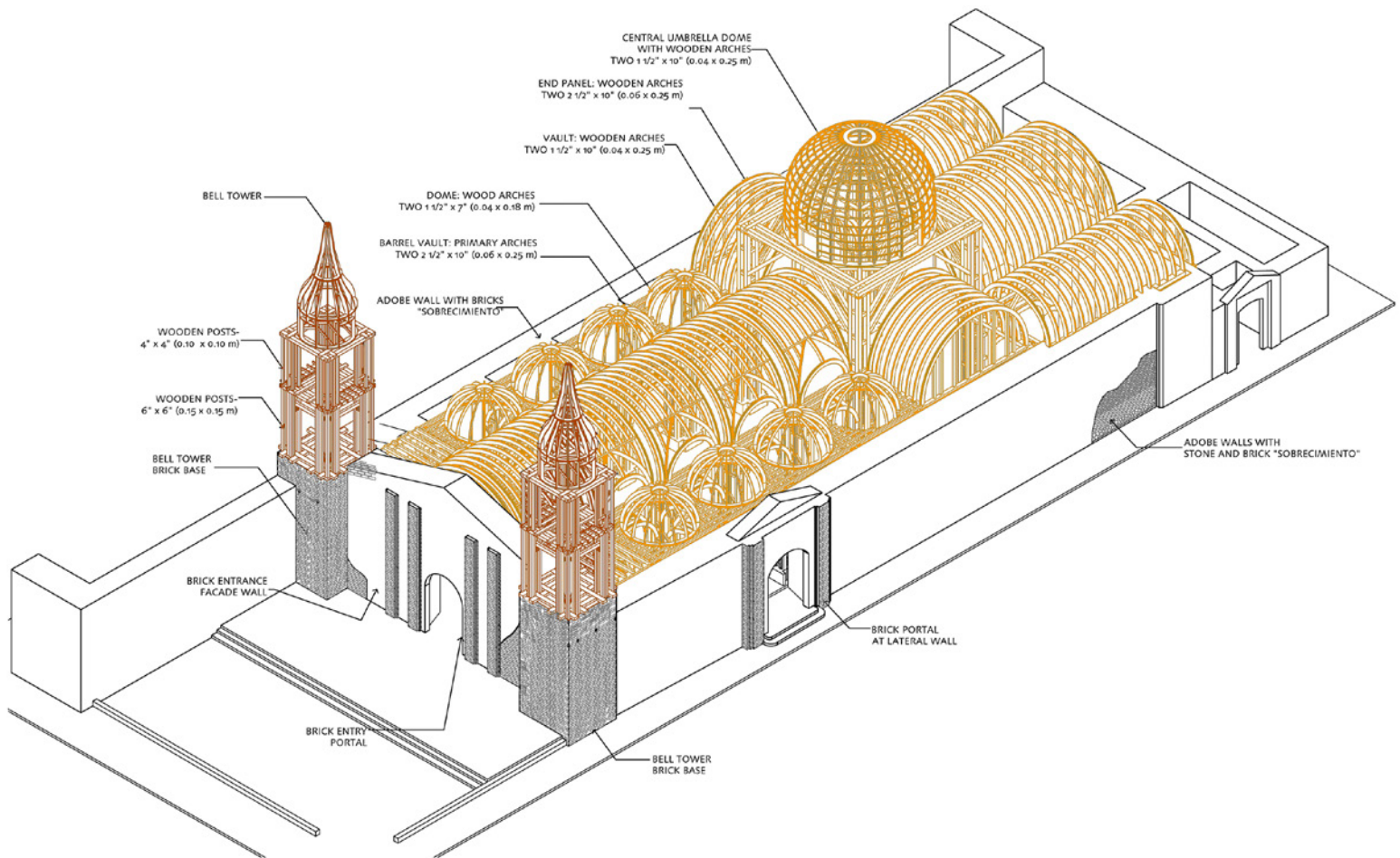
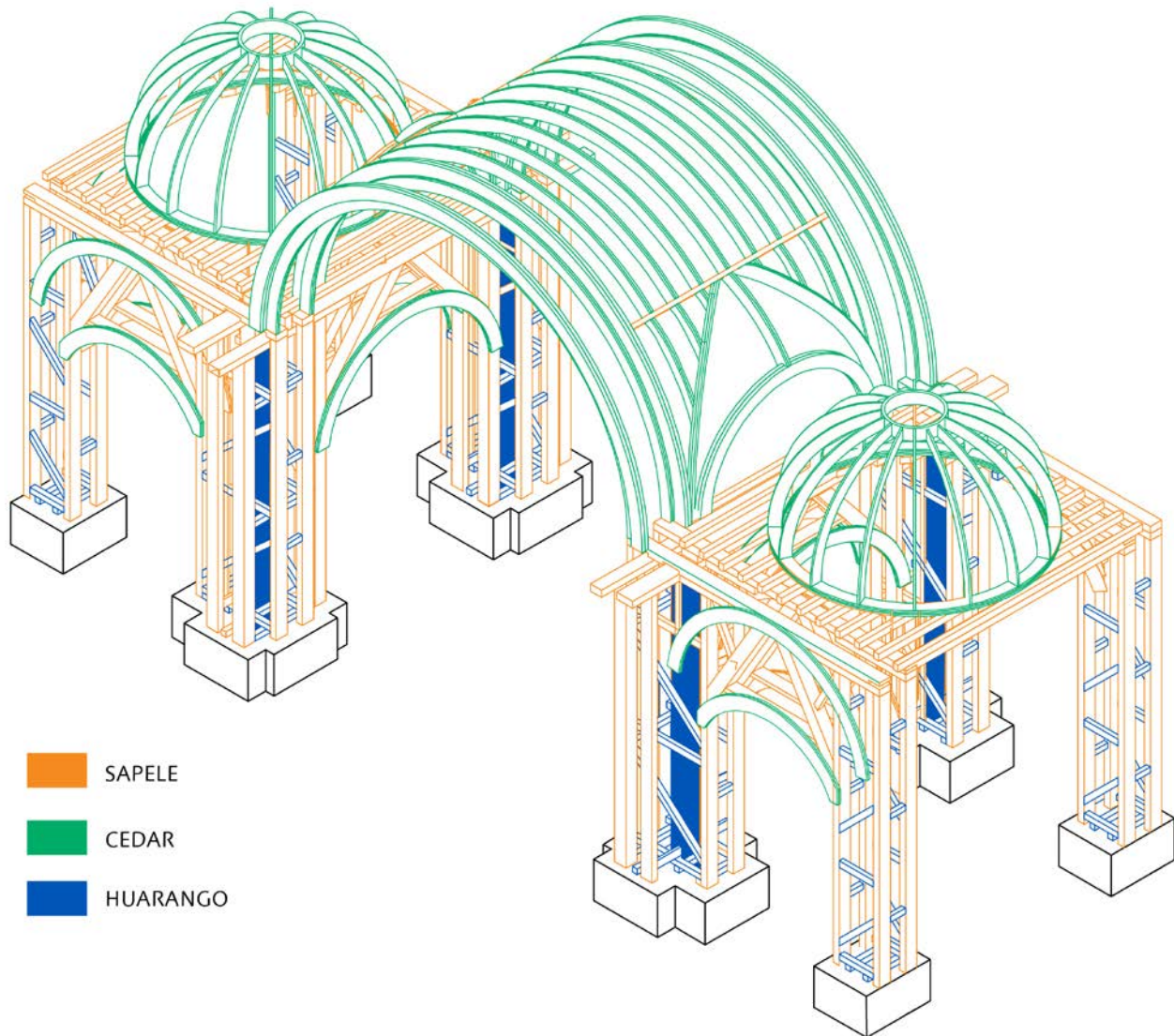


FIGURE 3.2.
Distribution of timber species in a
typical bay of Ica Cathedral.

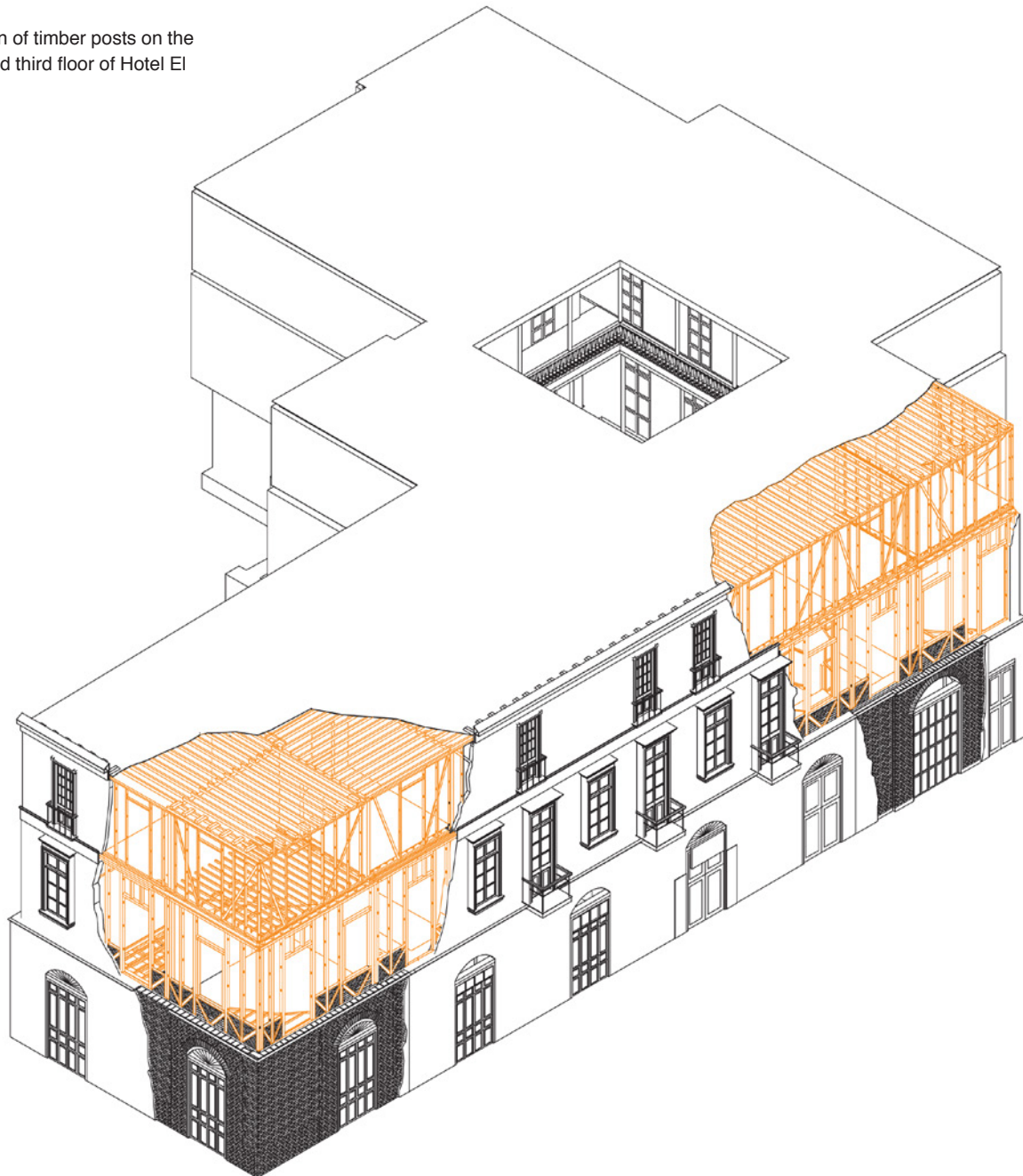


Hotel El Comercio

A major portion of the structural elements in Hotel El Comercio is made of timber. The quincha panels have timber frames, and the floors and roofs have timber beams, purlins, and joists (fig. 3.3). As in Ica Cathedral, sapele is a recurring wood species. The other two most prominent species are cypress (*Cupresses* sp.) and Oregon pine (*Pseudotsuga menziesii*). The timber is distributed as follows:

- The columns of the interior patio in the first floor are made of sapele.
- The beams and purlins of the first and second floors are made of sapele; the planking is made of cypress; the sleepers (timber used for support) and floor are made of Oregon pine.

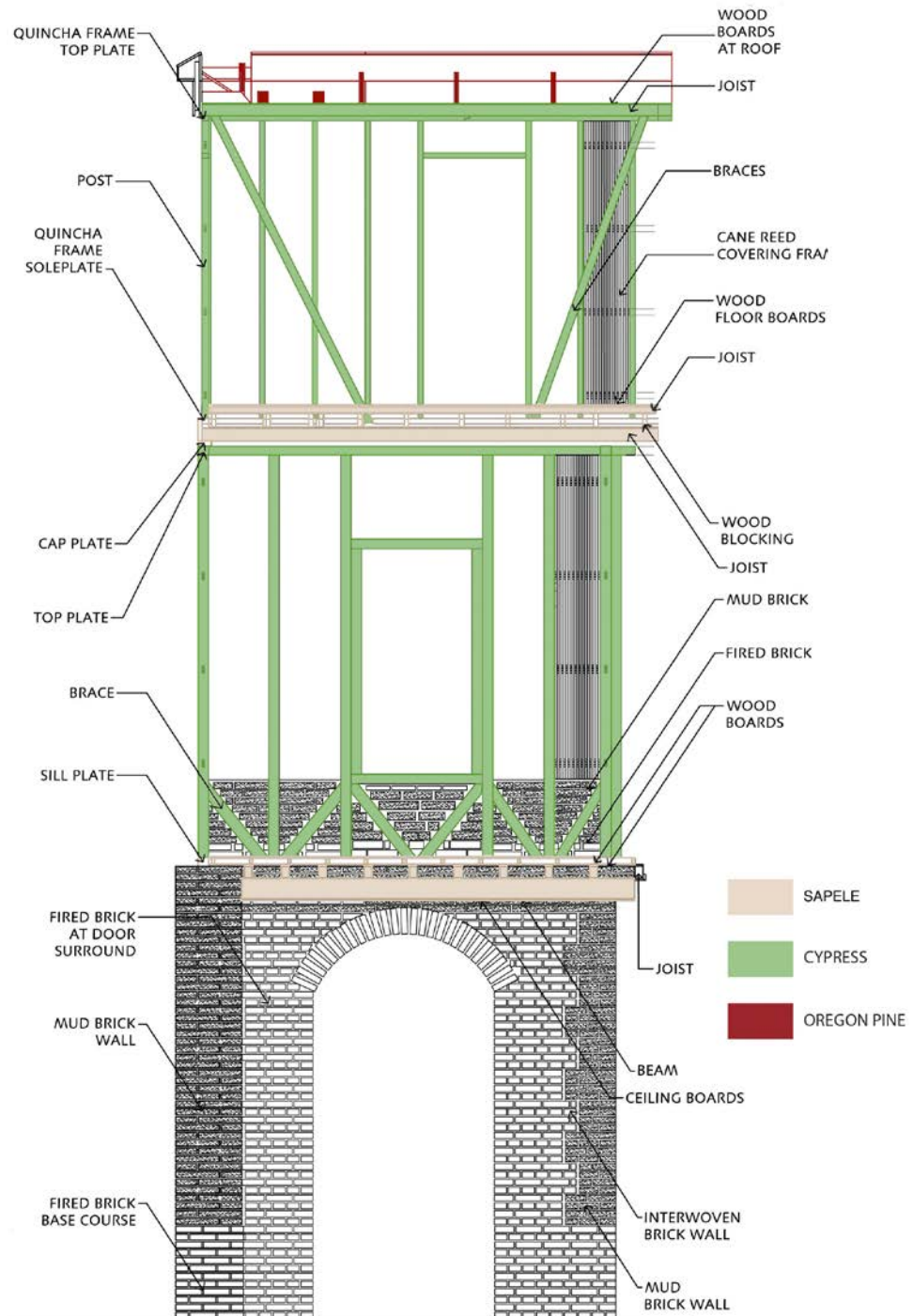
FIGURE 3.3.
Distribution of timber posts on the second and third floor of Hotel El Comercio.



- The lower and upper beams of the quincha panels on the second floor are made of sapele; the posts and diagonals are made of cypress.
- The lower beams of the quincha panels on the third floor are made of sapele; the upper beams, posts, and diagonals are made of cypress.
- The beams and planks of the roof are made of Oregon pine.

As seen in figure 3.4, sapele is found mostly on the first and second floor patios, which are the oldest parts of Hotel El Comercio. Cypress and Oregon pine are found on the third

FIGURE 3.4.
Distribution of timber species
in quincha panels on the sec-
ond and third stories of Hotel
El Comercio.



floor and roof, which were most likely added later. The presence of Oregon pine in some of the sleepers and planks of the first floor can probably be attributed to repair and replacement of these parts at some point during the building's lifetime.

Mechanical Characteristics

An overview of the mechanical characteristics of the wood species is presented in table 3.1. All mechanical properties were determined at the moisture content of the air dry density.

TABLE 3.1.

Overview of the mechanical characteristics of the wood species cedar, huarango, sapele, Oregon pine, and cypress.

Cedar						
PROPERTIES	CEDAR (<i>Cedrela odorata</i>)		SIMILAR SPECIES JUNAC*		VALUES OF "B" GROUP IN THE PERUVIAN TIMBER CODE E.010	GROUP OF CEDAR ACCORDING TO E.010
	FROM ICA CATHEDRAL (SRP)	FROM REFERENCES AITIM**	MANCHINGA (<i>Brosimum uleanum</i>)	HUAYRURO (<i>Ormosia coccinea</i>)		
Basic Density (g/cm ³)	0.33	0.45–0.60	0.68	0.6	0.56–0.70	B
M.O.R. (MPa)	75.77	69.0–72.0	78.2–104.4	84.3–109.5	150	
M.O.E. (MPa)	9380	7420–7930	11700–14000	13400–14800	7500–10000	
Parallel Compression (MPa)	27.26					
Perpendicular Compression (MPa)	4.1					
Parallel Shear (Mpa)	8.67					
Parallel Tension (Mpa)	21.19					
Perpendicular Tension (Mpa)	0.88					
Green Density (g/cm ³)	0,66	at 100.7%	moisture content			
Air Dry Density (g/cm ³)	0,38	at 11.7%	moisture content			
Huarango						
PROPERTIES	HUARANGO (<i>Prosopis</i> sp.)		SIMILAR SPECIES JUNAC*		VALUES OF "A" GROUP IN THE PERUVIAN TIMBER CODE E.010	GROUP OF HUARANGO ACCORDING TO E.010
	FROM ICA CATHEDRAL (SRP)	FROM REFERENCES UNALM***	ESTORAQUE (<i>Myroxylon peruiferum</i>)	PUMAQUIRO (<i>Aspidosperma macrocarpon</i>)		
BASIC DENSITY (g/cm ³)	0.91	1.07	0.78	0.67	0.71–0.90	A
M.O.R (MPa)	152.96	105.8	164.8–129.9	95.5–114.0	21	
M.O.E. (MPa)	16880	13200	16700–18600	14800–14500	9500–13000	
Parallel Compression (MPa)	92,18					
Perpendicular Compression (MPa)	22,55					
Parallel Shear (Mpa)	20,79					
Parallel Tension (Mpa)	61,86					
Perpendicular Tension (Mpa)	1,91					
Green Density (g/cm ³)	1,15	at 25.6%	moisture content			
Air Dry Density (g/cm ³)	1,04	at 10.9%	moisture content			

TABLE 3.1. (CONTINUED)

Overview of the mechanical characteristics of the wood species cedar, huarango, sapele, Oregon pine, and cypress.

Sapele						
PROPERTIES	SAPELE (<i>Entandrophagma</i> sp.)		SIMILAR SPECIES JUNAC*		VALUES OF "C" GROUP IN THE PERUVIAN TIMBER CODE E.010	GROUP OF SAPELE ACCORDING TO E.010
	FROM HOTEL EL COMERCIO (SRP)	FROM REFERENCES AITIM**	TORNILLO (<i>Cedrelinga catanaeformis</i>)	DIABLO FUERTE (<i>Podocarpus sp.</i>)		
BASIC DENSITY (g/cm ³)	0.4	0.64–0.70	0.44	0.53	0.40–0.55	C
M.O.R (MPa)	61.47	85.0–142.0	57.9–69.3	60.8–90.4	10	
M.O.E. (MPa)	7830	10300–13800	9900–10900	9900–11500	5500–9000	
Parallel Compression (MPa)	33.39					
Perpendicular Compression (MPa)	4.71					
Parallel Shear (MPa)	6.29					
Parallel Tension (MPa)	47.87					
Perpendicular Tension (MPa)	1.64					
Green Density (g/cm ³)	1.13	at 183.5%	moisture content			
Air Dry Density (g/cm ³)	0.49	at 17.3%	moisture content			
Oregon Pine						
PROPERTIES	OREGON PINE (<i>Pseudotsuga menziesii</i>)		SIMILAR SPECIES JUNAC*		VALUES OF "C" GROUP IN THE PERUVIAN TIMBER CODE E.010	GROUP OF PINE ACCORDING TO E.010
	FROM HOTEL EL COMERCIO (SRP)	FROM REFERENCES AITIM**	TORNILLO (<i>Cedrelinga catanaeformis</i>)	DIABLO FUERTE (<i>Podocarpus sp.</i>)		
BASIC DENSITY (g/cm ³)	0.49	0.47–0.52	0.44	0.53	0.40–0.55	C
M.O.R (MPa)	75.85	70–100	57.9–69.3	60.8–90.4	10	
M.O.E. (MPa)	10680	11000–13200	9900–10900	9900–11500	5500–9000	
Parallel Compression (MPa)	38.12					
Perpendicular Compression (MPa)	6.31					
Parallel Shear (MPa)	10.07					
Parallel Tension (Mpa)	64.12					
Perpendicular Tension (Mpa)	1.83					
Green Density (g/cm ³)	1.13	at 130%	moisture content			
Air Dry Density (g/cm ³)	0.6	at 16%	moisture content			

TABLE 3.1. (CONTINUED)

Overview of the mechanical characteristics of the wood species cedar, huarango, sapele, Oregon pine, and cypress.

Cypress						
PROPERTIES	CYPRESS (<i>Cupressus</i> sp.)		SIMILAR SPECIES JUNAC*		VALUES OF "C" GROUP IN THE PERUVIAN TIMBER CODE E.010	GROUP OF CYPRESS ACCORDING TO E.010
	FROM HOTEL EL COMERCIO (SRP)	FROM REFERENCES AITIM**	TORNILLO (<i>Cedrelinga catanaeformis</i>)	DIABLO FUERTE (<i>Podocarpus</i> sp.)		
BASIC DENSITY (g/cm ³)	0.39	0.40–0.60	0.44	0.53	0.40–0.55	C
M.O.R (MPa)	48.82	103	57.9–69.3	60.8–90.4	10	
M.O.E. (MPa)	5470	7500	9900–10900	9900–11500	5500–9000	
Parallel Compression (MPa)	31.69					
Perpendicular Compression (MPa)	4.83					
Parallel Shear (MPa)	7.79					
Parallel Tension (MPa)	60.96					
Perpendicular Tension (MPa)	2.96					
Green Density (g/cm ³)	0.86	at 120.8%	moisture content			
Air Dry Density (g/cm ³)	0.47	at 15%	moisture content			

*JUNAC: JUNTA DE ACUERDO DE CARTAGENA PADT REFORO

** AITIM: ASOCIACIÓN DE INVESTIGACIÓN TÉCNICA DE LAS INDUSTRIAS DE LA MADERA, MADRID

*** UNALM: UNIVERSIDAD NACIONAL AGRARIA LA MOLINA

Discussion and Conclusion

Timber identification and investigation of its properties provided the first set of data available on timber species in historic buildings in Peru. The identification process revealed that sapele, a native species from Africa, was present in both Ica Cathedral and Hotel El Comercio. This remarkable finding—that an African timber species is prevalent in historic buildings on the Peruvian coast—could not be readily explained. Historians specializing in the colonial era were consulted regarding this matter, but as trade with Africa was almost non-existent during this period, it remains an open question on how sapele arrived on the Peruvian coast. The samples of sapele found in Ica Cathedral were in an advanced state of deterioration, but undamaged samples suitable for testing were obtained from Hotel El Comercio.

Comparing the mechanical characteristics of the timber found in situ to the values reported in literature showed that the obtained cedar had a much greater elasticity modulus (E-modulus) than expected. However, the value retrieved from literature was obtained at a very high moisture content, which can explain this difference. In all other cases the values of the mechanical properties of the wood from the historic sites were lower than the values obtained from literature. Huarango had by far the best mechanical properties and was thus unsurprisingly used in the more critical structural elements in Ica Cathedral. All other historical wood specimens had mechanical properties of which the values were about 40% lower than those reported in literature. The strength values of sapele, particularly shear strength, were lower than expected. In contrast, the values obtained for cypress and Oregon pine corresponded to the values for new wood.

Three non-native wood species were identified in main structural elements in Hotel El Comercio: cypress and Oregon pine from central America and, as mentioned above, sapele from Africa. The African wood was found in the first floor of the building and is assumed to be the oldest one. Cypress and sapele were found in the quincha walls on the second and third floors. Oregon pine was introduced in Lima around the end of the nineteenth century to the beginning of the twentieth century, and would have been used for repair and replacement of older wood.

Peruvian Design Code E-010 classifies the wood species in three categories based on its mechanical properties, where category A is of higher quality than categories B and C (Ministerio de Transportes 2006b). Based on the tests performed on original timber samples, the following classification can be made: huarango pertains to group A; cedar to group B; and sapele, cypress, and Oregon pine to group C.

References

- ASTM International. 2007. *Standard Test Methods for Density and Specific Gravity (Relative Density) of Wood and Wood-based Materials*. ASTM 2395-07a. West Conshohocken, PA: ASTM International.
- _____. 2009. *Standard Test Methods for Small Clear Specimens of Timber*. ASTM D143-09. West Conshohocken, PA: ASTM International.
- Baas, Pieter, Peter E. Gasson, Elisabeth A. Wheeler, and International Association of Wood Anatomists. 1989. "IAWA List of Microscopic Features for Hardwood Identification: With an Appendix on Non-anatomical Information." *IAWA Journal* 10(3): 219–332.
- Cancino, C., S. Lardinois, D. D'Ayala, C. Fonseca, D. Torrealva, E. Vicente, and L. Villacorta. 2012. *Seismic Retrofitting Project: Assessment of Prototype Buildings*. 2 vols. Los Angeles: Getty Conservation Institute.
- COPANT (Comisión Panamericana de Normas Técnicas). 1974. *Maderas: Método para la descripción de las características generales, macroscópicas y microscópicas de las maderas angiospermas y dicotiledóneas: anteproyecto de Norma*. COPANT 30:1-019. Caracas, Venezuela, 25pp.
- Coradin, V. T. R., and G. I. Bolzon de Muniz. 1991. *Normas de procedimentos em estudos de anatomia de madeira I. Angiospermae. II. Gimnospermae*. Serie Técnica 15. Brasília: IBAMA, DIRPED, Laboratório de Produtos Florestais.
- Hidayat, S., and W. T. Simpson. 1994. *Use of Green Moisture Content and Basic Specific Gravity to Group Tropical Woods for Kiln Drying*. Research note FPL-RN-0263. Madison, WI: US Department of Agriculture, Forest Service, Forest Products Laboratory.

Quincha Testing

Introduction to Quincha Systems

Quincha, a lightweight construction system that is composed of a timber frame filled with cane and mud, is a primary building component of many buildings in the historic center of Lima, including Hotel El Comercio. The typical historical house in Lima has a ground floor of thick adobe masonry wall, and the walls of the upper floors are made of quincha.

In Hotel El Comercio, two types of quincha paneling can be found. The second-floor walls are made of quincha with an adobe brick base called the citara (fig. 4.1). These walls have a height of 4.80 m, and the elements are constructed from timber posts and upper and bottom timber beams. A citara of 90 cm high is situated at the lower part of the second-floor wall and is characterized by a set of diagonal timber struts (cross section of 10 × 10 cm) that are infilled with adobe masonry, thus providing cross bracing for the wall base. Beams and posts have similar dimensions, with cross sections of 10 × 10 cm. The horizontal distance between posts varies between 50 and 80 cm but is typically 60 cm. The posts are connected to the upper and lower beams by mortise-and-tenon joints (fig. 4.2). Whereas the citara is infilled with adobe masonry, the rest of the wall is infilled with woven

FIGURE 4.1. Diagram showing the structural characterization of the three-story Hotel El Comercio.

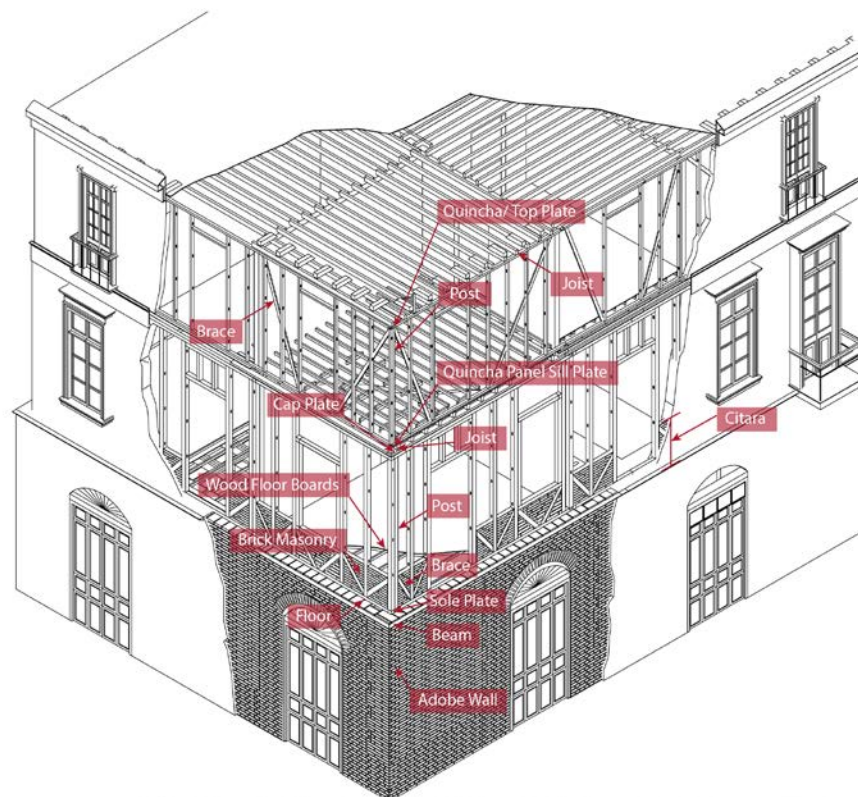


FIGURE 4.2. Schematic (a) and photograph (b) of a typical mortise-and-tenon connection. These joints connect the posts to the upper and lower beams in Hotel El Comercio.

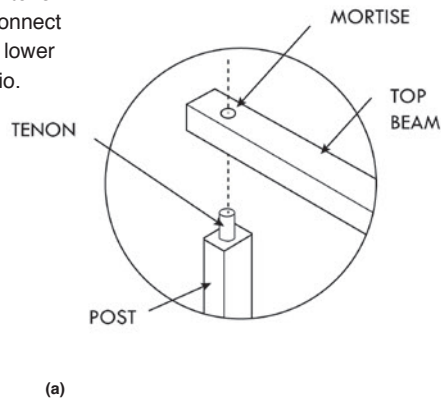
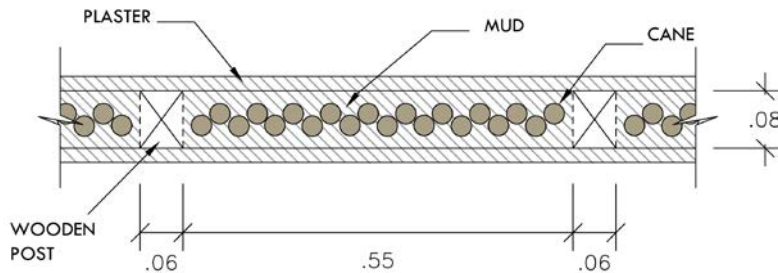


FIGURE 4.3. Transversal section of a quincha wall on the third floor of Hotel El Comercio, showing the woven cane and mud mortar.



cane and mud mortar. The surface of the wall is coated with additional layers of mud plaster and a fine layer of gypsum.

On the third floor of Hotel El Comercio, the walls are quincha with diagonal elements, but without citara. These walls are 3.20 m high and are similarly composed of timber posts and upper and lower beams, which have a smaller cross section (8 × 6 cm) than those on the second floor. Instead of a citara, the quincha elements have a diagonal timber element (3 × 9 cm) that crosses the entire panel and functions as a cross brace over the entire height of the wall. Distance between the posts is, as on the second floor, typically 60 cm. The third-floor quincha panels are filled with woven cane and mud mortar, coated with layers of mud plaster, and finished with a fine gypsum layer (fig. 4.3).

Full-scale reproductions of both types of quincha panels were constructed and tested under lateral cyclic load to evaluate their in-plane shear stiffness and strength.

Testing Methodology

Thirteen quincha panels were tested: of these, twelve were newly constructed and one original panel (fig. 4.4) was taken from the second floor of Hotel El Comercio. The upper beam of the original panel was severely damaged and was replaced with an existing beam found on site. The twelve new quincha test sample panels were constructed of new wood and cane to match the original design of the existing walls. Six panels matched the configuration found on the second floor (quincha with citara), referred to as specimens MA (fig. 4.5); the remaining six matched the configuration found on the third floor with the diagonal across the panel, referred to as specimens MB (fig. 4.6).

FIGURE 4.4.
Diagram showing configuration of original quincha panel.

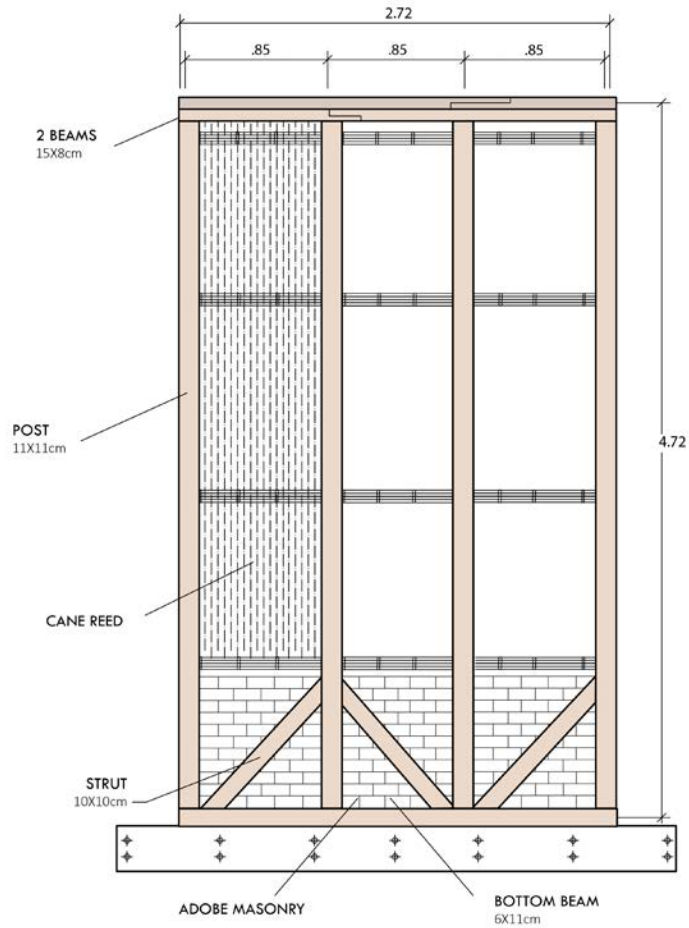


FIGURE 4.5.
Diagram showing configuration of the six panels matching the second floor, known as specimens MA.

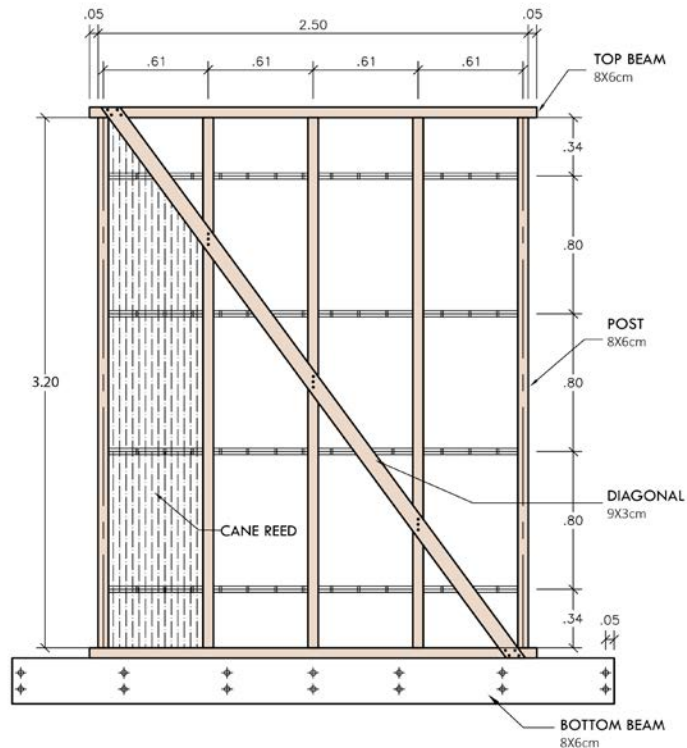
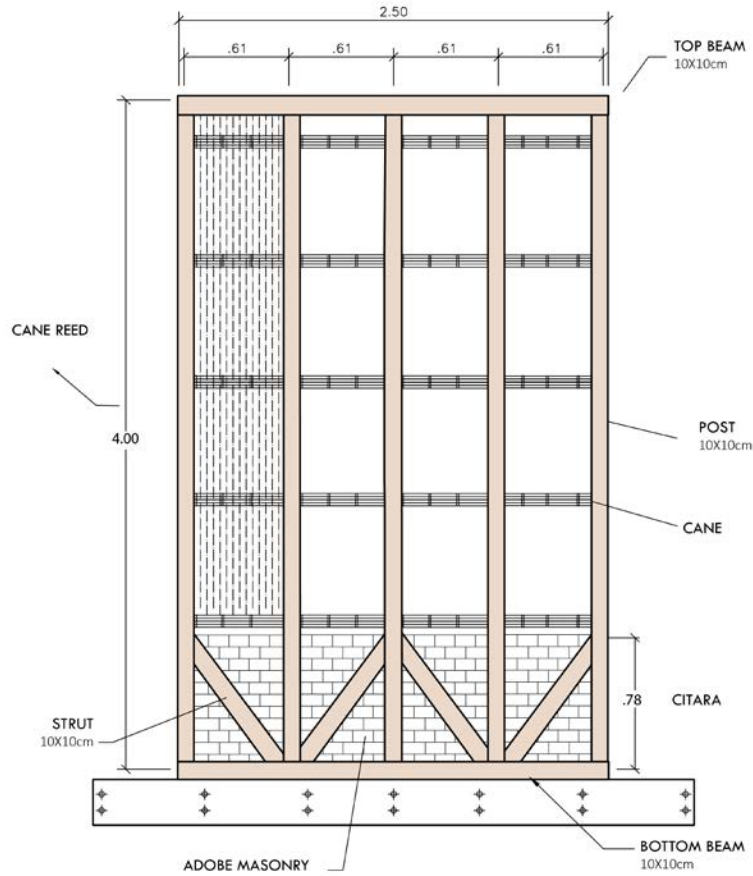


FIGURE 4.6.
Diagram showing configuration of the six panels matching the third floor, known as specimens MB.



The beams of the original panel consisted of sapele, and the posts and struts were made of cypress. For the construction of the twelve new panels, two timber species were used: moena alcanfor (*Ocotea costulata*) and moena amarillo (*Aniba* sp.) (table 4.1); their mechanical properties are shown in table 4.2.

The timber connections were executed as follows: beams and posts were connected using mortise-and-tenon joints, and the diagonal elements of the citara were nailed. The horizontal canes pass through holes in the posts. The masonry used to infill the citara of the quincha panels (MA) typically consisted of adobe blocks (or bricks, in some cases) and mud mortar. The primary purpose of the citara is to provide a base that is stiffer than the cane and mud fill above, making the specific infill material (adobe or brick) of secondary importance. During testing, two rows of new brick units and seven rows of new adobe units

TABLE 4.1.
Timber species used for the construction of specimens MA and MB.

Structural Elements	Timber Species		
	Original	Second floor (MA)	Third floor (MB)
Lower Beam	Sapele	Moena Alcanfor	Moena Alcanfor
Upper Beam	Sapele	Moena Alcanfor	Moena Alcanfor
Posts	Cypress	Moena Alcanfor	Moena Alcanfor
Struts (Citara)	Cypress	Moena Amarillo	–
Full diagonal	–	–	Moena Alcanfor

TABLE 4.2.
Mechanical properties of the timber species used for the construction of specimens MA and MB.

Properties	Moena Alcanfor	Moena Amarillo
Density (g/cm ³)	0.55	0.47
Moisture content at the time of testing (%)	19.00	16.80
Elasticity modulus in bending MOE (×1000 MPa)	10.92	9.93
Bending strength parallel to grain test (MPa)	76.67	75.43
Compression parallel to grain test (MPa)	44.37	40.57
Compression perpendicular to grain test (MPa)	6.20	6.95
Shear strength parallel to grain test (MPa)	10.03	10.04
Tension parallel to grain test (MPa)	52.81	62.92
Tension perpendicular to grain test (MPa)	4.37	3.80

with one-inch thick mud mortar joints were used for the one original quincha panel; for the six new quincha panels, all masonry infill consisted of new adobe units. Figure 4.7 shows the construction process of the newly constructed quincha panels. The original quincha panel was dismantled and rebuilt in the laboratory, as detailed in figure 4.8.



FIGURE 4.7.
Construction of new quincha test sample panel: (a) fastening of the citara (diagonal element at base), representative of the second-floor structure (MA); (b) insertion of transversal canes into posts; (c, d) construction of third-floor panel (MB) with diagonal timber element; (e) infilling of the panel (MA) with mud mortar; (f) quincha panel showing shrinkage cracks in the first layer of mud plaster; (g) quincha panel after application of a second layer of mud plaster.

FIGURE 4.8. Construction of original quincha test sample panel: (a) original quincha panel in existing location (second floor of Hotel El Comercio); (b) reassembly of panel; (c) insertion of masonry infill at citara base; (d) panel prior to mud plaster finish, with mud mortar over canes and complete infill at base.



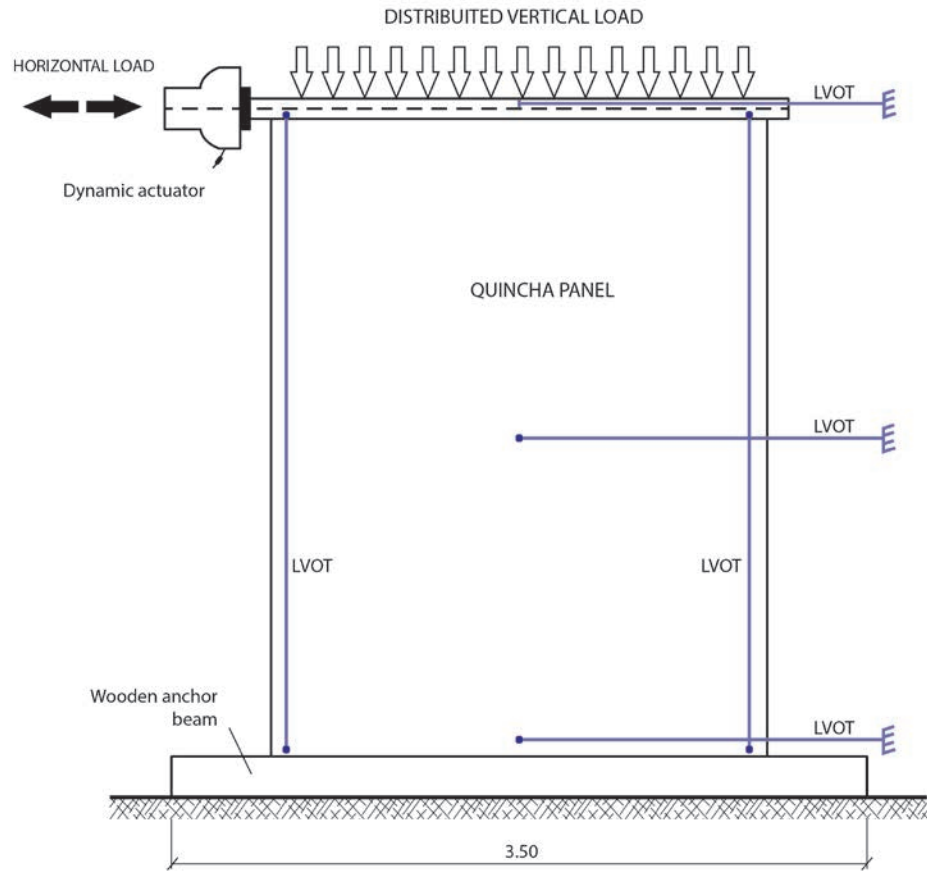
Test Setup

The quincha panels were subjected to lateral cyclic load exerted by a servo-hydraulic actuator with a maximum displacement capacity of 150 mm in two directions. The test setup is shown in figure 4.9. Each panel was anchored to a timber beam at the base, which in turn was anchored to a reactive floor.

Vertical loads were placed on top of a set of the panels to simulate the vertical loads (from roof, or upper floor). Five panels—the original panel from Hotel El Comercio, two MA specimens (MA1 and MA2), and two MB specimens (MB1 and MB2)—were tested without any additional vertical load. Specimens MA3, MA4, MB3, and MB4 were loaded with the expected weight of the panels of an exterior wall in Hotel El Comercio (40 kN for type A and 16 kN for type B). Specimens MA5, MA6, MB5, and MB6 were loaded with the equivalent weight of an internal wall (80 kN for type A and 32 kN for type B). The weight exerted on type A was larger than that exerted on type B, as type A corresponds to the second floor and type B corresponds to the third floor. The vertical load was applied before the first phase of the cyclic displacement and was manually controlled with a load cell during the complete test. Tables 4.3–4.6 provide an overview of the history of loading for each type of panel.

The original panel was subjected to three symmetrical cyclic phases and a final phase in which the center of the actuator was moved to provide further displacement in one direc-

FIGURE 4.9.
Test setup diagram for the quincha panels.



tion (see table 4.3). The MA panels were subjected to four symmetrical cyclic phases with a maximum horizontal displacement of ± 150 mm and similarly to one final phase where the center of the actuator was shifted to allow for further displacement in one direction (except for panel MA1; see table 4.4). The additional unilateral displacement was imposed because little damage to the panels occurred in the symmetrical cyclic phase, making it necessary to increase the relative displacement in one direction. Panels MB1 through MB4 were subjected to only four symmetrical cyclic phases (table 4.5) until a maximum displacement of ± 150 mm was achieved. Panels MB5 and MB6 were also subjected to the additional phase, which provided a maximum displacement of 300 mm in one direction.

TABLE 4.3.
Loading phases of the original quincha test sample panel.

Phases	Original Specimen
Phase 0 Vertical load (kN)	0
Phase 1 Max. displ. (mm)	± 30
Phase 2 Max. displ. (mm)	± 60
Phase 3 Max. displ. (mm)	± 140
Phase 4 Max. displ. (mm)	+300

TABLE 4.4.
Loading phases of specimens MA.

Phases	Specimens MA					
	1	2	3	4	5	6
Phase 0 Vertical load (kN)	0	0	40	40	80	80
Phase 1 Max. displ. (mm)	+/-25	+/-25	+/-25	+/-25	+/-25	+/-25
Phase 2 Max. displ. (mm)	+/-50	+/-50	+/-50	+/-50	+/-50	+/-50
Phase 3 Max. displ. (mm)	+/-100	+/-100	+/-100	+/-100	+/-100	+/-100
Phase 4 Max. displ. (mm)	+/-140	+/-140	+/-140	+/-140	+/-140	+/-140
Phase 5 Max. displ. (mm)	–	+200/-100	+250/-50-	+230/-70-	+220/-80	+230/-70

TABLE 4.5.
Loading phases of specimens MB.

Phases	Specimens MB					
	1	2	3	4	5	6
Phase 0 Vertical load (kN)	0	0	16	16	32	32
Phase 1 Max. displ. (mm)	+/-25	+/-25	+/-25	+/-25	+/-25	+/-25
Phase 2 Max. displ. (mm)	+/-50	+/-50	+/-50	+/-50	+/-50	+/-50
Phase 3 Max. displ. (mm)	+/-100	+/-100	+/-100	+/-100	+/-100	+/-100
Phase 4 Max. displ. (mm)	+/-140	+/-140	+/-140	+/-140	+/-140	+/-140
Phase 5 Max. displ. (mm)	–	–	–	–	+300/-0	+300/-0

Results

The maximum shear force sustained by specimens MA and MB and the corresponding lateral stiffness are presented in table 4.6. Specimens with citara (MA) had an average lateral stiffness of 0.23 kN/mm, while specimens with a diagonal had an average stiffness of 0.47 kN/mm. The maximum sustained force depended largely on the vertical load and ranged from 8 to 13 kN for specimens MA and 12.5 to 17 kN for specimens MB.

All tested quincha panels reached large lateral displacements without losing load capacity and none of the elements collapsed. The posts and beams, which are the main structural elements, did not present significant damage, although cracks in the mud always formed at the interface of the flexible wooden elements and the stiffer, more brittle mud mortar. A detailed description of the crack propagation is given for each of the three types of panels below.

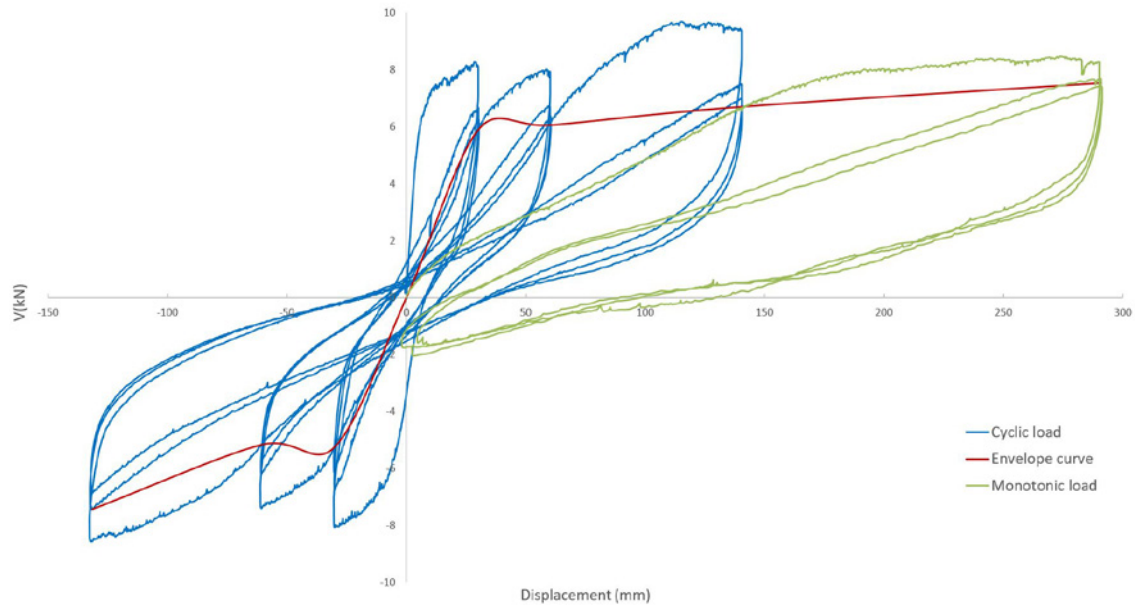
Original Panel from Hotel El Comercio

The original panel from Hotel El Comercio showed cracking around the posts and the columns, as well as an uplifting of the wall base of 1 to 2 cm, but there were no signs of structural damage during the tests.

TABLE 4.6.
Maximum force and lateral stiffness achieved by the twelve newly constructed quincha panels.




Type	Specimen	Maximum Force (kN)	Lateral Stiffness (kN/mm)
MA (quincha with adobe base)	Original	8.01	0.23
	MA1	7.09	0.19
	MA2	9.14	0.23
	MA3	9.14	0.23
	MA4	12.95	0.25
	MA5	12.38	0.24
	MA6	13.00	0.23
MB (quincha only)	MB1	12.50	0.40
	MB2	13.06	0.40
	MB3	14.50	0.50
	MB4	13.66	0.45
	MB5	17.00	0.56
	MB6	14.95	0.50

FIGURE 4.10.
Graph showing hysteresis curve of original test sample panel (monotonic loading).



The hysteresis loops for the panel under cyclic loading are shown in figure 4.10. Each test peak corresponds to a hysteresis loop associated with the displacements shown in table 4.3. The envelope curve (in orange) shows that the maximum obtained lateral capacity before entering the inelastic range is 7.17 kN. The greatest shear strength measured is 9.53 kN. The maximum deformation in the elastic range is around 9.8 mm when forced displacement is 150 mm. Due to application of the unidirectional monotonic displacement of 290 mm, the cracks widened and mud portions detached around the upper and lower beams, as well as around the posts (fig. 4.11). The lower left side of the wall lifted 7 cm.

FIGURE 4.11.
Description of conditions of original panel after testing from Hotel El Comercio.

	Original Panel	Description
Phase 1 – Max. D = 30mm		Cracks appeared close to the position of the posts and upper beam, due to cracking of the dried mud. Only small cracks were detected.
Phase 2 – Max. D = 60mm		Width of the cracks around the wooden elements observed in the first phase increased. Cracks also appeared in the struts at the level of the citara.
Phase 3 – Max. D = 140mm		Width of the existing cracks increased further. Additionally, a small detachment of mud at the top of the wall next to the second post from the left was observed. An uplifting of 1 cm at the bottom right and of 2 cm at the lower left of the wall base was observed.

Quincha Panels with Citara (specimens MA)

The quincha panels with citara showed a damage pattern similar to that of the original panel: cracks concentrated around the wooden elements that increased in width when displacements increased. When maximum displacement occurred, the tenon lifted from the mortise.

Behavior of all six panels is quantified in the load-displacement curves of the panel under horizontal cyclic shear force (fig. 4.12). The blue curves in each graph represent the behavior for the cyclic displacements of up to 150 mm in two directions. The red line in each graph represents the envelope curve of the elastic loading. Finally, the green line represents the part of the load test when the total displacement of 300 mm was applied in the positive direction. This unilateral displacement was applied because the normal cyclic test induced little damage, and no sign of strength decay was observed. However, even after applying the additional displacement, the quincha panels were still far from collapse (figs. 4.13, 4.14).

FIGURE 4.12. Graphs showing hysteresis curves of quincha panel specimens (a) MA1, (b) MA2, (c) MA3, (d) MA4, (e) MA5, and (f) MA6.

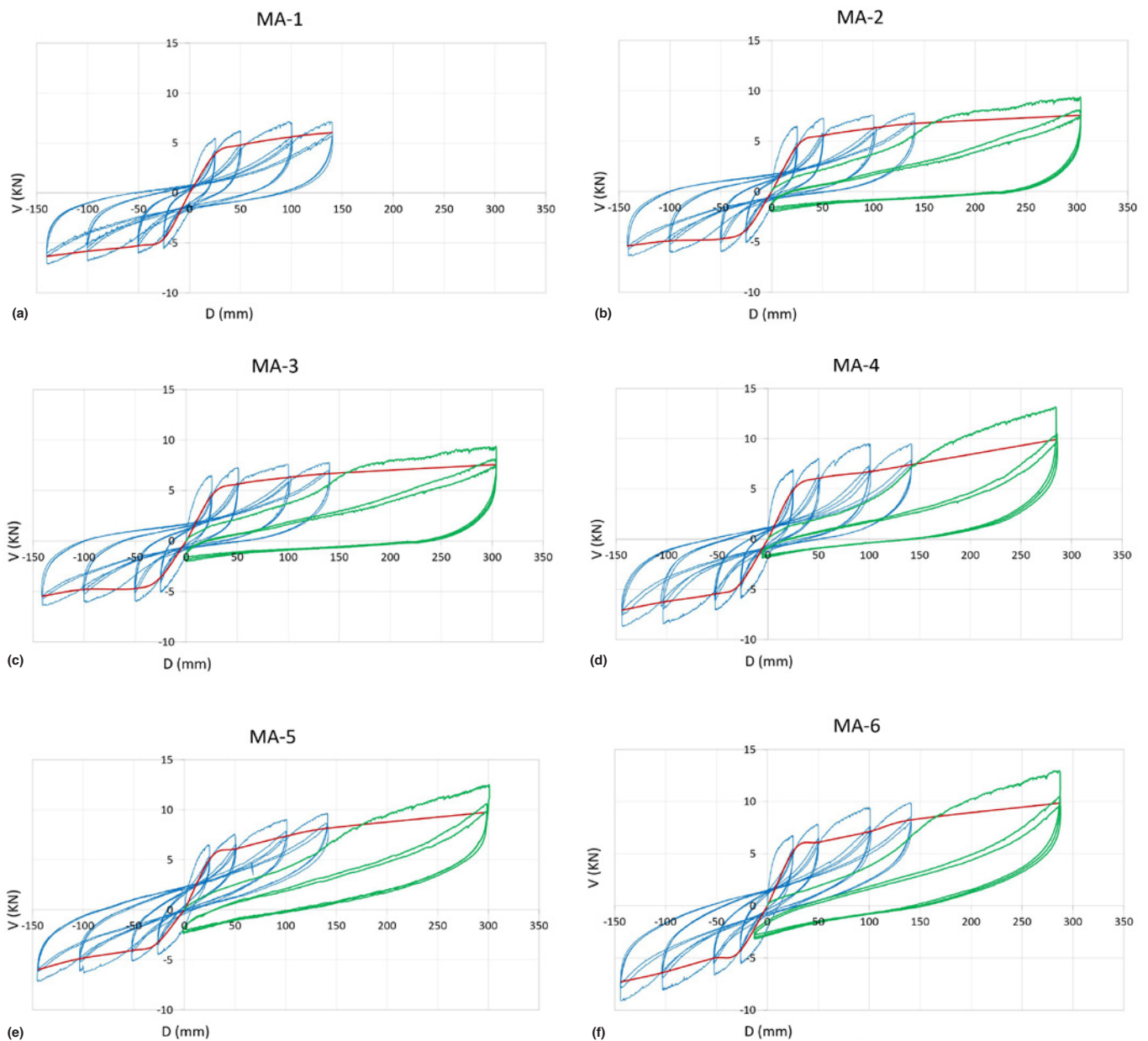


FIGURE 4.13.
Description of MA panel after test-
ing under different loads from Hotel
El Comercio.





MA	Description
<p data-bbox="521 359 570 491">Phase 1 – Max. D = 50mm</p> 	<p data-bbox="987 814 1479 1050">The damage due to the cyclic loading on the panel with citara is limited to the deterioration of the mud plaster finish and the development of cracks in the masonry infill at the citara. Due to this cracking of the citara, the stiffness reduces every cycle. The tenon at the base of the post also came loose from the mortise (see figure 4.12 above) due to the forward and backward motion, but the connection did not fail. In conclusion, the test did not lead to failure of any structural elements.</p>
<p data-bbox="521 785 570 917">Phase 2 – Max. D = 100mm</p> 	
<p data-bbox="521 1211 570 1344">Phase 3 – Max. D = 140mm</p> 	
<p data-bbox="521 1631 570 1764">Phase 3 – Max. D = 300mm</p> 	

FIGURE 4.14.
Image showing the tenon lifting from the mortise (red circle) at maximum horizontal displacement of specimen MA.



Quincha Panels with Diagonal (specimens MB)

Specimens MB1 through MB6 cracked primarily around the locations of the timber elements, as observed in the other quincha panels. However, because these elements also have diagonal timber elements, additional cracks were observed around these diagonals (see the detailed description of each panel in figs. 4.15–4.17). Furthermore, connection of the diagonal element to the rest of the frame failed, reducing the stiffness of the panels, as reflected in the hysteresis curves (fig. 4.18).

FIGURE 4.15.
Condition description of panels MB1 and MB2 after testing from Hotel El Comercio.

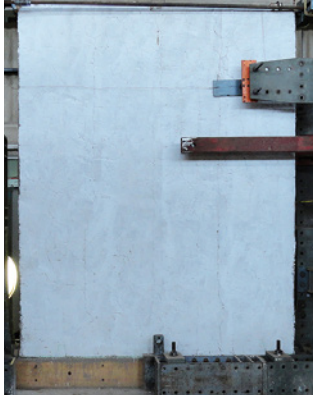







	MB1	MB2	Description
Phase 1 – Max. D = 25mm D/H = 0.0078			Cracks appeared on the plaster aligned with the posts and the base. Note: The diagonal was located on the opposite side of the one displayed in the images.
Phase 2 – Max. D = 50mm D/H = 0.0156			Crack width increased and new cracks appeared randomly in the panel surface. The tenons in the lower part of the posts started to detach from the mortises. The nails that connected the diagonal to the posts started to bend, and a crack appeared along the diagonal element.
Phase 3 – Max. D = 100mm D/H = 0.0313			Cracks increased in width. The lower tenons lifted 1 cm from the mortises. The timber diagonal (not displayed) cracked at the locations of the nailed connections. The nails in the intermediate connections became bent. In MB1 the plaster started to detach.
Phase 4 – Max. D = 140mm D/H = 0.0438			Extensive plaster detachment in MB1. Plaster detached from the posts in MB2. The timber diagonal detached at both ends, and the nails at the intermediate connections were bent even further. The tenons in the lower part lifted 2.5 cm from the mortises. Both panels maintained lateral load capacity.

FIGURE 4.16.
Condition description of panels MB3 and MB4 after testing from Hotel El Comercio.

















	MB3	MB4	Description
Phase 1 – Displ. = 25mm D/H = 0.0078			Some cracks appeared on the upper section of the panel due to application of the vertical load. Cracks also appeared along the timber diagonal and in the base. Note: In these panels the diagonal was on the front side.
Phase 2 – Displ. = 50mm D/H = 0.0156			Cracks formed along the posts and the timber diagonal and were distributed over the entire. The lower tenons started to lift from their mortises. The nailed connections of the diagonal started to detach.
Phase 3 – Displ. = 100mm D/H = 0.0313			The plaster detached along the posts and diagonal. Cracks increased, and the tenons lifted 1 cm from the lower mortises. Timber diagonal detached almost completely from the ends, and the nails of the intermediate connections started to bend.
Phase 4 – Displ. = 140mm D/H = 0.0438			Severe detachment of the plaster and the mud infill near the diagonal occurred at this stage. The timber diagonal broke at both ends, and the nails of the intermediate connections bent further. The lower tenons lifted 3 cm from the mortises in each loading and unloading cycle.

FIGURE 4.17.
Condition description of panels
MB5 and MB6 after testing
from Hotel El Comercio.

	MB5	MB6	Description
Phase 1 – Displ. = 25mm D/H = 0.0078			Some cracks appeared on the upper part due to vertical load application. Cracks also appeared along the timber diagonal and in the base. Note: In these panels the diagonal was on the front side.
Phase 2 – Displ. = 50mm D/H = 0.0156			Cracks increased along the posts and the timber diagonal. The lower tenons start to lift from their mortises. The nailed connections of the diagonal started detaching at both ends. Plaster started detaching along the diagonal.
Phase 3 – Displ. = 100mm D/H = 0.0313			Plaster detached along the posts and diagonal. Crack widths increased and tenons lifted from the lower mortises. The timber diagonal detached almost entirely from their ends, and the nails in the intermediate connections started to bend.
Phase 4 – Displ. = 140mm D/H = 0.0438			The plaster detachment increased and the connections of the diagonal failed almost entirely. The lower tenons lifted 3 cm from the mortises. In MB5 loss of infill occurred as well.

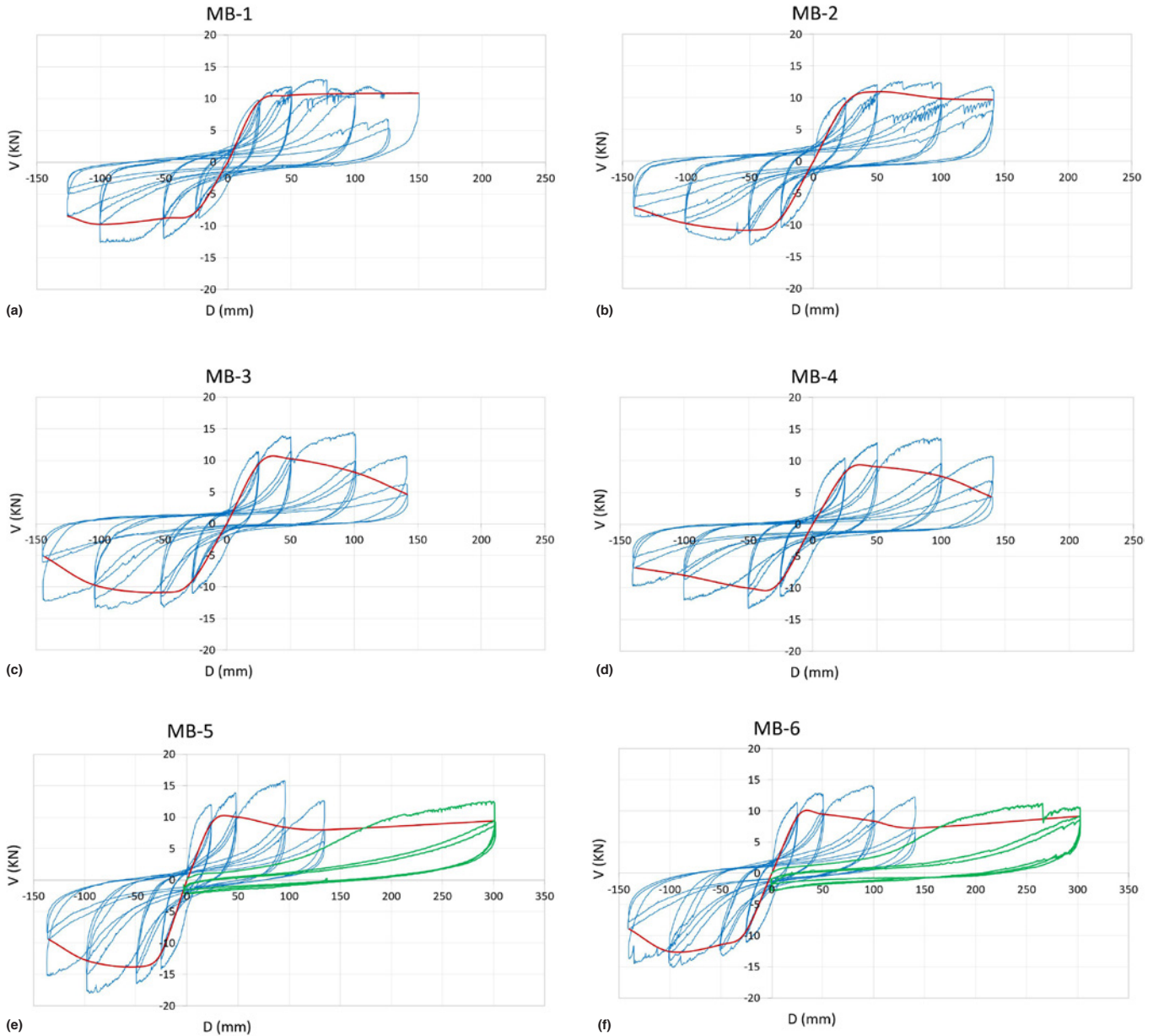


FIGURE 4.18. Graphs showing hysteresis curves of quincha panels (a) MB1, (b) MB2, (c) MB3, (d) MB4, (e) MB5, and (f) MB.

Discussion and Conclusion

None of the panels tested suffered structural damage, which can be attributed largely to the flexibility of the quincha system due to mortise-and-tenon connections of the posts and beams. These connections work as pins, allowing large deformations without causing failure. While the global behavior of all quincha elements was similar, the most important difference between the panels with citara (MA) and the panels without citara (MB) is that the stiffness of the MB panels is almost double that of the MA panels. The original panel behaves very similarly to the MA panels, as it has the same typology.

FIGURE 4.19.
Combined envelope
curves for MA panels.

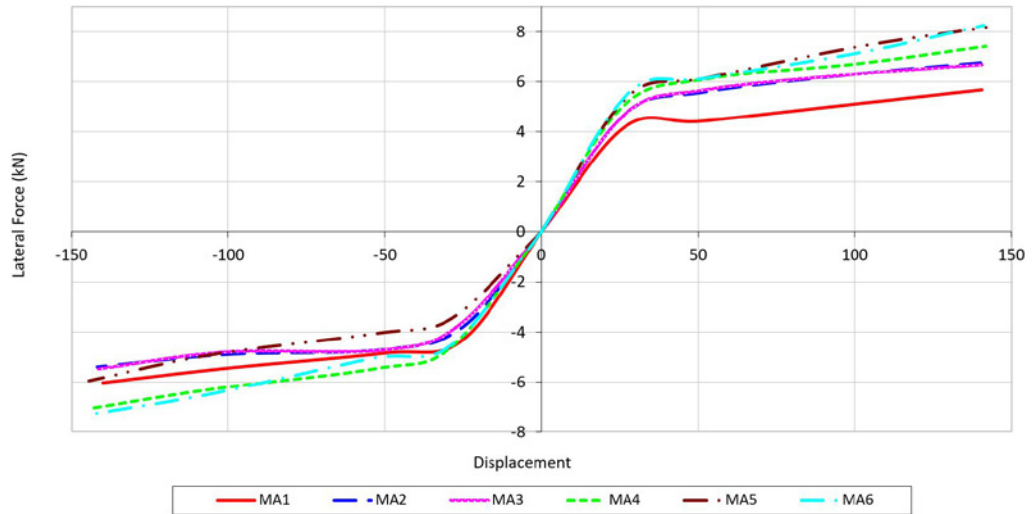


FIGURE 4.20.
Graph showing
evolution curves for
all MB panels.

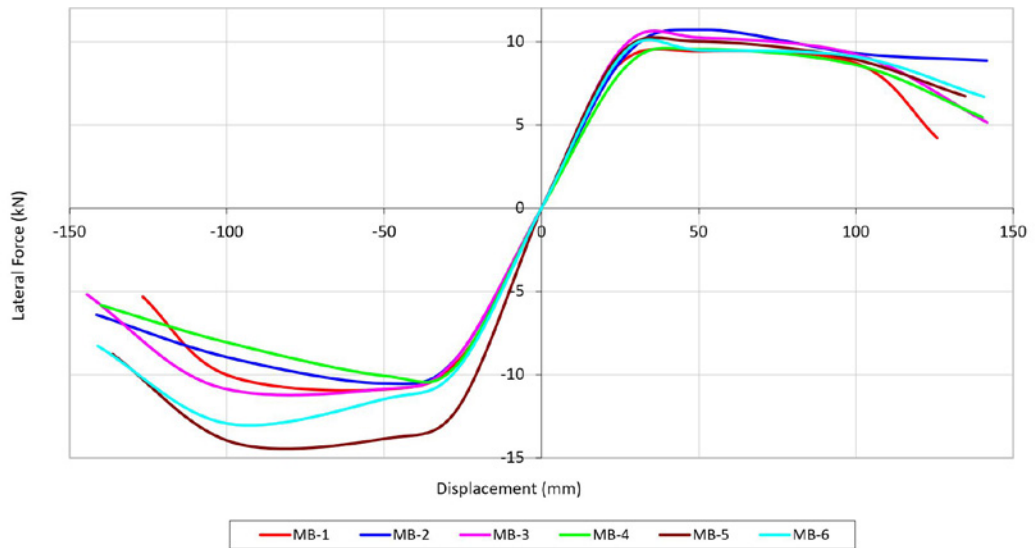
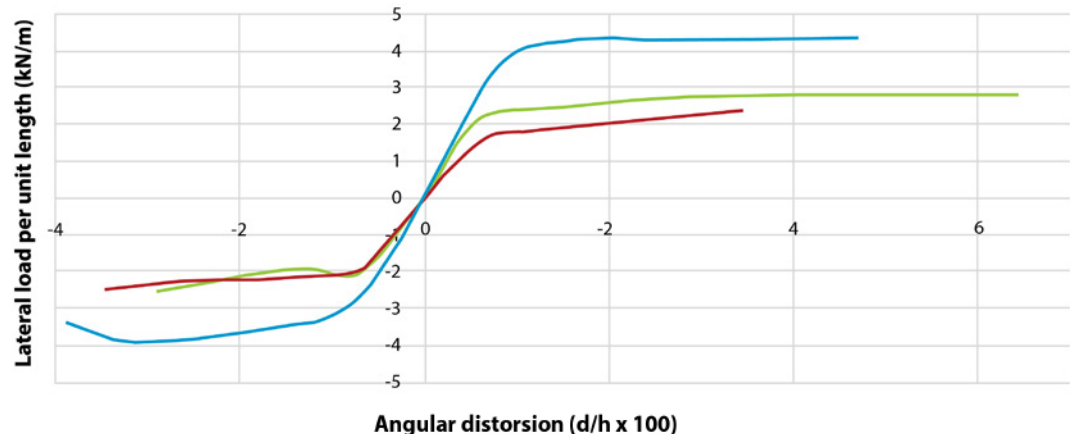


FIGURE 4.21.
Shear per unit length
vs. angular distortion
for the three types of
quincha panels.



Stiffness of the MA panels (0.23 kN/mm) is influenced by the presence of the citara. This element reduces the free height of the posts and thereby provides additional stiffness compared to systems without an infill base. Still, the stiffness is less than that of the panels with diagonal; however, the stiffness does not provide information on maximum capacity of the panels. The hysteresis curves for the MA panels show that after achieving the maximum displacement in both directions, the panels have not yet reached maximum displacement capacity during these tests. This is illustrated in figure 4.19, which combines all envelope curves obtained for specimens MA. As all envelope curves have a positive slope, there is no softening behavior of the panels, which implies that maximum capacity of the panels has not yet been reached. Therefore, it can be concluded that the panels indeed have a very large in-plane flexibility, allowing them to deform without significant damage.

Similar curves for all specimens with diagonal (MB) are shown in figure 4.20. The diagonal element in these panels increases the initial stiffness. Maximum capacity is reached when the top displacement is around +/-100 mm, at which point the nailed connections between the diagonal timber element and the posts fail. At this point, stiffness decreases significantly. Nonetheless, the panels remain stable, and as the diagonal bracing is lost, the panels start behaving like MA walls, similarly relying only on the vertical posts connected to the horizontal beams and the cane and mud infill.

Figure 4.21 compares behavior of the three types of quincha panels. The MB panels have the highest lateral resistance, which can be attributed to the diagonal brace. The original quincha panel performed slightly better than the newly constructed MA panels. This is probably due to the presence of a double upper beam (connected with a longer pin to posts), which increased the stiffness of the panel and provided greater load capacity.

Figures 4.22 and 4.23 show the load-displacement curves for MA6 and MB6, respectively. These curves correspond to the panels exposed to the larger vertical loads. In both figures, the dashed red lines represent the maximum lateral drift allowed by the Peruvian Design Code (NTE E-010) for timber design in new construction (Ministerio de Transportes 2006b). The code specifies that the maximum lateral displacement allowed for timber structures is the height of the wall multiplied by 0.01, which amounts to an admissible drift of 42 mm for MA panels and 35 mm for MB panels. The panels tested reached displacement values seven times higher than the maximum allowable drift specified in the standard (300 mm for MA, 250 mm for MB) without collapsing. Therefore, it can be concluded that the limit of lateral deformation imposed by the Peruvian standard is very conservative when applied to the traditional quincha panels.

FIGURE 4.22. Comparison of the MA6 curve, showing maximum lateral drift (dashed red lines) for timber structures according to the Peruvian Design Code (E-010).

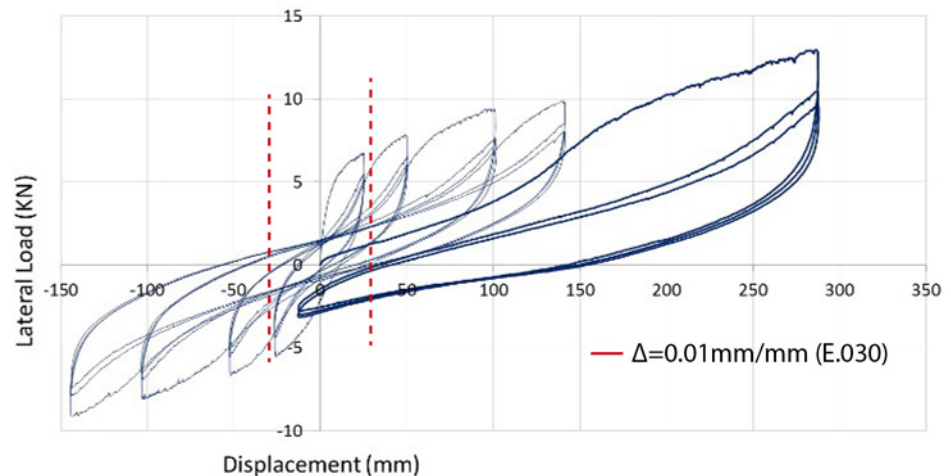
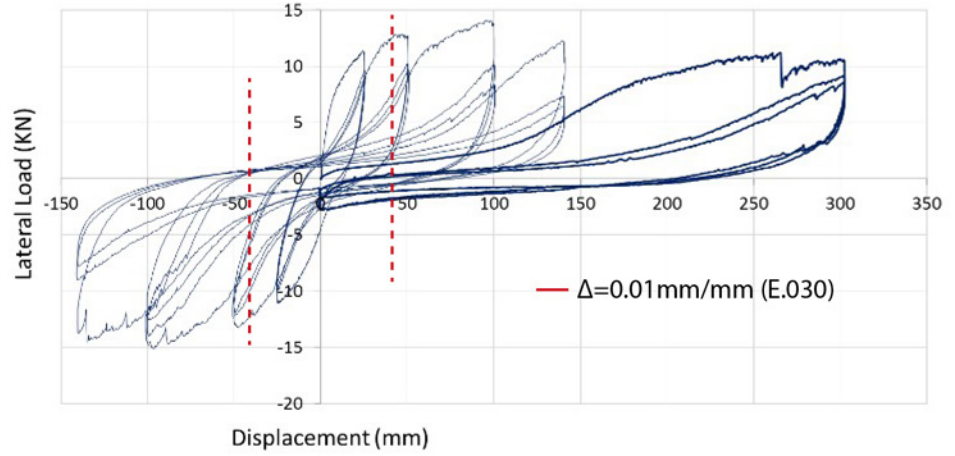


FIGURE 4.23.
Comparison of the MB6 curve,
showing maximum lateral drift
(dashed red lines) for timber struc-
tures according to the Peruvian
Design Code (E-010).



References

Ministerio de Transportes, Comunicaciones, Vivienda y Construcción. 2006b. *Normativa de madera*. NTE E-010. Lima: Ministerio de Transportes, Comunicaciones, Vivienda y Construcción.

Testing of Timber Connections at Ica Cathedral

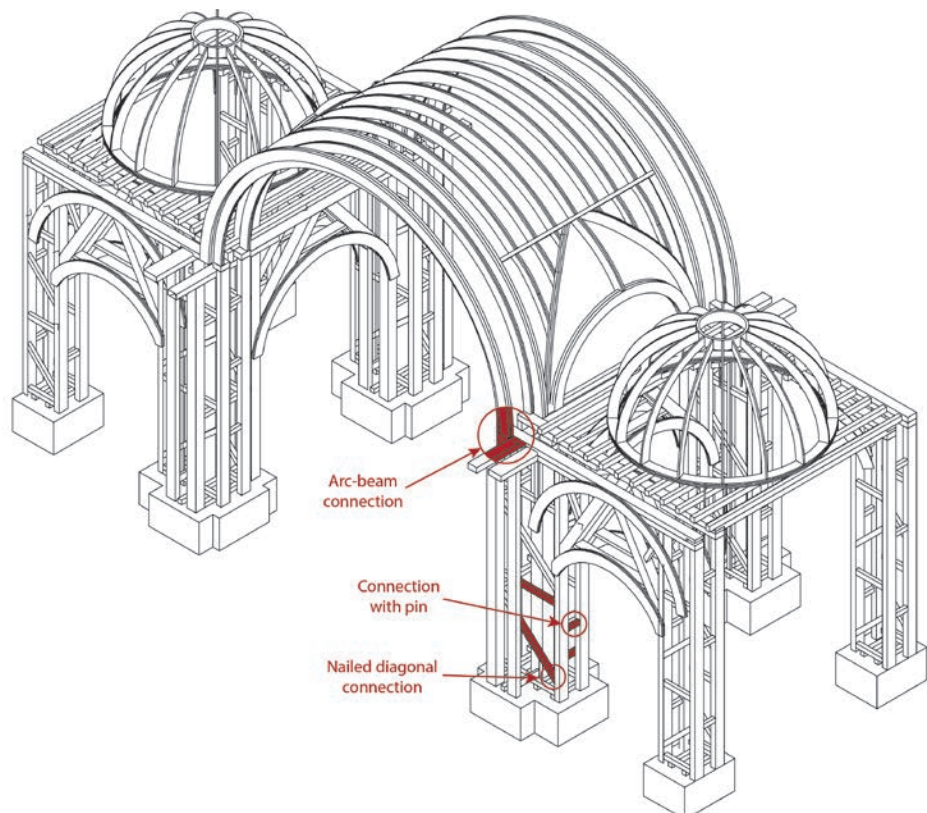
Selected Connections and Testing Methodology

Ica Cathedral is a sophisticated timber structure composed of pillars, beams, cupolas, vaults, arches, and towers. Seismic behavior of the structure is therefore likely to be dependent on the behavior of the timber joints tying these parts together. Three main types of connection have been identified for testing and further investigation:

1. Connection between post and horizontal bracing (pinned). The horizontal elements have two pins at the edges, which fit into two holes in the posts.
2. Connection between post and diagonal bracing (nailed). The diagonal bracing is nailed to the vertical posts.
3. Connection between arches and beams (mortise and tenon). This connection is typically mortise and tenon, in which the supporting beam has a rectangular hole and the element of the arch has a tenon that fits into this hole.

The locations of the three connections are shown in figure 5.1. Photographs of the pinned connection and its test setup are shown in figures 5.2 and 5.3.

FIGURE 5.1. Diagram of Ica Cathedral, showing locations of three typical connections studied: pinned, nailed, and mortise and tenon.



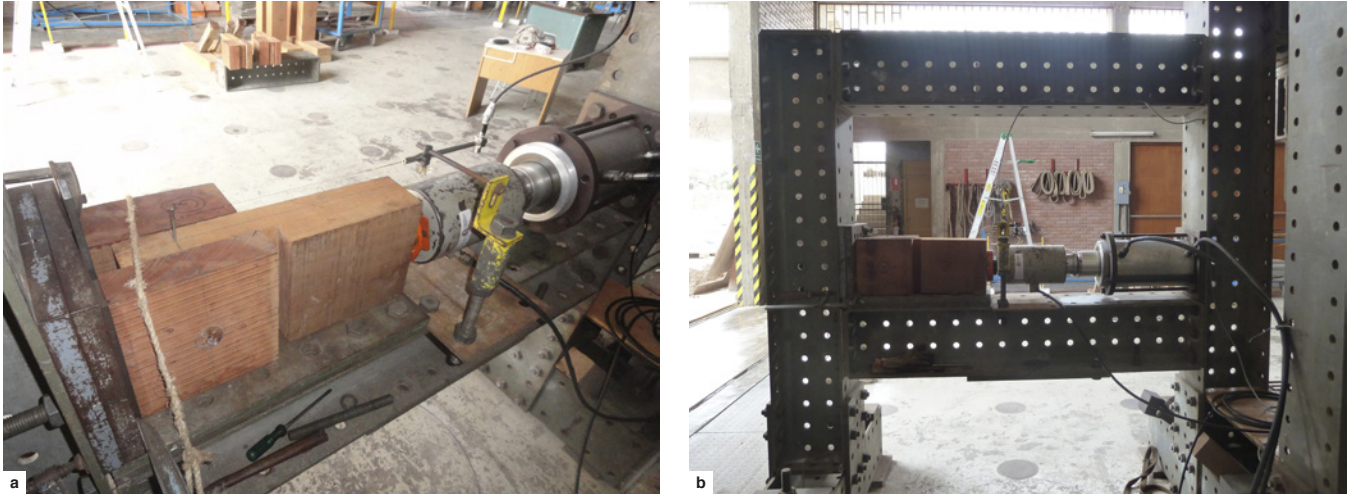
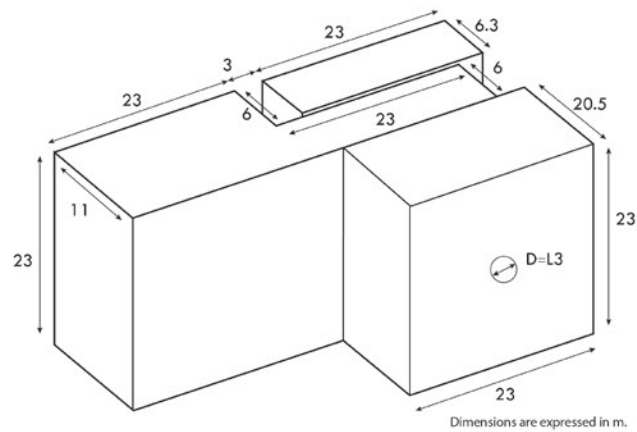


FIGURE 5.2.

Pinned connection between post and horizontal bracing: (a) view of the specimen; (b) view of the test setup.

FIGURE 5.3.

Diagram showing dimensions of the pinned connection between post and horizontal bracing, built in the laboratory.



The main objective of the testing was to identify whether these connections act as hinged connections, or if they allow for the transfer of bending moments.

A test was developed for each of the three connections shown in figure 5.1. Each test reproduced elements similar in size to those found on site, and full-scale specimens were constructed using new wood with properties similar to those found on site. The mechanical actions that each joint was expected to sustain was mimicked as closely as possible.

Connection between Post and Horizontal Bracing (pin)

Test Setup

Three specimens were constructed from quinilla colorada (*Manilkara bidentata*), which belongs to the same wood category (type A) specified in the Peruvian Design Code (NTE E.010) as the original timber huarango (*Prosopis pallida*) (Ministerio de Transportes 2006b). Today huarango is a protected wood species. The mechanical properties are shown in table 5.1.

TABLE 5.1.

Characterization of the mechanical properties of *Quinilla colorada*, used to construct the test specimens.

Values Presented	Moisture content	Bending			Compression		
		Limit of linear elastic behavior	Maximum capacity	Modulus of elasticity	Limit of linear elastic behavior	Maximum capacity	Modulus of elasticity
	%	MPa	MPa	GPa	MPa	MPa	GPa
Average	46	69.8	118	18.1	46.7	59.6	19.2
Characteristic		15.7	15.8	1.76	9.41	8.53	3.82
Coefficient of variation		25.5	1.05	1.08	2.25	1.57	2.25

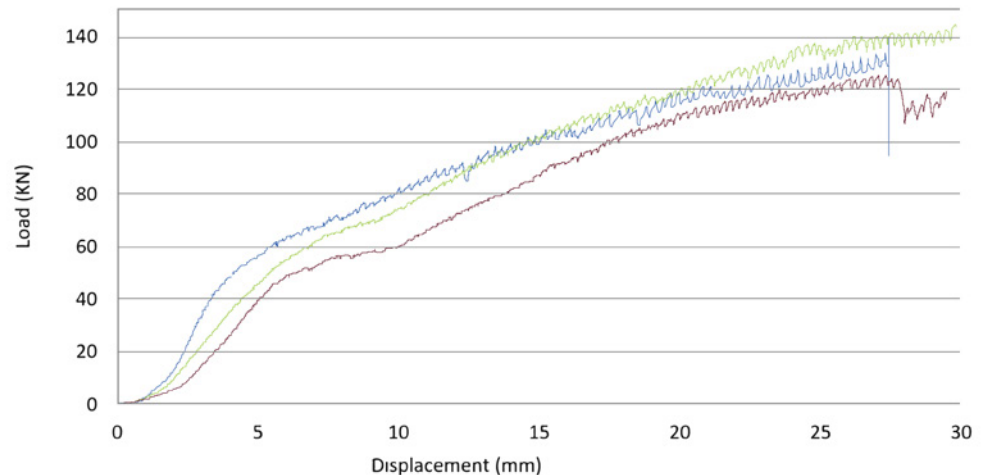
Results and Conclusion

In all executed tests, the pin bent and crushed the adjacent areas of the supports without breaking. This confirmed the field observation that none of these pins had failed during the Pisco earthquake in 2007 experienced by Ica Cathedral. The maximum loads sustained by the three samples were 140 kN, 144 kN, and 125 kN, respectively. The results showed that the capacity of the pinned joint is very high and that the pinned connection will behave elastic under the expected loads. This is illustrated by the load-displacement curves in figure 5.4.

In conclusion, the ultimate load capacity of the connection is very high: an average maximum load of 132 kN associated with a displacement of 27 mm that is unlikely to be exceeded during seismic action. Therefore, it can be safely assumed that the connection itself will not fail during strong seismic events and will continue behaving like a pin.

FIGURE 5.4.

Graph showing load-displacement curves for the three specimens with pinned connections.



Connection between Post and Diagonal Bracing (nailed)

Test Setup

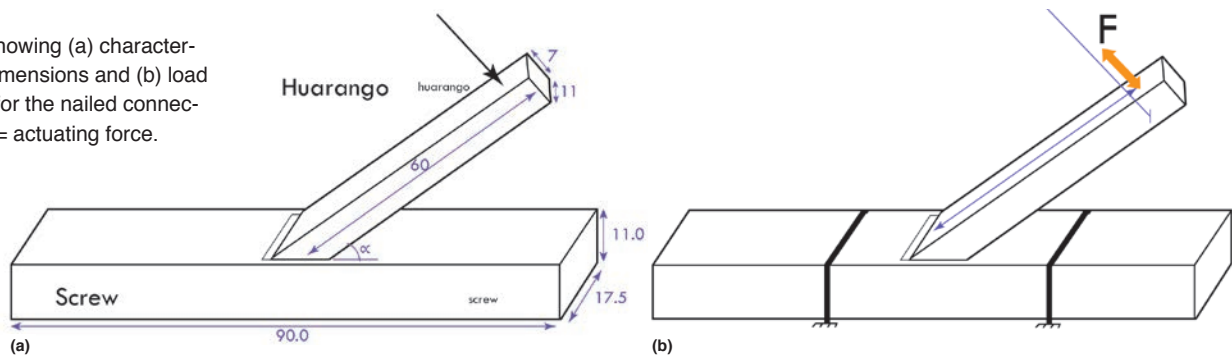
Three specimens were also constructed to gain further insight into the behavior of the nailed connections between the posts and diagonal bracing. Originally in Ica Cathedral, sapele (*Entandrophragma cylindricum*) was used for the posts, and huarango (*Prosopis pallida*) for the diagonals. As sapele is also an exotic timber species, it was replaced by tornillo

(*Cedrelinga catanaeformis*), from the same type C timber class specified in the Peruvian code. Original pieces of huarango timber in good condition were collected from the collapsed material in Ica Cathedral and used in the testing. The diagonal was connected to the base with an original, single nail. The test was performed in a cyclic manner, controlling the displacement and measuring the force. The force was applied at the end of the diagonal perpendicular to its axis. The three specimens were tested in three phases of maximum displacement of 20, 40, and 80 mm, respectively. Three cycles were performed for each phase. The test setup is shown in figures 5.5 and 5.6.

FIGURE 5.5.
Test setup for the nailed connection between post and diagonal bracing.



FIGURE 5.6.
Diagrams showing (a) characteristics and dimensions and (b) load application for the nailed connection, with F = actuating force.



Results and Conclusion

Figure 5.7 shows the position of the nail and its distance from the center of rotation in the cyclic test. These rotation centers are at both ends of the area of contact between the two elements. When the actuating force (F) pulls the diagonal outward, the distance to the center of rotation in the three specimens is greater (10, 10, and 7.5 cm) than when F acts in the opposite direction (6, 4, and 7 cm). This asymmetry of the centers of rotation, combined with the asymmetry of the nail, results in much higher loads experienced by the joint in one direction than in the other (fig. 5.8). Figure 5.9 shows the asymmetrical load-displacement curves obtained for the three specimens. This plot is proportional to the moment-rotation curve, since the values displayed on the axis are $moment = force \times d$; and $angle\ of\ rotation = displacement/d$.

FIGURE 5.7.

Distance between the nail and the center of rotation. When F pulls the diagonal outward, distance is greater (a) than when F pulls in the opposite direction (b).

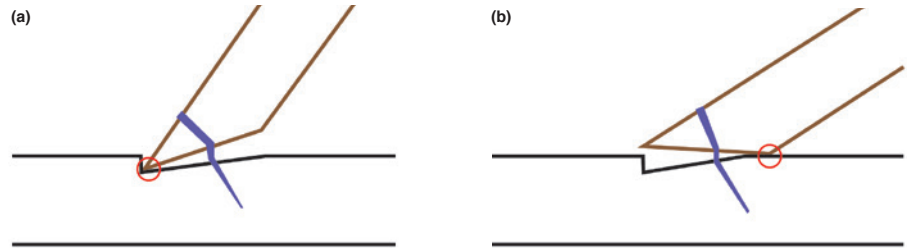


FIGURE 5.8.

(a) Direction of F (yellow arrow) and distance to the center of rotation (double red arrow). (b) Detail showing rotation of diagonal at distance d from center when the pulling force (dashed yellow line) is acting.

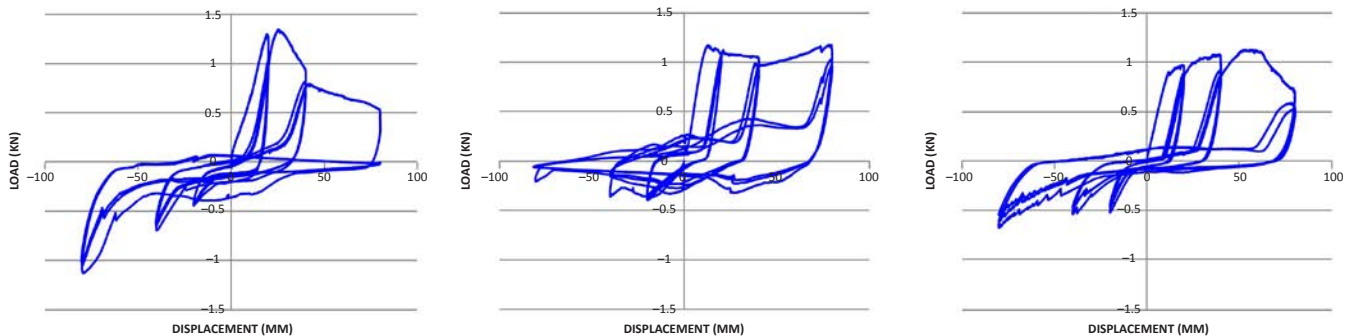


FIGURE 5.9.

Load-displacement curves for the nailed connections between post and diagonal.

The rotational stiffness of the connection is almost zero after the first load application, as the nail is extracted almost right away, allowing the two pieces of wood to separate. From this point on, the diagonal only rotates around the nail until the diagonal reaches the base at one end or the other. When the diagonal touches the base, additional moment resistance is generated.

The cyclic test shows that the behavior of the connection is asymmetrical, as the nail connecting both elements is not at the center of the contact surface. Because of the different distances from both ends to the nail, different resisting moments occur when the diagonal rotates. From the load-displacement curves, it can be concluded that the connection will lose its moment resistance and will start to behave as a pin once a bending moment of 0.72 kNm has been exceeded.

Connection between Arches and Beams (mortise and tenon)

Test Setup

Six specimens replicating the connection between arches and beams were tested. Tornillo (*Cedrelinga catanaeformis*) was used for the beams to replace the unavailable sapele timber. Cedar (*Cedrela odorata*) was used for the arches as in the original structure. The test was set up so that the tenon was in the middle of the longitudinal direction of the beam. The load was applied cyclically at the end of the element representing the arch. Three of the six specimens were subjected to a force parallel to the longitudinal direction of the beam; the remaining three were subjected to a force perpendicular to the longitudinal direction of the beam (figs. 5.10, 5.11). In the transversal direction, however, the tenon was located off center, creating an asymmetrical setup (fig. 5.12). Testing was performed in a displacement-controlled environment while measuring the force. Each test was subjected to three phases of maximum displacement: ± 20 , ± 25 , and ± 50 mm.

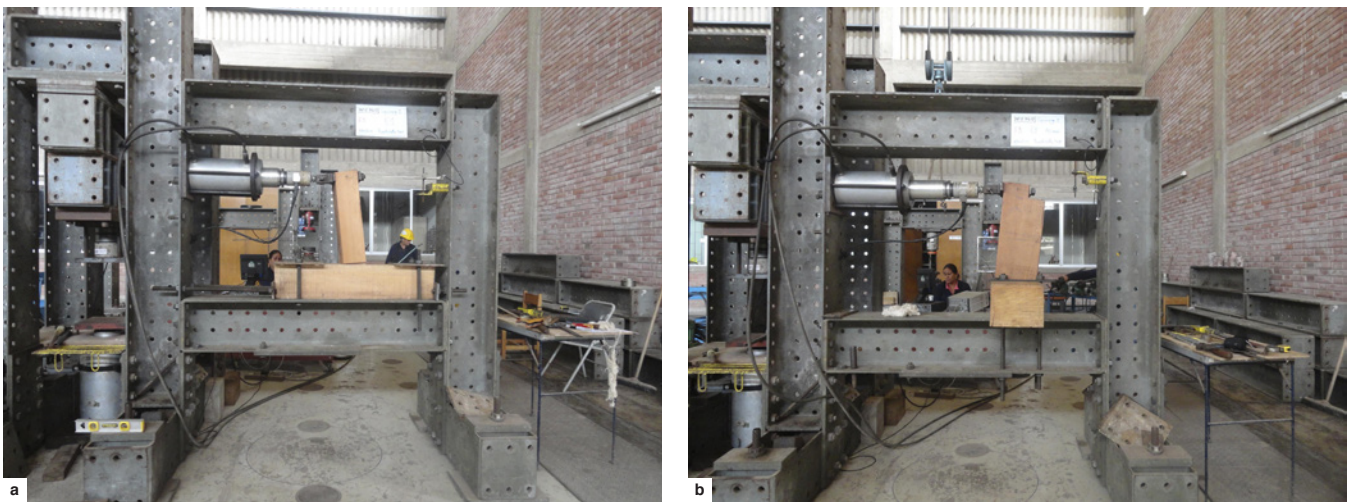


FIGURE 5.10.

Test setup for the connection between arches and beams (mortise and tenon): (a) test parallel to beam; (b) test perpendicular to beam.

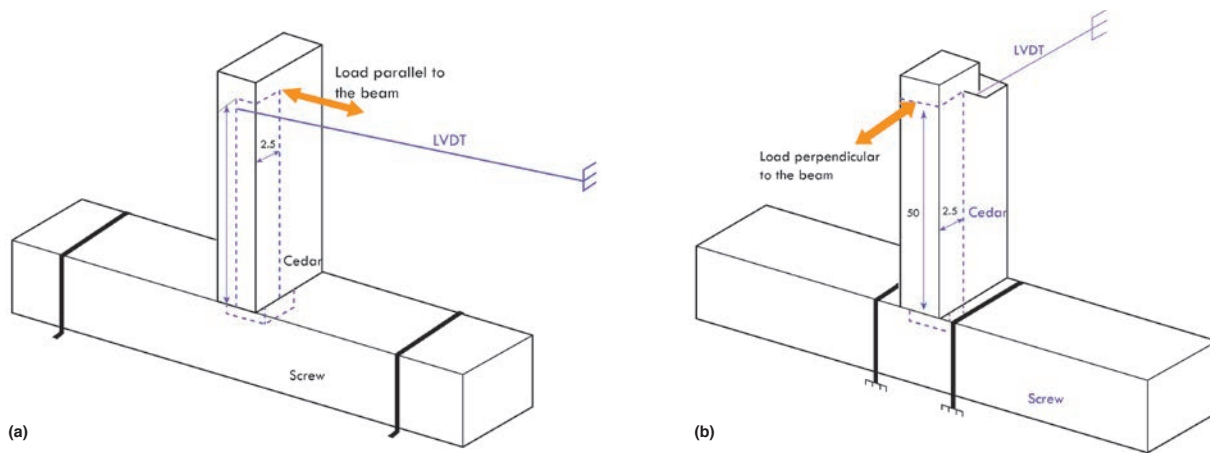
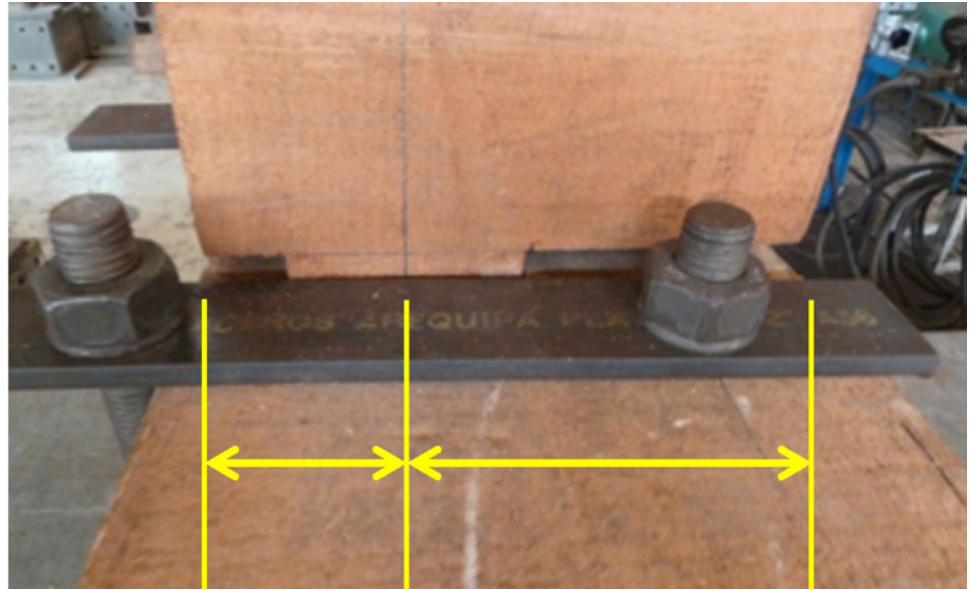


FIGURE 5.11.

Test schematics showing load (a) parallel to the beam; (b) perpendicular to the beam.

FIGURE 5.12.

Setup of transversal direction, showing the tenon placed off center, creating an asymmetrical setup.



Results and Conclusion

The load-displacement curves for parallel loading (specimens 1, 2, and 3) and perpendicular loading (specimens 4, 5, and 6) to the longitudinal direction of the beam are displayed in figures 5.13 and 5.14, respectively. When the connection is loaded in the parallel direction, its behavior is slightly asymmetrical. In fact, even though the tenon is symmetrically

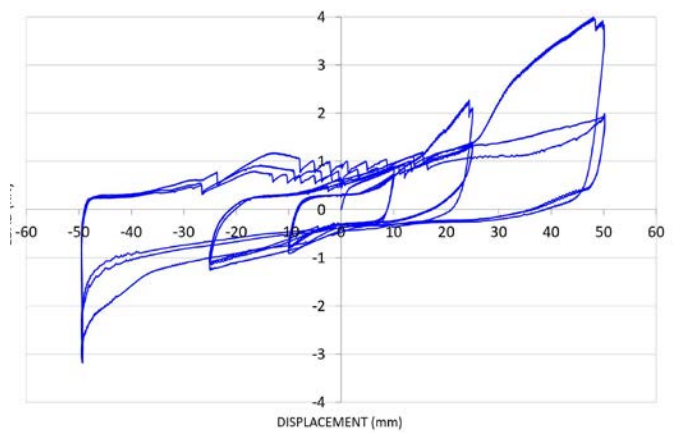
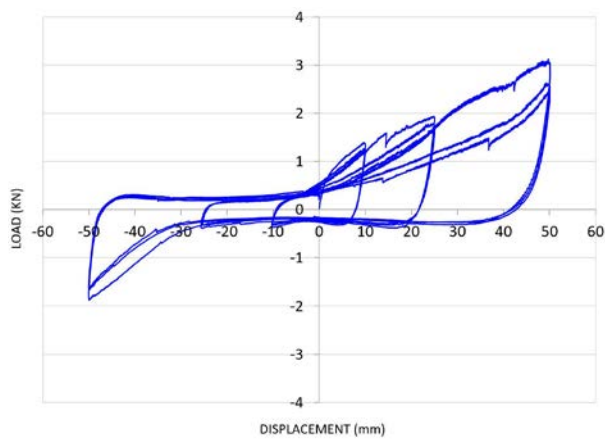
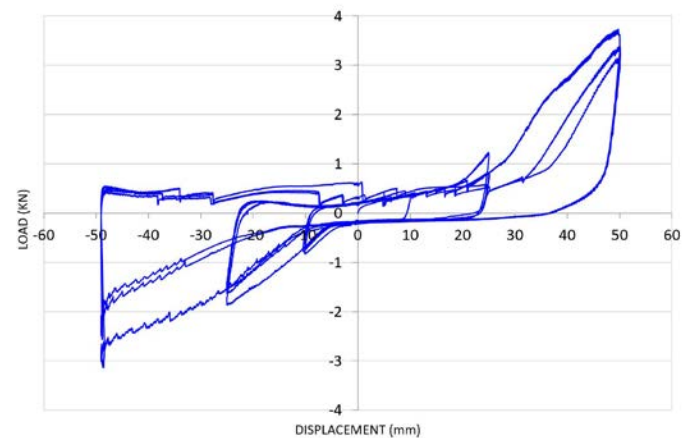


FIGURE 5.13.

Load-displacement curves for the arch-and-beam connection for specimens 1, 2, and 3 (parallel loading).



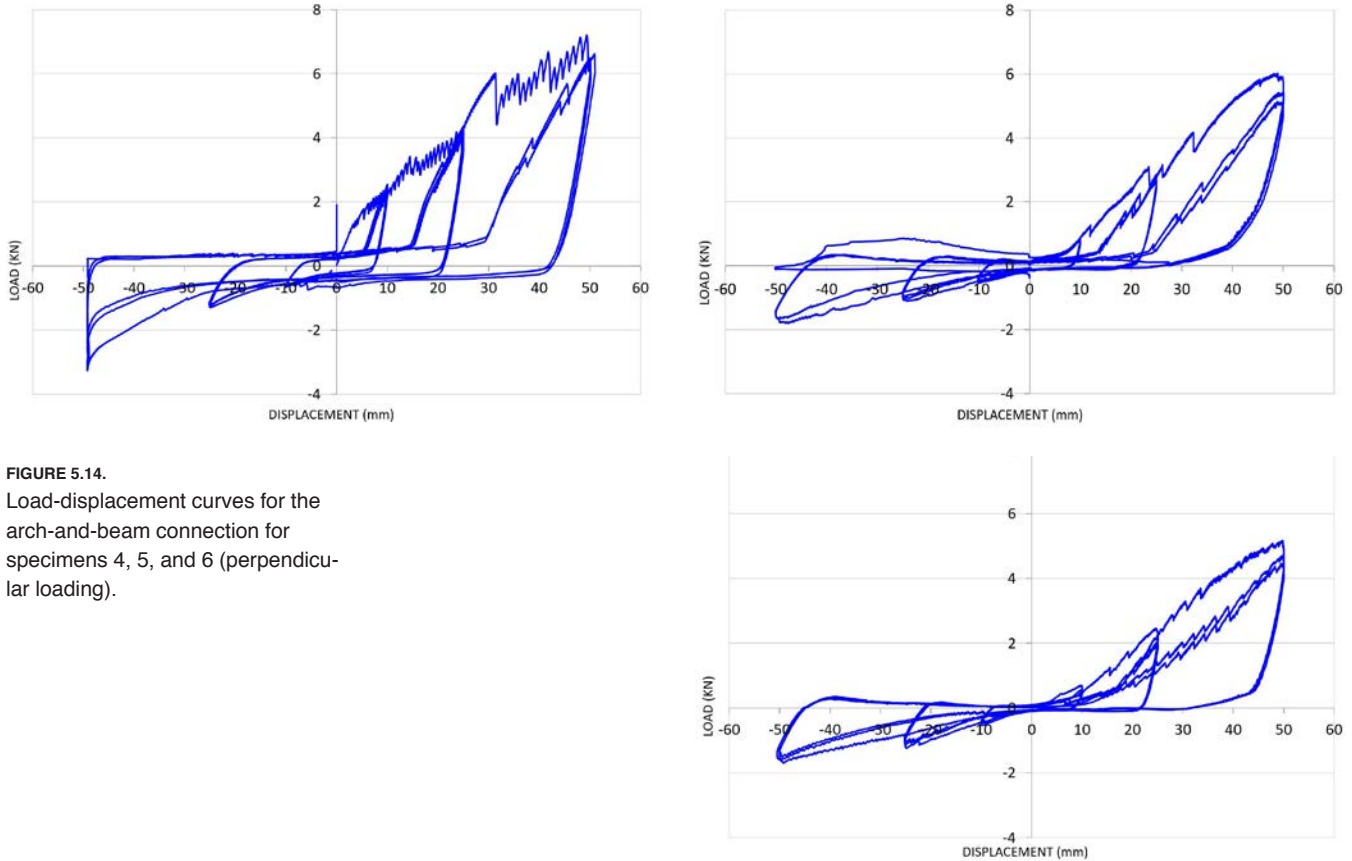


FIGURE 5.14. Load-displacement curves for the arch-and-beam connection for specimens 4, 5, and 6 (perpendicular loading).

located, it pulls out from the mortise and returns fully to its initial position because of friction. The moment resistance of the connection can be computed by multiplying the forces obtained in each direction (3 kN and 3.6 kN on average) by the distance to the base (0.50 m). The resisting bending moments of the connection in the direction, aligned with the beam, thus become 1.5 kNm and 1.8 kNm depending on whether the force is exerted in a positive or negative direction along the beam. The central part of the load-displacement curve for all specimens loaded parallel to the beam shows a near-horizontal slope, indicating that the bending stiffness is almost zero. Therefore, the rotational stiffness is also close to inexistent, and the connection behaves like a hinge. The connection did not fail, nor did the tenon loosen from the mortise.

In the case of perpendicular loading, the measured loads were highly asymmetrical. This is due to the asymmetrical position of the tenon in relation to the axis of the beam. When the timber element representing the arch rotates, the distance to the center of the tenon changes. The bending moment can again be computed by multiplying the exerted forces by the vertical distance to the base (0.50 m). The values for the maximum bending moment then become 2.5 kNm in one direction and 0.75 kNm in the other direction. Also in perpendicular loading, the central part of the load-displacement curve shows an almost horizontal slope with almost zero force, again demonstrating that the stiffness is close to zero. Therefore, the rotational stiffness is near zero. Again, we can conclude that the connection behaves like a hinge. The connection did not fail, nor did the connection become loose between the tenon and mortise.

Furthermore, the connection between the arch and the beam can be considered a pinned connection.

Conclusions

The testing of the timber connections allowed identification of a clear structural behavior for all three connections. None of the connections showed fragile behavior, and no connections failed during the tests. All connections can be represented as pinned: in the case of both the nailed diagonal and the arch-and-beam connections, there is a small initial capability to transfer bending moments; however, once the nail and the tenon slide from their original location, they no longer resist rotation.

References

Ministerio de Transportes, Comunicaciones, Vivienda y Construcción. 2006b. *Normativa de madera*. NTE E-010. Lima: Ministerio de Transportes, Comunicaciones, Vivienda y Construcción.

Traditional Techniques for Seismic Stabilization

Traditional techniques that enhance the stability of adobe buildings have been part of the adobe architectural heritage for centuries. The main stabilization techniques that have been used traditionally are wooden ring beams, wooden tie beams (that interconnect parallel walls), wooden corner keys, and buttresses (Michiels 2015). These techniques have been used for retrofitting but have also been incorporated in historic adobe structures at the time of construction. This chapter describes the physical testing of two of these techniques: wooden tie beams and wooden corner keys.

Pull-out Testing of Tie Beams

Tie beams—horizontal elements that connect parallel walls and allow the transfer of horizontal loads—are a recurring building element in many adobe churches. These beams, usually made from timber, form an essential part of many adobe masonry buildings, as they tie together parallel walls, thereby improving the box behavior of structures and contributing to the out-of-plane resistance of the walls (Michiels 2015). Tie beams are mostly employed where there are few transversal walls. They can serve as complementary structural elements to buttresses but are often used instead of buttresses.

The anchoring of tie beams to adobe walls is often a critical factor in determining the effectiveness of the beams (fig. 6.1). Therefore, the objective of pull-out testing is to understand the behavior of a system of tie beam and anchor key as it connects to an unfired-brick masonry wall. Testing was accomplished by analyzing the system's failure mode and defining the maximum capacity of the connection.

FIGURE 6.1.

- (a) Tie beams as seen in the outside wall of a house in Cuzco.
 (b) Tie beams visible at the roof level inside the church of Kuñotambo.



Prior to the laboratory testing program, a field survey was performed in the Cuzco area in Peru to identify the dimensions, construction details, and building materials typically used for tie beams. In the historic center of Cuzco, the thickness of the adobe walls varies from 0.60 to 1.20 m in houses and from 1.00 to 2.00 m in churches. In houses, tie beams typically have a diameter of 15 cm and can be found at the roof level as well as between the first and second floors of two-story homes. In churches, the diameter of the cross section of the tie is between 20 and 25 cm. Spacing between tie beams varies from 2 to 5 m, and anchor keys tend to be 50 cm long and 10 cm in diameter.

Methodology

For the testing, nine walls with embedded ties were constructed following the schematic shown in figure 6.2. Each of the nine walls had a width of 1.90 m and a height of 1.50 m (fig. 6.3). The walls were divided into three test groups; the three walls in each group had a thickness of 0.26, 0.54, and 0.84 m, respectively (fig. 6.4). Larger vertical load (w) was placed on the two thicker samples (0.54 and 0.84 m) in each group (fig. 6.5). Width, height, thickness, and load for the nine wall samples are provided in table 6.1. Each wall was restrained both at the bottom and at the top. The placement of a restraint at the top inhibited the rotation around the bottom hinge. A tensile force (P) was applied at the end of the tie beam using a hydraulic jack, while the horizontal displacement was recorded using a linear variable differential transformer (LVDT).

The masonry walls were built using unfired artisanal bricks as a substitute for adobe units. These unfired clay bricks were fabricated following a process similar to the production of adobe and were hand molded and sun dried. The elements have smaller dimensions ($203 \times 118 \times 92$ mm) and a higher clay content than typical adobe blocks, however. Average

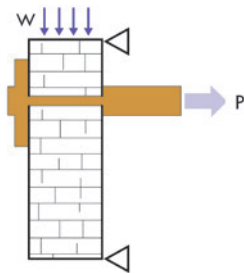


FIGURE 6.2. Schematic used for construction of the nine test walls, with w = vertical load and P = tensile force.

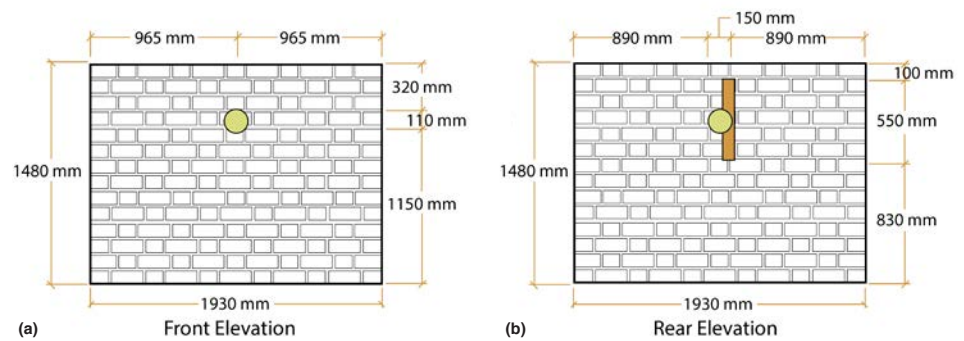


FIGURE 6.3. (a) Front and (b) back views of the test-sample walls, showing the main dimensions.

FIGURE 6.4.

Side views of the test samples, showing the three different thicknesses: (a) 0.26 m, (b) 0.54 m, and (c) 0.83 m.

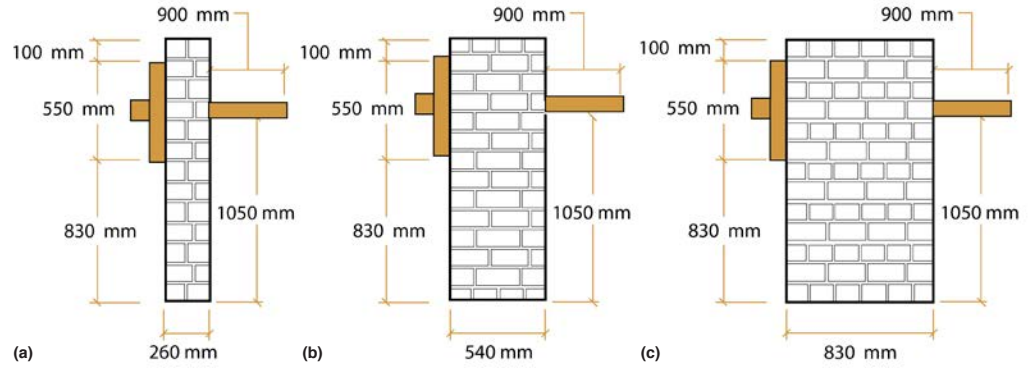


FIGURE 6.5.

Photograph of test setup, showing the application of the vertical load on a wall sample.



TABLE 6.1.

Characteristics (width, height, thickness, and load) of the nine walls constructed for the pull-out test

Wall	Width (m)	Height (m)	Thickness (m)	Top Load (kN)
M1	1.90	1.50	0.26	3.5
M2	1.90	1.50	0.26	3.5
M3	1.90	1.50	0.26	0
M4	1.90	1.50	0.54	7.0
M5	1.90	1.50	0.54	7.0
M6	1.90	1.50	0.54	0
M7	1.90	1.50	0.84	10.5
M8	1.90	1.50	0.84	10.5
M9	1.90	1.50	0.84	0

compression strength of the blocks was 2 MPa, which is high compared to the values obtained for the historic adobe units. The mud mortar used for the masonry was composed of 3 parts soil, 1 part sand, and 1 part straw by volume. The thickness of the horizontal and vertical mortar joints was about 20 mm. Uniaxial compression strength tests on piles were executed as well, and an average compression strength of 1.13 MPa and Young's modulus of 246 MPa were measured (based on three test specimens). Shear strength of the masonry was successfully obtained through diagonal compression tests and measured 0.044 MPa. The walls were coated with a thin limewash that allowed crack developments to be seen more easily.

Results

The load-displacement curves and the corresponding crack formations on the outside wall surfaces are shown in figure 6.6. All walls experienced a conical shear failure that started from the anchor and developed toward the inside wall (fig. 6.7). The 0.26-m-thick walls (M1 to M3) experienced out-of-plane bending at first, but as the load increased, the failure mechanism turned into a punching shear failure. The 0.54-m- and 0.83-m-thick walls (M4 to M6 and M7 to M9, respectively) similarly failed due to punching shear (fig. 6.8). In the 0.83-m-thick walls, the failure surface did not reach the frontal face of the wall; instead, cracks appeared on the lateral sides.

The maximum pull-out force applied to the nine wall specimens is shown in table 6.2. It can be observed that the 0.26-m-thick walls (M1 to M3) reached values that are independent from the vertical load, whereas for the remaining walls, the maximum pull-out force increased approximately 20% when a vertical load was applied. Shear strength for the 0.54-m- and 0.83-m-thick walls was computed assuming a conical failure surface that crossed the entire width of the wall. However, this failure cone developed only for the wall with a thickness of 0.54 m. It was noted that for this thickness, the computed value of shear strength without vertical load was 0.043 MPa, which is very close to the value obtained from the diagonal compression tests (0.044 MPa). The shear cone (see fig. 6.7) could not fully develop in the other tests because of the geometric setup.

TABLE 6.2.
Maximum pull-out force and vertical force applied to the nine wall samples.

Wall	Thickness (m)	Vertical Load (kN/m)	Maximum Load (kN)	Associated Shear Stress (MPa)
M1	0.26	1.83	16.04	–
M2	0.26	1.83	17.46	–
M3	0.26	0	16.60	–
M4	0.54	3.67	34.28	0,053
M5	0.54	3.67	35.69	0,055
M6	0.54	0	28.21	0,043
M7	0.83	5.50	52.35	0,034
M8	0.83	5.50	49.40	0,032
M9	0.83	0	41.83	0,027

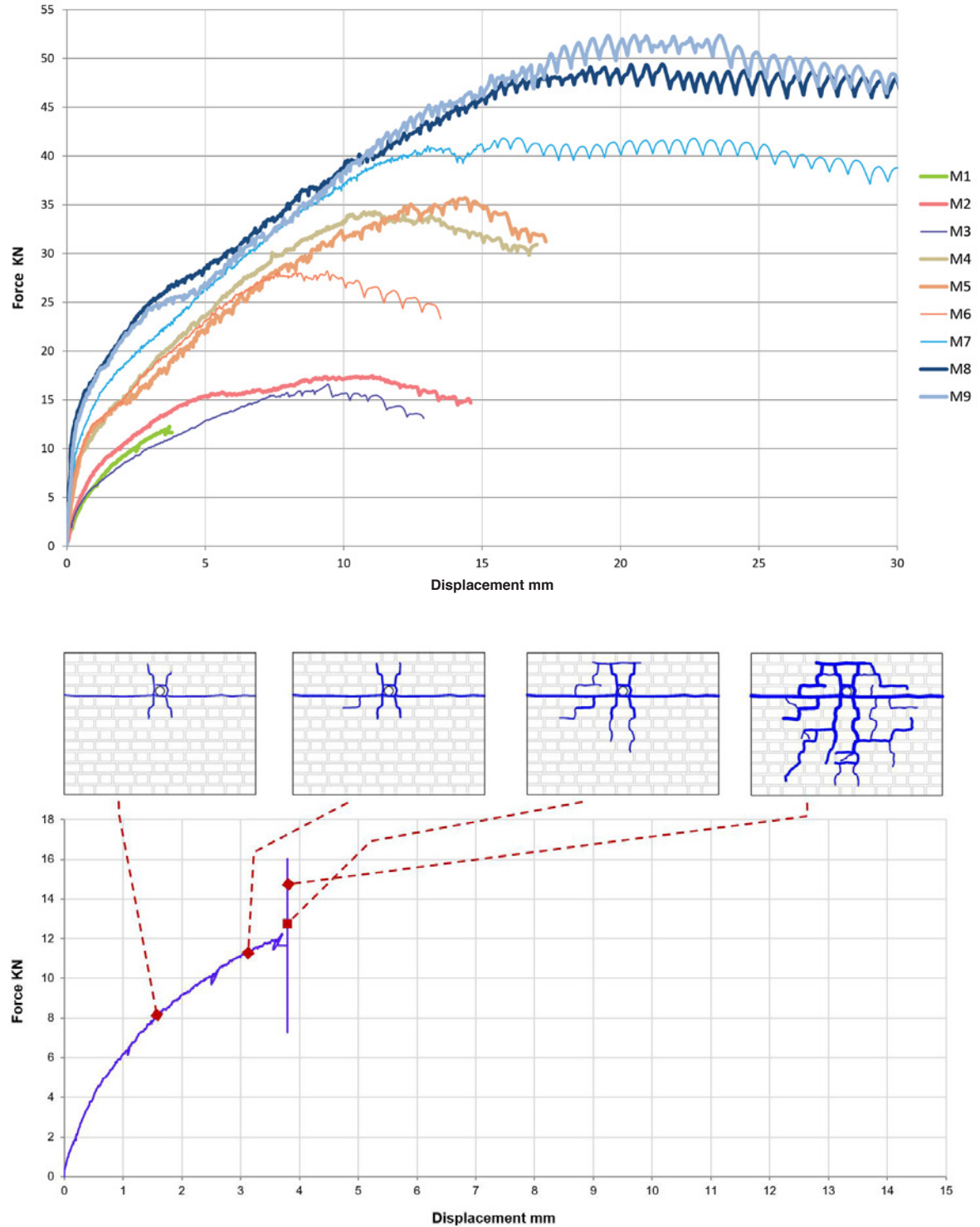


FIGURE 6.6.

Graph showing load-displacement curves and corresponding crack formations on the outside plane of the nine wall samples.

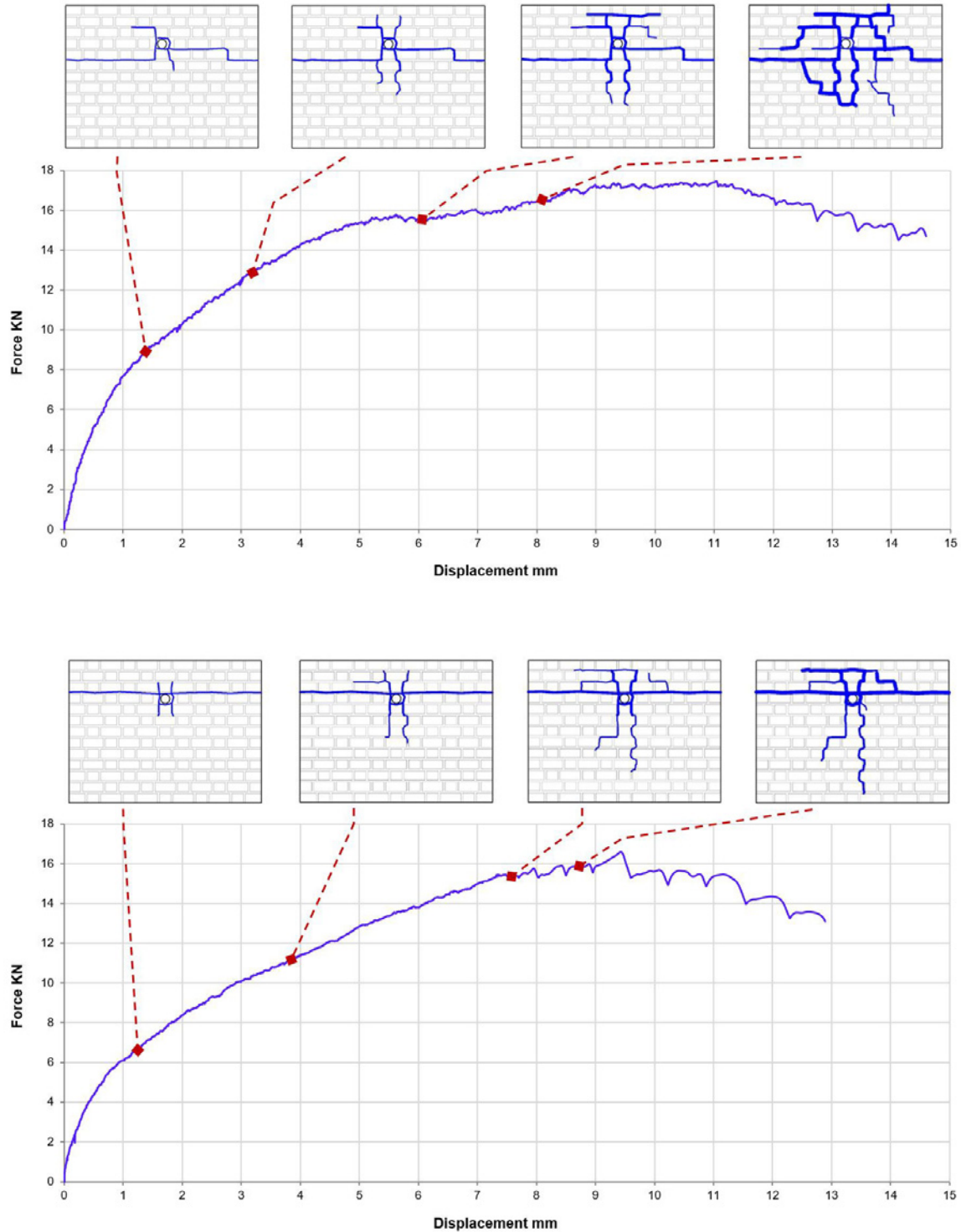


FIGURE 6.6. (CONTINUED)

Graph showing load-displacement curves and corresponding crack formations on the outside plane of the nine wall samples.

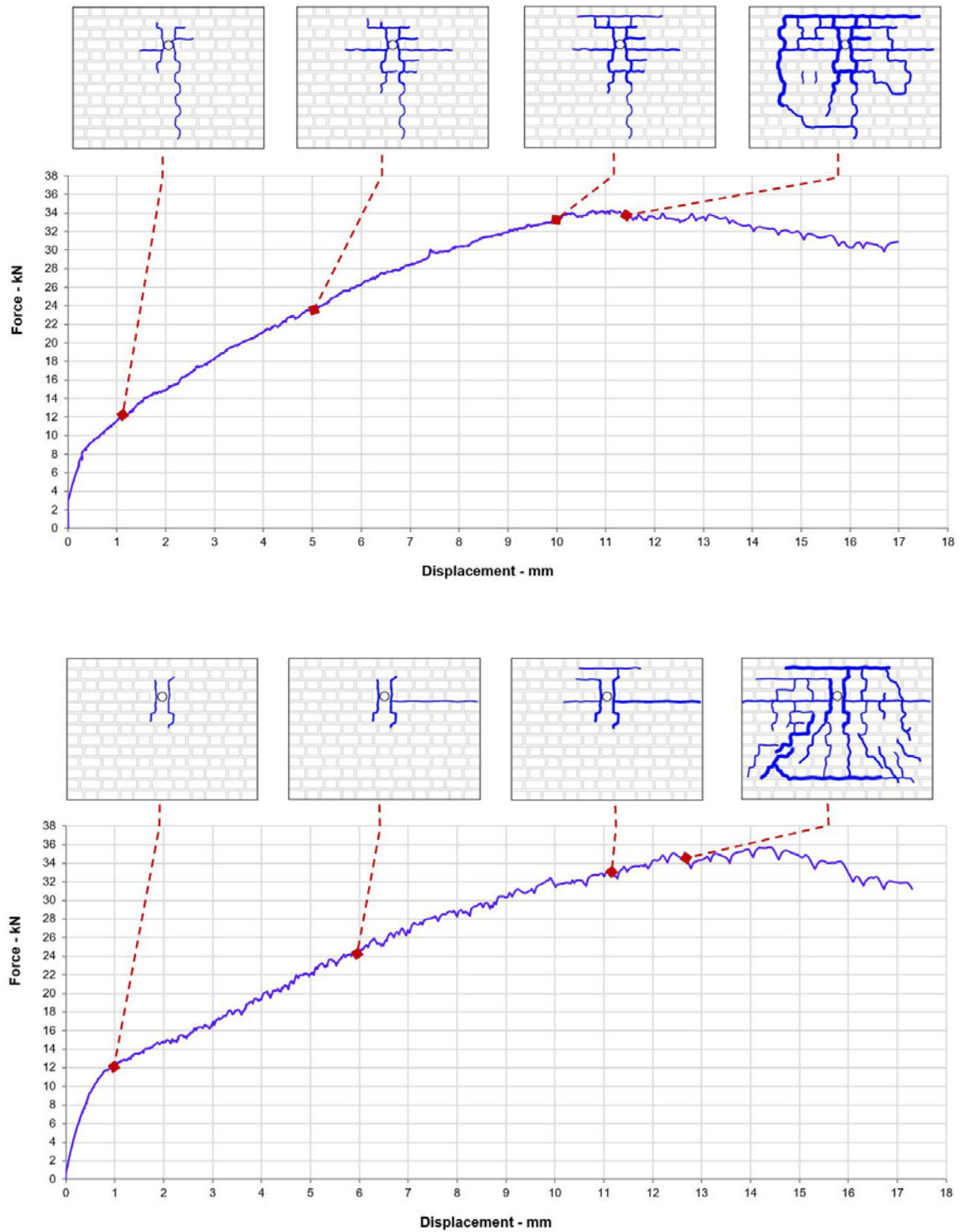


FIGURE 6.6. (CONTINUED)

Graph showing load-displacement curves and corresponding crack formations on the outside plane of the nine wall samples.

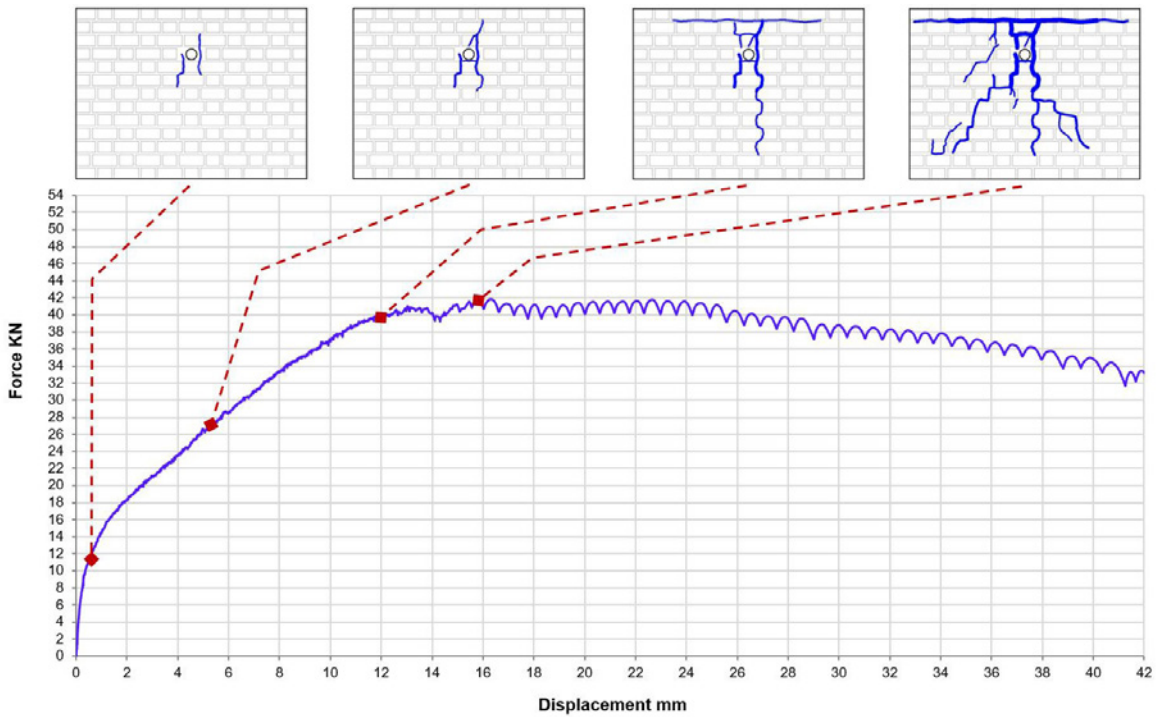
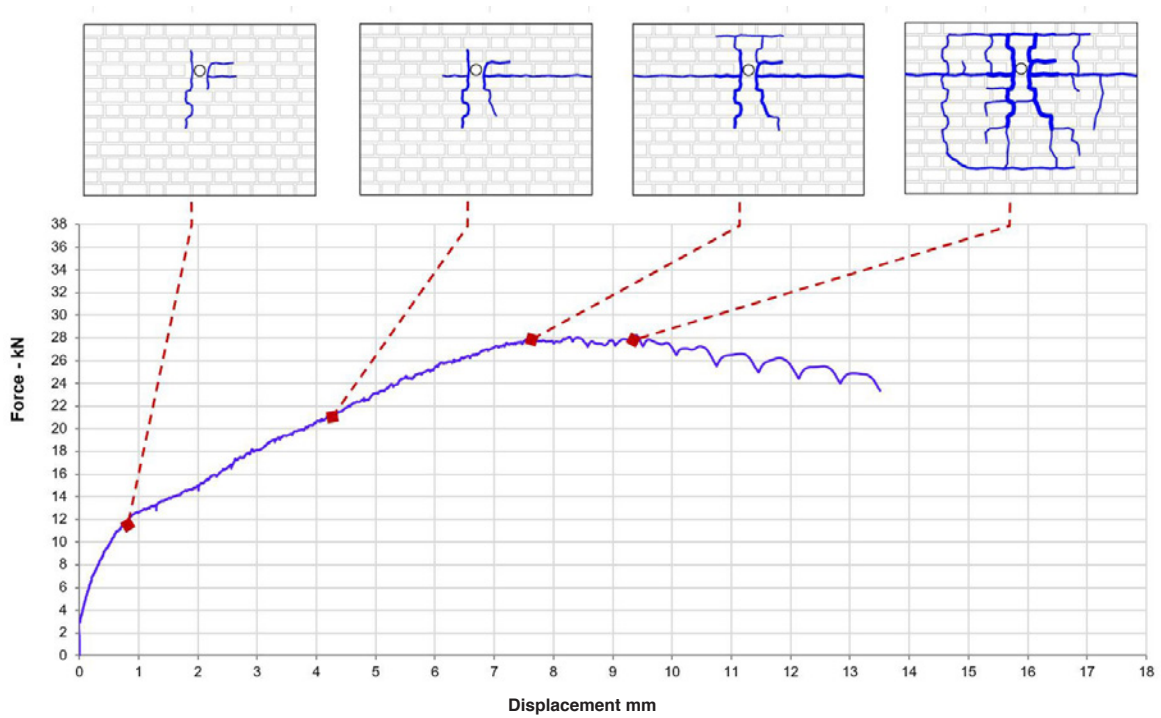


FIGURE 6.6. (CONTINUED)

Graph showing load-displacement curves and corresponding crack formations on the outside plane of the nine wall samples.

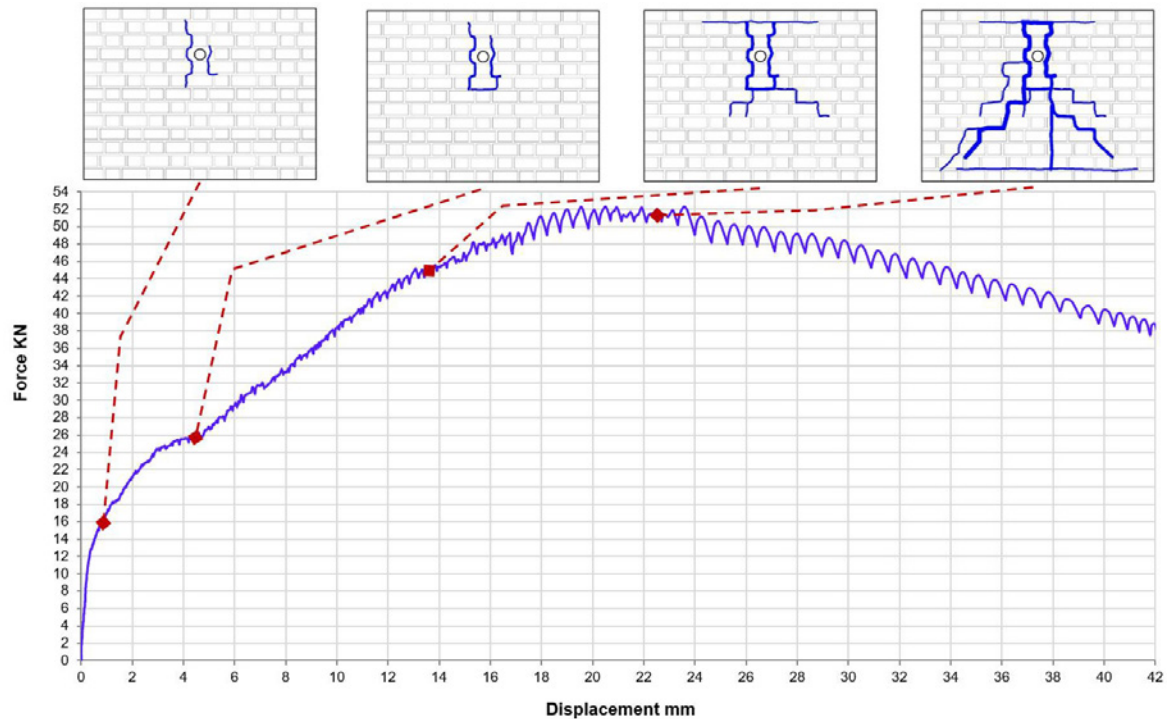
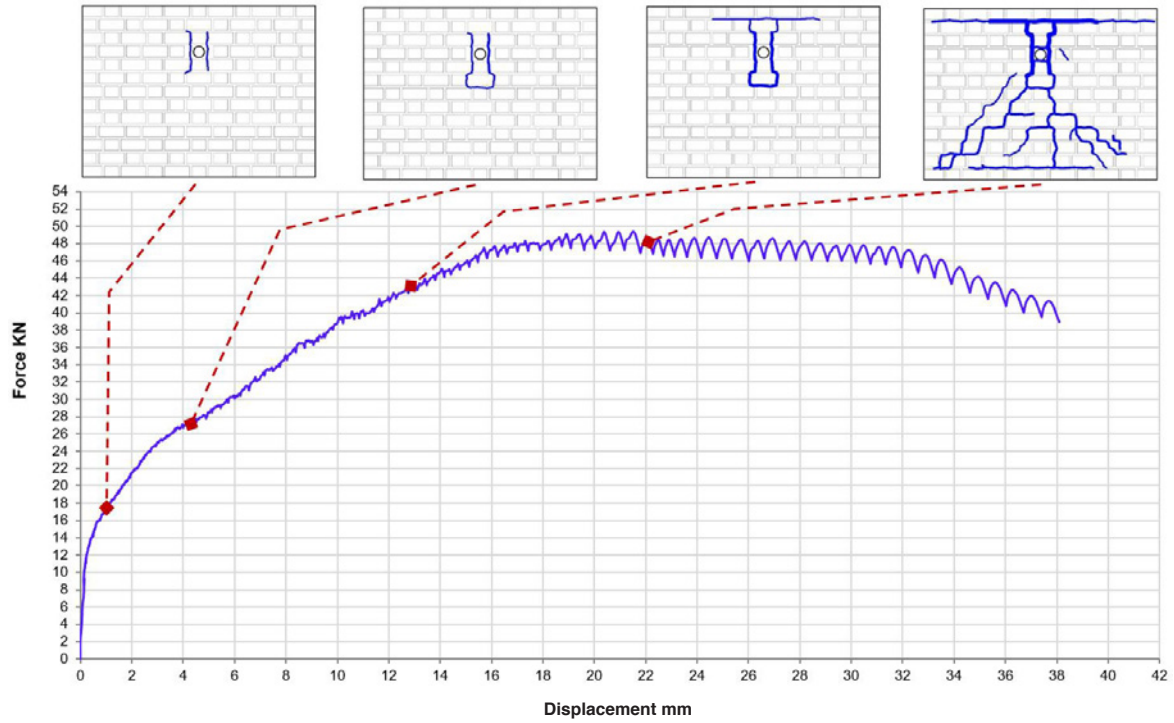


FIGURE 6.6. (CONTINUED)

Graph showing load-displacement curves and corresponding crack formations on the outside plane of the nine wall samples.

FIGURE 6.7.

Diagrams showing (a) front view and (b) side view of failure surfaces.

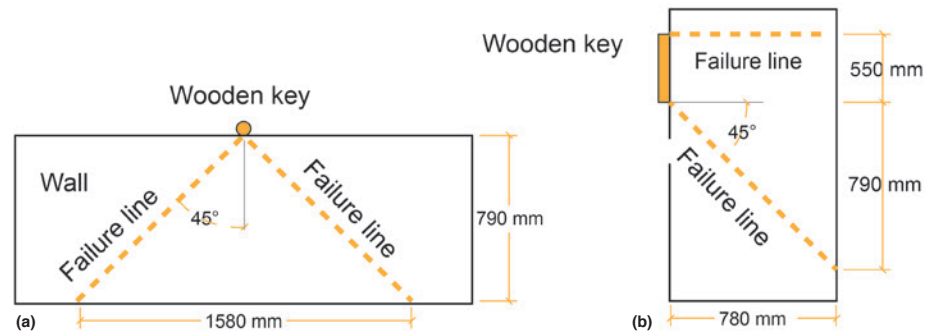


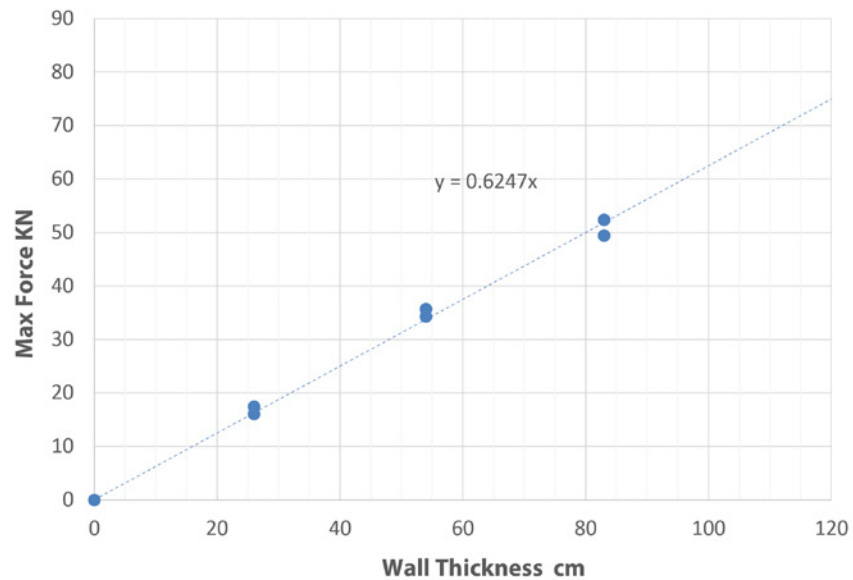
FIGURE 6.8.

Photographs of wall specimens (a) M5 and (b) M8, showing failure mode due to punching shear of the tie through the masonry.



FIGURE 6.9.

Graph showing correlation between the maximum tensile capacity of the ties and the thickness of the walls.



Conclusions

In this program, pull-out tests were executed on adobe walls of varying thickness. Failure occurred through punching shear of the tie through the adobe masonry, as the test setup inhibited overturning failure. A clear linear relationship could be discerned between the ultimate load capacity of the tie and the thickness of the wall. In turn, this relationship can be traced back to a shear-strength calculation based on a 45-degree failure cone. Due to the presence of the upper support, however, the wall could not rotate around a point at its base. Therefore, failure due to bending, or combined shear-bending behavior, was ruled out through the test setup, while these failure mechanisms or even failure of the key are likely to occur during a real seismic event.

Testing of Corner Keys

Corner keys are wooden elements that are employed at different heights of perpendicular walls to stitch these walls together. Cracks commonly occur between orthogonal walls due to the differences in out-of-plane and in-plane motion; accordingly, corner keys are installed to allow the members to work together (fig. 6.10).

Installation of corner keys is a traditional technique throughout Peru with the objective of providing additional internal bracing to improve lateral resistance during seismic activity. One of the main vulnerabilities of earthen structures is the connection between orthogonal walls. A common failure mechanism during an earthquake is the formation of a vertical crack that starts from the top of the wall connection and subsequently pulls both walls apart due to out-of-plane movement of the longitudinal wall.

To provide connectivity of orthogonal walls, a timber corner key composed of a 90-degree assembly with two longitudinal members and transversal members is placed at the corners of buildings and embedded in adobe walls. Each corner key is typically located at each one-third of the wall height, beginning from the top of the wall, and commonly inserted from the interior. Originally, the keys were made of cedar. Today, eucalyptus is the wood most widely used. Even though there are no predefined dimensions for the corner-key members found throughout Cuzco, they are generally constructed of square timber sections with sides of about 13 to 15 cm and extend along walls between 1.20 and 2.00 m from the wall joint.

FIGURE 6.10.

- (a) Timber corner key assembly;
(b) worker installing corner key installed in wall.



FIGURE 6.11.
Structural scheme of the mechanism of a typical corner key.

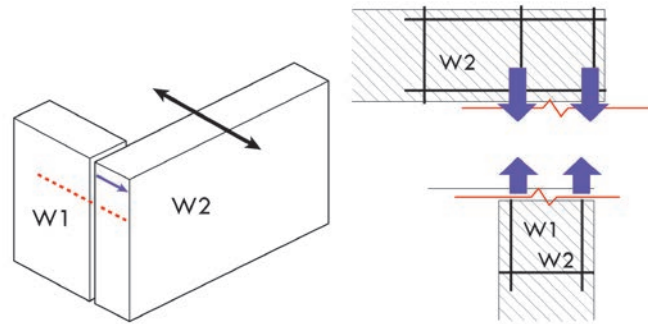


Figure 6.11 shows a schematic of the mechanism of a typical corner key. When cracks are activated between perpendicular walls, they typically appear on a plane that belongs to the wall perpendicular to the one that tends to overturn outward. Wall W2 is the one that tends to fail, and the vertical crack will develop in wall W1.

Methodology

Six masonry walls with embedded corner keys were needed for testing. These walls were built using the same type of unfired bricks as those used for the tie beams (dimensions 90 × 115 × 205 mm, compression strength 2 MPa). Composition of the mortar was 1 part soil, 1/4 part sand, and 1/20 part straw. The timber species used was tornillo (*Cedrelinga catenaeformis*). The connections were executed half-lapped with nails. For a photo of the full test setup, see figure 6.12.

Three different geometric configurations of the wall specimens were built (types A, B, and C) in order to represent the behavior of the corner key. Two tests were executed for each configuration. The first configuration, type A, consisted of a timber assembly in which the key was embedded in longitudinal wall W1 and pulled out in the direction parallel to the wall (fig. 6.13). In contrast, in the second configuration, type B, part of the key was embedded in wall W2 and pulled out in the direction perpendicular to the wall (fig. 6.14). A third set of tests (type C) was set up similar to the configuration of type B but with an additional anchor key added at the outer end of the assembly in an attempt to increase load capacity (fig. 6.15). A pull-out force was applied incrementally at a constant rate of 2 kN/min using

FIGURE 6.12.
Corner-key full test setup.



a hydraulic jack until failure. Top and bottom of wall displacement were restricted, thus simulating a ring-beam or upper corner key above and below the corner key. LVDTs were installed to record displacement of the timber assembly.

FIGURE 6.13.

Type A specimen (timber assembly), where key is embedded in the longitudinal wall (W1) and pulls out parallel to the wall.

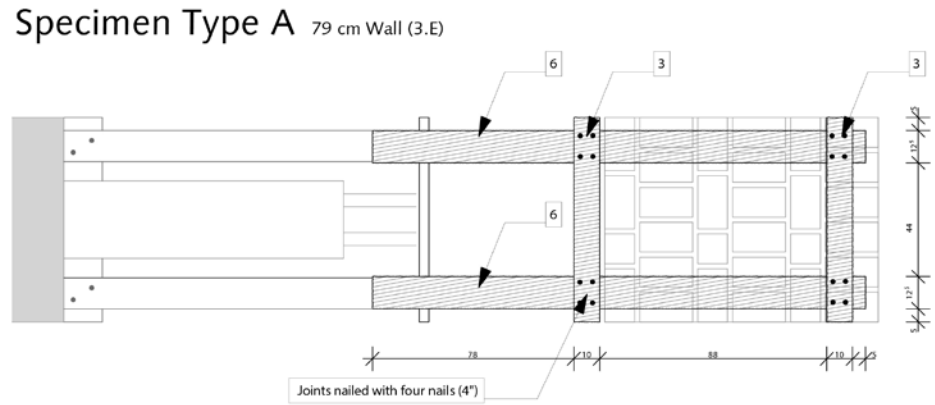


FIGURE 6.14.

Type B specimen, where part of key is embedded in wall W2 and pulls out perpendicular to the wall.

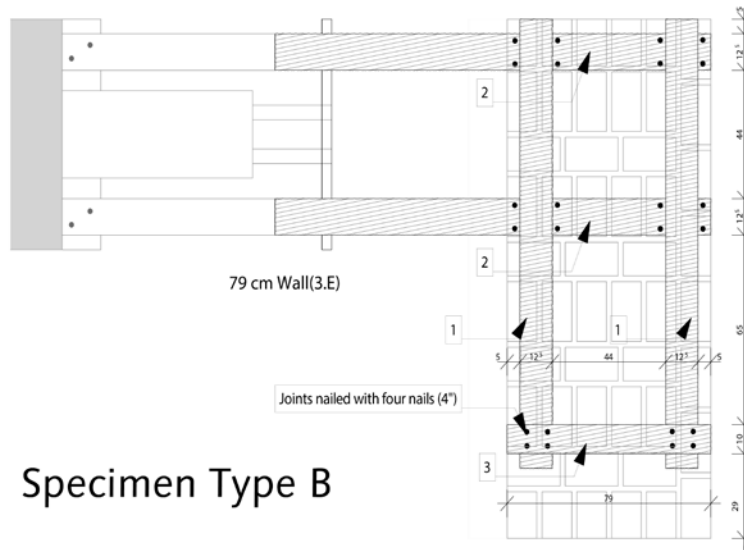


FIGURE 6.15.

Type C specimen, similar to type B except for an additional anchor key added to increase load capacity.

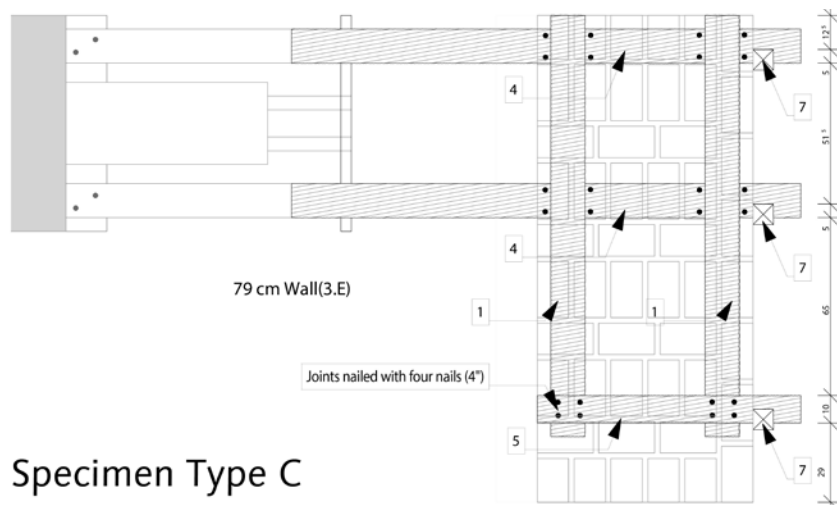


TABLE 6.3.

Maximum pull-out force applied to the six specimens.

Specimen	Dimensions of Wall length x height (m x m)	Maximum Load (kN)	Associated Shear Stress (MPa)
A1	1.05 x 2.00	26.97	0.023
A2	1.05 x 2.00	26.91	0.023
B1	1.75 x 2.00	30.57	0.015
B2	1.75 x 2.00	32.78	0.016
C1	1.75 x 2.00	37.13	0.018
C2	1.75 x 2.00	37.20	0.018

Results

Table 6.3 shows the maximum pull-out force for all six specimens. Figures 6.16 and 6.17 show the load-displacement curves for type A specimens and type B and C specimens, respectively. Figures 6.18, 6.19, and 6.20 show development of crack patterns during testing. The maximum pull-out force is governed by the failure in shear of the masonry wall, on a plane inclined approximately 45 degrees with the horizontal plane of the key. The load-displacement curves indicate an elastoplastic behavior until the timber key detaches from the adobe wall.

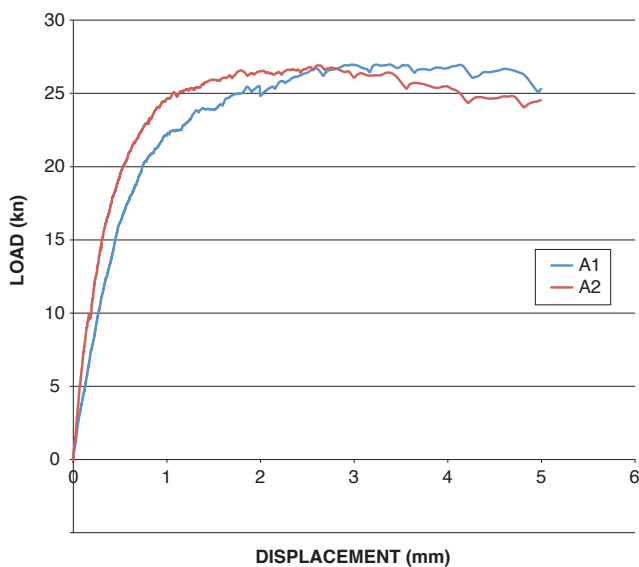


FIGURE 6.16. Graph showing load-displacement curves for type A specimens.

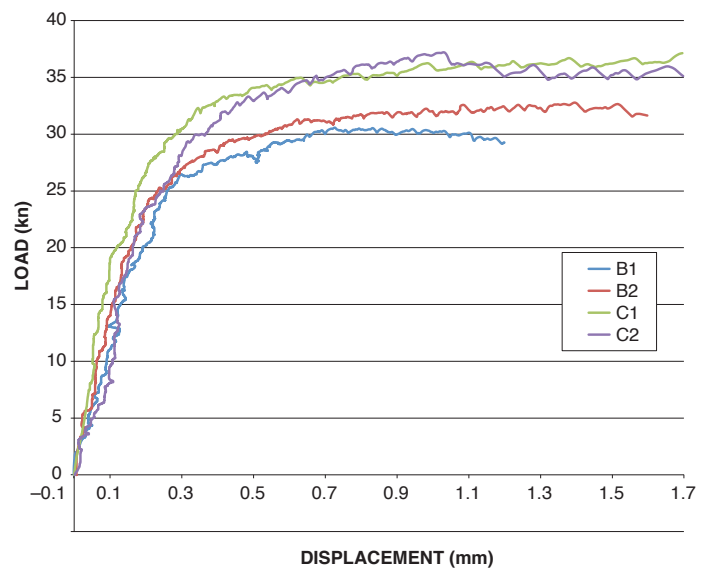


FIGURE 6.17. Graph showing load-displacement curves for type B and C specimens.

FIGURE 6.18.
Crack propagation during testing of
type A specimens.



FIGURE 6.19.
Crack propagation during testing of
type B specimens.

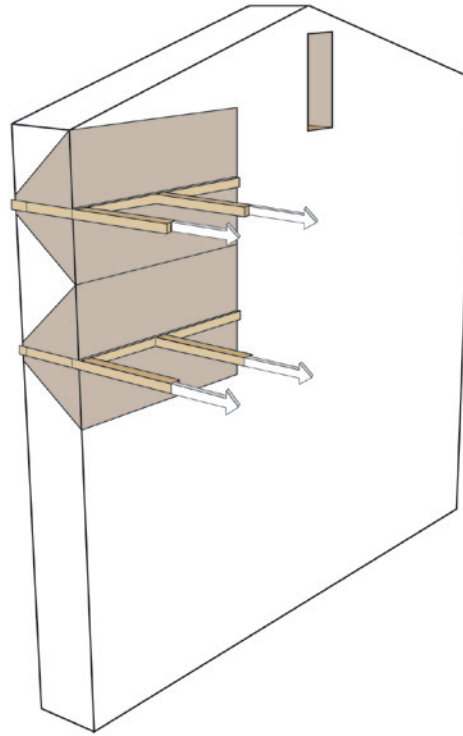


FIGURE 6.20.
Crack propagation during testing of
type C specimens.



FIGURE 6.21.

Diagram showing the shear cone that is activated through pull-out of the corner keys, which can inform the vertical distance between keys.



Conclusions

In this test setup, failure of the corner key is governed by the section embedded in wall W1, as the masonry of this wall fails when subjected to a pull-out force (27 kN, type A) lower than the pull-out force needed to cause shear failure in the transversal wall (31 kN, type B). The overall shear capacity of wall W1 is lower than the shear capacity of the transversal wall (W2); the latter has a larger area to develop the shear failure cone (fig. 6.21). Calculating the associated shear stress for type A specimens, assuming a 45-degree failure plane, results in a shear-compression stress of 0.023 MPa, about half the shear strength capacity measured in diagonal compression tests. For type B and C specimens, the failure plane is not uniform over the section due to the fact that the force is applied off center, leading to an asymmetrical loading pattern. Assuming a uniform plane of failure for the calculation of the associated shear stress in types B and C, this leads to even lower shear stress values. The incorporation of vertical anchors at the end of the corner key in the type C specimens increased the ultimate force by 20%. Development of the failure plane starts in the transversal piece of the key, embedded in W1 located farthest from the intersection of the walls. Therefore, maximum load capacity is directly related to length of the key.

References

Michiels, T. L. G. 2015. "Seismic Retrofitting Techniques for Historic Adobe Buildings." *International Journal of Architectural Heritage* 9 (8): 1059–68.

Conclusions

The objective of this research program was to gain a more profound understanding of the mechanical properties and structural behavior of traditional building materials and components used in historic adobe structures in Peru. This goal was accomplished by performing a series of tests on original materials collected in historic buildings, as well as by mimicking traditional connection and seismic stabilization systems using new materials.

The collection of original materials from historic buildings proved to be an extremely complicated endeavor. As it is not permissible from a conservation perspective to extract large portions of undamaged material from historic sites, the sample size of tests on original material was small. Moreover, documentation of the exact origin, age, or deterioration history of the samples was complicated. Excess elements presented in the buildings—for example, an unused adobe block found in the sacristy of the church of Kuñotambo—were often used for testing purposes. After collecting the samples, it was sometimes necessary to manipulate the fragile material. The reader should keep in mind that these factors may have had an impact on the results. Given the variation of the obtained values of some tests, the presented data should be used with caution. Nonetheless, valuable results were obtained through the testing of original timber and historical adobe blocks and quincha panels.

Characterizing the material properties of the basic elements of the historic sites was undertaken through in-depth material testing of adobe and brick masonry, as well as through extensive wood characterization tests. Research confirmed that the compressive strength of historical adobe blocks can be considerably lower than the strength of their new counterparts and can vary greatly from site to site. In addition, because adobe piles showed significantly lower capacity in compression than adobe units, the compressive strength of adobe masonry should not be predicted by relying solely on the compressive strength of the units. This could lead to overestimates of the compressive strength of the masonry. It was found that applying tests developed for traditional masonry on the much more brittle and lower-strength adobe is a challenge. Most importantly, the brittleness of the adobe prevented accurate estimation of the elastic and shear modulus of the masonry in the employed test setups. As the understanding of the elastic behavior of adobe is key to increasing the accuracy of numerical modeling, it is advised to improve testing methodologies in future research.

One of the great revelations of the adobe material testing, however, was the efficacy of the shear-compression tests on triplets to characterize the shear behavior of adobe masonry. The reliability of these tests stood in stark contrast to the results obtained using diagonal compression tests, which proved to be unreliable because adobe test samples were often so brittle that they could not even be placed on the testing device without breaking. As such, it is recommended that researchers consider replacing or complementing diagonal compression tests with shear-compression tests on triplets.

The timber species present in two historic buildings on the Peruvian coast were identified and their mechanical properties detailed. This was the first such investigation carried out to date in Peru. Surprisingly, a North African wood species called sapele was found in both Hotel El Comercio and Ica Cathedral. Huarango, a tropical hardwood, and cedar were found in Ica Cathedral, whereas in Hotel El Comercio, cypress and Oregon pine complemented the sapele. The mechanical properties of each of these species were reported and each wood species was classified based on the Peruvian standard (NTE E-010).

As quincha panels are an essential feature of many houses in Lima, an extensive full-scale testing program was set up to characterize the dynamic in-plane response of these panels. For the first time, a full-scale historical quincha panel was tested to characterize its in-plane capacity and ductility. The results of the tests on this original panel were compared to the results of newly constructed quincha panels with identical typology as found in Hotel El Comercio. The tests showed that the original panel had sustained little deterioration over time, as it outperformed some of the newly constructed samples. In general, the tests proved that the in-plane capacity of quincha panels is unlikely to be surpassed during seismic events, as none of the structural components of the panel failed during testing. It could be concluded that the wooden frames of quincha, and the relatively lightweight infill of cane and mud, are very flexible and therefore can accommodate large displacements without suffering significant damage. Nonetheless, only the in-plane behavior of the quincha was characterized, and while the out-of-plane behavior is unlikely to cause problems, it would be interesting to further detail this out-of-plane behavior.

Three types of timber connections in Ica Cathedral were subjected to cyclic load testing to identify their properties. The most important conclusion of these tests is that all considered connection types effectively behaved as pinned connections. Furthermore, none of the connections are likely to fail even under extreme loading (assuming they are properly executed and have not been affected by wood deterioration).

Finally, two large-scale tests on building components were executed by investigating the interaction of masonry walls with tie beams and corner keys. In both cases, the tests were set up to reproduce failure governed by shear strength of the material. The adobe masonry was the factor governing failure, rather than the ties or keys themselves. These tests could capture one possible failure mode of the systems accurately, thereby showing the great potential of doing macro-scale testing on larger elements. In the future, it could be valuable to repeat the tests reproducing other failure mechanisms.

Overall, the testing program detailed in this report sheds new light on several aspects of the building materials and components used in historic earthen structures in Peru. Though new insights inevitably lead to more questions, this report forms a basis toward a better understanding of these earthen structures, and will therefore contribute to safer and better-preserved monuments.

Bibliography

- ASTM International. 2006. *Standard Practice for Classification of Soils for Engineering Purposes (Unified Soil Classification System)*. ASTM D2487. West Conshohocken, PA: ASTM International.
- _____. 2007. *Standard Test Methods for Density and Specific Gravity (Relative Density) of Wood and Wood-based Materials*. ASTM 2395-07a. West Conshohocken, PA: ASTM International.
- _____. 2007. *Standard Test Method for Particle-Size Analysis of Soils (Withdrawn 2016)*, ASTM D422-63(2007)e2. West Conshohocken, PA: ASTM International.
- _____. 2009. *Standard Test Methods for Small Clear Specimens of Timber*. ASTM D143-09. West Conshohocken, PA: ASTM International.
- _____. 2017. *Standard Test Methods for Liquid Limit, Plastic Limit, and Plasticity Index of Soils*, ASTM D4318-17e1. West Conshohocken, PA: ASTM International.
- _____. *Standard Classification of Peat Samples by Laboratory Testing*, ASTM D4427-18. West Conshohocken, PA: ASTM International.
- Baas, Pieter, Peter E. Gasson, Elisabeth A. Wheeler, and International Association of Wood Anatomists. 1989. "IAWA List of Microscopic Features for Hardwood Identification: With an Appendix on Non-anatomical Information." *IAWA Journal* 10(3): 219–332.
- British Standards Institution. 2002. *Methods of Test for Masonry, Part 3: Determination of Initial Shear Strength*. BS EN 1052-3. London: BSI Group.
- Cancino, Claudia. 2014. Estudio de daños a edificaciones históricas de tierra después del terremoto del 15 de agosto del 2007 en Pisco, Perú. Los Angeles: Getty Conservation Institute. http://hdl.handle.net/10020/gci_pubs/damage_assess_esp
- Cancino, Claudia, and Sara Lardinois. 2012. Seismic Retrofitting Project: Assessment of Prototype Buildings. 2 vols. Los Angeles: Getty Conservation Institute. http://hdl.handle.net/10020/gci_pubs/assess_prototype
- Cancino, C., S. Lardinois, D. D'Ayala, C. Fonseca, D. Torrealva, E. Vicente, and L. Villacorta. 2012. *Seismic Retrofitting Project: Assessment of Prototype Buildings*. 2 vols. Los Angeles: Getty Conservation Institute.
- COPANT (Comisión Panamericana de Normas Técnicas). 1974. *Maderas: Método para la descripción de las características generales, macroscópicas y microscópicas de las maderas angiospermas y dicotiledóneas: anteproyecto de Norma*. COPANT 30:1-019. Caracas, Venezuela, 25pp.
- Coradin, V. T. R., and G. I. Bolzon de Muniz. 1991. *Normas de procedimentos em estudos de anatomia de madeira I. Angiospermae. II. Gimnospermae*. Serie Técnica 15. Brasília: IBAMA, DIRPED, Laboratório de Produtos Florestais.
- Ferreira, C. F., and D. D'Ayala. 2014. "Structural Analysis of Timber Vaulted Structures with Masonry Walls." In *Proceedings of the SAHC 2014 9th International Conference on Structural Analysis of Historical Constructions, Mexico City, Mexico, 14–17 October 2014*. Wrocław, Poland.
- Ferreira, C. F., D. D'Ayala, J. L. Fernandez Cabo, and R. Díez. 2013. "Numerical Modeling of Historic Vaulted Timber Structures." *Advanced Materials Research*, 778, 517–25.
- Fonseca, C., and Dina D'Ayala. 2012a. "Numerical Modelling and Structural Analysis of Historical Ecclesiastical Buildings in Peru for Seismic Retrofitting." In *Proceedings of the 8th International*

- Conference on Structural Analysis of Historical Constructions, 15–17 October 2012*. Wrocław, Poland.
- _____. 2012b. "Seismic Assessment and Retrofitting of Peruvian Earthen Churches by Means of Numerical Modeling." In *Proceedings of the Fifteenth World Conference on Earthquake Engineering*. Lisbon.
- Haesebrouck, L., and T. Michiels. 2011. "Improving Durability of Adobe: A Case Study for Cuenca, Ecuador." Master's thesis, University of Leuven, Belgium.
- Hardy, Mary, Claudia Cancino, and Gail Ostergren, eds. 2009. *Proceedings of the Getty Seismic Adobe Project 2006 Colloquium: Getty Center, Los Angeles, April 11–13, 2006*. Los Angeles: Getty Conservation Institute. http://hdl.handle.net/10020/gci_pubs/gsap
- Hidayat, S., and W. T. Simpson. 1994. *Use of Green Moisture Content and Basic Specific Gravity to Group Tropical Woods for Kiln Drying*. Research note FPL-RN-0263. Madison, WI: US Department of Agriculture, Forest Service, Forest Products Laboratory.
- Hurtado, P. 2011. "Bóvedas encamonadas: Origen, evolución, geometría y construcción entre los siglos XVII y XVIII en el Virreinato del Perú, dirigida por E. Nuere y J. Fernández." Doctoral thesis, Universidad Politécnica de Madrid, Escuela Técnica Superior de Arquitectura.
- International Council on Monuments and Sites (ICOMOS). 1999. *Principles for the Preservation of Historic Timber*. Paris: ICOMOS.
- Michiels, T. L. G. 2015. "Seismic Retrofitting Techniques for Historic Adobe Buildings." *International Journal of Architectural Heritage* 9 (8): 1059–68.
- Ministerio de Transportes, Comunicaciones, Vivienda y Construcción. 2000. *ININVI: Adobe Construction. Technical Standard for Adobe Building. Special Disposition for Seismic-resistant Adobe Building*. NTE E-080. Lima: Ministerio de Transportes, Comunicaciones, Vivienda y Construcción.
- _____. 2006a. *Albañilería*. NTE E-070. Lima: Ministerio de Transportes, Comunicaciones, Vivienda y Construcción.
- _____. 2006b. *Normativa de madera*. NTE E-010. Lima: Ministerio de Transportes, Comunicaciones, Vivienda y Construcción.
- Ottazzi, G. P., J. F. L. Yep, M. S. Blondet, M. G. Villa-García, and J. F. Ginocchio. 1989. *Ensayos de simulacion sismica de viviendas de adobe*. Lima: Pontificia Universidad Católica del Perú, Departamento de Ingeniería.
- Quinn, N., and D. D'Ayala. 2013. "Assessment of the Realistic Stiffness and Capacity of the Connections in Quincha Frames to Develop Numerical Models." *Advanced Materials Research*, 778: 526–33.
- _____. 2014. "In-plane Experimental Testing on Historic Quincha Walls." In *Proceedings of the SAHC 2014 9th International Conference on Structural Analysis of Historical Constructions, Mexico City, Mexico, 14–17 October 2014*. Wrocław, Poland.
- Quinn, N., D. D'Ayala, and D. Moore. 2012. "Numerical Analysis and Experimental Testing of Quincha under Lateral Loading." In *Proceedings of the 8th International Conference on Structural Analysis of Historical Constructions, 15–17 October 2012*. Wrocław, Poland.
- Tolles, E. Leroy, Edna E. Kimbro, and William S. Ginell. 2002. *Planning and Engineering Guidelines for the Seismic Retrofitting of Historic Adobe Structures*. GCI Scientific Program Reports. Los Angeles: Getty Conservation Institute. http://hdl.handle.net/10020/gci_pubs/seismic_retrofitting_english
- Tolles, E. Leroy, Edna E. Kimbro, Frederick A. Webster, and William S. Ginell. 2000. *Seismic Stabilization of Historic Adobe Structures: Final Report of the Getty Seismic Adobe Project*. GCI Scientific Program Reports. Los Angeles: Getty Conservation Institute. http://hdl.handle.net/10020/gci_pubs/seismic_stabilization
- Tolles, E. Leroy, Frederick A. Webster, Anthony Crosby, and Edna E. Kimbro. 1996. *Survey of Damage to Historic Adobe Buildings after the January 1994 Northridge Earthquake*.

GCI Scientific Program Reports. Los Angeles: Getty Conservation Institute.
http://hdl.handle.net/10020/gci_pubs/damage_adobe_structures

- _____. 2014. "Experimental Behavior of Traditional Seismic Retrofitting Techniques in Earthen Buildings in Peru." In *Proceedings of the SAHC 2014 9th International Conference on Structural Analysis of Historical Constructions, Mexico City, Mexico, 14–17 October 2014*. Wroclaw, Poland.
- Torrealva Dávila, Daniel and Erika Vicente Meléndez. 2012. Proyecto de Reforzamiento Sísmico: Evaluación Experimental del Comportamiento Sísmico de Muros de Quincha del Centro Histórico de Lima—Perú. In *11th International Conference on the Study and Conservation of Earthen Architectural Heritage*. Lima, Perú.
- Torres, R., and J. Alva. 1983. *Propiedades físico-mecánicas de adobes no estabilizados utilizados en el Perú*. Lima: Universidad Nacional de Ingeniería, Departamento de Estructuras y Construcción.
- Vargas, J., J. Bariola, and M. Blondet. 1983. *Informe final del proyecto resistencia sísmica de la mampostería de adobe*. Convenio AID-PUCP. Lima: Pontificia Universidad Católica del Perú, Departamento de Ingeniería, Sección Ingeniería Civil.
- Vargas, J., J. Bariola, M. Blondet, and P. K. Mehta. 1986. Seismic Strength of Adobe Masonry. *Materials and Structures* 19 (4): 253-58. <https://doi.org/10.1007/BF02472107>
- Vargas, J., and G. Ottazzi. 1981. *Investigaciones en adobe*. Lima: Pontificia Universidad Católica del Perú, Departamento de Ingeniería, Sección Ingeniería Civil.
- Vargas-Neumann, Julio, Daniel Torrealva, and Marcial Blondet. 2007. Construcción de casas saludables y sismorresistentes de adobe reforzado con geomallas—Zona de la costa (1st ed.). Lima: Fondo Editorial de la Pontificia Universidad Católica del Perú.
- Varum, H., A. Costa, H. Pereira, and J. Almeida. 2006. "Comportamento estrutural de elementos resistentes em alvenaria de adobe." Paper presented at TerraBrasil 2006: I Seminário Arquitetura e Construção com Terra no Brasil / IV Seminário Arquitetura de Terra em Portugal, Ouro Preto, Minas Gerais, Brazil, November 2006.
- Yamakawa, R. 2013. "Investigation and Analysis of Wood Pathologies in Quincha Construction at Hotel Comercio in Lima, Peru; with Recommendations for Its Treatment." Master's thesis, University of Pennsylvania, Philadelphia.
- Yamin, L., C. Phillips, D. Reyes, and D. Ruiz. 2004. "Seismic Behavior and Rehabilitation Alternatives for Adobe and Rammed Earth Buildings." In *Proceedings of the 13th World Conference on Earthquake Engineering, Vancouver, BC*. Bogotá: CITEC, Universidad de Los Andes.



The Getty Conservation Institute